An innovative application of Nuclear Magnetic Resonance technology to complex flows

Jiaju Hong, BEng.

Thesis submitted to the University of Nottingham

for the degree of Doctor of Philosophy

September 2016

Abstract

In the present work, an inter principle research is carried out on complex fluid flow and heat transfer, using an innovative technology Nuclear Magnetic Resonance (NMR), from the Department of Physics. To enhance heat transfer performance of complex fluid flow, the present work mainly focuses on two different parts, one is the adoption of nanofluid; the other is flow forces analysis through bionic engineering studies on plant water migration system.

Nanofluids are attracting considerable attention from both academic and industrial communities. Comparing with conventional pure fluids or solutions, nanofluids have higher thermal conductivity, due to the high surface to volume ratio of nanoparticle and liquid interface, which exhibits a great potential in enhancing heat transfer performance in various occasions. It is believed that different types and concentrations of nanofluid could strongly affect the thermal performance, and a great number of papers have been published to illustrate the phenomenon. However, none has really focused on the possible concentration change of nanofluid while flowing. Otherwise, the thermal performance of nanofluid flow could never be quantified.

In the present work, a novel method to measure the dynamic concentration of nanofluid is proposed, using NMR technology. The experiments were carried out with ferrofluid under different concentration and temperature. A new parameter T_2^* was introduced in the study. T_2^* is a

relaxation time of the signals that is released by hydrogen atoms after Radio Frequency (RF). And this signal intensity can be strongly affected by nanofluids. Experiments were carried out to obtain the T_2^* of nanofluid in the pipe. An empirical equation based on T_2^* and temperature was proposed to calculate the concentration of nanoparticles. Then, experiments were carried out with flowing ferrofluid in pipe. The dynamic concentration was calculated with the empirical equation. And with the series of experiment, it is confirmed that the flowing nanofluid consists of an obvious concentration gradient, and thus cause different layers of thermal performance from boundary to central line of a laminar pipe flow. Furthermore, the experiment result also gives out a chance to investigate the mechanism of nanoparticle movement in laminar flow with the concentration gradient along radius.

Bionic Engineering is another research field that has been more and more interesting to researches from various fields. Since life has been evolving for over millions of years, many functions in lives has become extremely high efficiency and adaptive. These functions can be very worthy for researchers to study and utilize in industries. For heat transfer in fluid flow, it is very important to enhance the flow pattern. And thus water migration system in plants become very attractive. Plant can take water from soil up to several metres high. Learning from the water migration process in plants has been attracting interests from scientist for over a hundred years. The water migration in plant stem, especially xylem, involves various driving forces including

capillary effect, osmosis effect, Marangoni effect and transpiration effect, etc.

This present work mainly focuses on the water transport process within xylem. As xylem system is simplified as micro channel, a mathematic model is presented based on micro channel theory, with critical analysis and simplification. With a simplified micro channel from xylem structure and the calculation using the model of water migration in xylem, the relationship between various forces and water migration velocity is identified. The velocity of water migration within the plant stem is considered as detail as possible using all major forces involved. And a full mathematical model is proposed to calculate and predict the velocity of water migration in plants. Comparison between the calculated result and experimental one is made, to confirm the accuracy of the mathematical model. The present work proved that the mathematical model should be enough to predict the water migration in plants, and could also be critical for future water transport prediction in complex fluid flow in industry applications such as heat pipe.

List of Publications

1. Jiaju Hong, Sheng Liu, Paul Glover, Yuying Yan, Innovative application of NMR to evaluate the dynamic concentration of nanofluids laminar flow in pipe, submitted to International Journal of Heat and Mass Transfer, September 2016.
2. Jiaju Hong, Sheng Liu, Yuying Yan, Mathematical model of water migration in plant xylem, submitted to International Journal of Heat and Mass Transfer, September 2016.
3. Jiaju Hong, Sheng Liu, Yuying Yan, An application of NMR to investigate water migration in plant xylem, submitted to Journal of Bionic Engineering, September 2016.
4. Qian Wang, Jiaju Hong, Yuying Yan, Biomimetic Capillary Inspired Heat Pipe Wicks, Journal of Bionic Engineering, 11(3), 469-480, 2014.
5. Yong Li, Jiaju Hong, Yuying Yan, Nature inspired innovation of heat pipe technology for energy harvesting and thermal management, submitted to Applied Thermal Engineering, September 2016.

List of Selected Conference Papers

1. Jiaju Hong, Sheng Liu, Yuying Yan, Bionic inspired study of heat pipe from plant water migration, 1st International Conference on Energy and Power, 2016
2. Jiaju Hong, Sheng Liu, Yuying Yan, Mathematical model of water migration in plant xylem, 5th International Conference of Bionic Engineering, 2016.
3. Jiaju Hong, Paul Glover, Yuying Yan, An experimental study of dynamic concentrations of nanofluid flow, 4th Micro and Nano Flows Conference UCL, 2014.
4. Jiaju Hong, Y. Gan, P. Glover, Y. Yan, Y. Tomohiko, B. Li, An experimental study of dynamic flow of nanofluid with different concentrations, IHTS140135, International Heat Transfer Symposium, 2014.
5. Tomohiko Yamaguchi, Qian Wang, Yuying Yan, Jiaju Hong, Numerical simulation of liquid-gas two phase flow with large density difference in multi-layered sintered wick by the lattice boltzmann method, IHTC15-9543, International Heat Transfer Conference, 2014.
6. Yuying Yan, Jiaju Hong, Nature inspired innovation of heat pipe technology for energy harvesting and thermal management, keynote paper at ISHT9, International symposium on heat transfer, 2016.

Acknowledgement

First and foremost, I would like to express my sincere gratitude to my supervisor, Prof. Yuying Yan, for all the support, encouragement and guidance all across my PhD study with his experience, patience and kindness. Without him, this thesis would not be possible. Prof. Yan's support is of great value to me in stepping into a relative unfamiliar inter disciplinary field such as NMR and bionic engineering.

I'm also grateful to my colleagues in SRB for their support and encouragement. Special thank goes to Dr. Sheng Liu for the excellent cooperation and helpful suggestions and discussions during his visit in our group.

My thanks are extended to my friends made in Nottingham during these four years. Thanks to them, my life in Nottingham was colourful and enjoyable.

Finally, I would like to thank all my family: my parents, my grandparents, my uncle and ants for their support and endless love.

Contents

List of Tables

List of Figures

Chapter 1

Chapter 2

Chapter 3

Chapter 4

Chapter 5

Chapter 6

Nomenclature

Roman Letters

Chapter 2

Q	Heat flux (J)
A	Surface area (m^2)
h	Heat transfer coefficient ($W/(m^2 \cdot K)$)
ΔT	Temperature (°C)

Chapter 3, 4 &5

M	Nuclear spin magnetization (A/m)
h	Planck constant ($6.626*10^{-34}$ m^2kg/s)
γ	Nucleus constant (gyromagnetic ratio)
w_0	RF frequency
ΔE	RF energy
t	Time (ms)
T	Temperature (°C)
S	Non-dimensional signal strength
T_1	Longitudinal relaxation time (ms)
T_2	Transverse relaxation time (ms)
v	Nanofluid flow velocity (mm/s)
k	Slope of decaying line
ΔB_0	Local varying field strength difference
J	Mass flow rate (kg/s)
D	Diffusion coefficient
N_{BT}	Ratio of Brownian force to Thermophoresis force

Chapter 6

r	Radius of xylem conduit (nm)
E	Evaporation flux density ($kg \cdot s^{-1} \cdot m^{-2}$)
A	Surface area of conduit water-air interface (m^2)
K_h	Hydraulic conductivity (kg·m/s)
Q	flow rate (m^3/s)
h	conduit height (m)
w	diameter of helical structure bump in xylem (nm)
a	height of simplified bump (nm)
p	Pressure (Pa)
g	Gravity (m/s^2)
h_f	Head loss (m)
f	Friction factor
u	Water transport velocity in xylem (mm/s)
x	Distance along the tube or conduit
Re	Reynolds number

Greek Letters

ρ	Density (kg/m^3)
φ	Gyromagnetic ratio
θ	Contact angle (°)
γ	Surface tension (N/m)
λ	Thermal conductivity ($W \cdot m^{-1} \cdot K^{-1}$)

δ	Distance between two helical structure bump (nm)
ε	Width of helical structure bump (nm)
ϕ	Volume concentration (%)

Subscripts and superscripts

xy	Surface formed by x and y axis
z	Z axis
f	Fluid (thermal conductivity)
ef	Effective (thermal conductivity)
eq	Equilibrium state
p	Particle
h	Hydraulic
f	Friction
c	Capillary
g	Gravity
t	Transpiration
x	Along the tube or conduit
e	Eddies

Abbreviations

NMR	Nuclear Magnetic Resonance
CT	Computed Tomography
TEM	Transmission Electron Microscopy

EG	Ethylene Glycol
SWNT	Single Wall Nanotube
MWNT	Multiwall Nanotube
MNF	Magnetic Nanofluid
OLPHP	Open Loop Pulsating Heat Pipes
ACO	Ant Colony Optimization
BA	Bees Algorithm
RF	Radio Frequency
SPIO	Superparamagnetic Iron Oxides
USPIO	Ultrasmall Superparamagnetic Iron Oxides
SDS	Sodium Dodecyl Sulphate
PID	Proportional - Integral – Derivative
AC	Alternating Current
DC	Direct Current
HA	Hydraulic Architecture

Chapter 1: Introduction

1.1 General Background

Complex flow involves multi-phase flow and fluid flow through complex structures such as micro channel. And heat transfer of complex flows can be widely seen in daily life and industrial process. It is commonly used in many areas such as petroleum engineering, mechanical engineering, electrical engineering, bionic engineering and so on. Many researches have been carried out in these fields, including theoretical, numerical and experimental studies [1-5]. The performance of heat transfer devices, such as heater or cooler, directly influences the performance of modern industrial machines. And because of it, heat transfer problem became a major research field, and there has been a great number of researches on enhancing heat transfer, especially in fluid flow.

In recent years, methods to enhance fluid flow and heat transfer are mainly considered in the two following ways:

First, improving the working agent in the heat transfer process, where in most cases would be water, oil or other organic coolants. And here a state of art product is studied, nanofluid.

Adding nanoparticles into carrier liquid could strongly affect the thermal performance of the carrier liquid, and thus using nanofluid as working agent become very interesting to researchers.[6-8] Nanofluid has very unique

properties that could potentially suit for applications in thermal engineering industries such as thermal engine, fuel cell, thermal management and so on.[9, 10] Researchers have found influence from nanoparticles on the carrier fluid, enhancement on both thermal conductivity and convective heat transfer coefficient.[11] And there're many different types of nanoparticles in nanofluid, each with different thermal properties, as shown in Fig. 1.1. Therefore, using nanofluid to enhance heat transfer become a very critical research field in engineering.

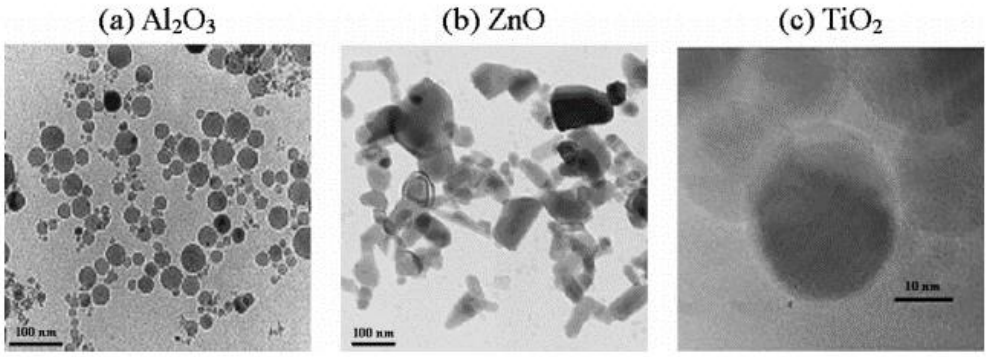

Figure 1. 1: Type of nanofluid under TEM[12]

Second, enhance flow pattern of working agent through bionic engineering. Bionic engineering, or biomimetic, is a new inter-disciplinary field that use biological methods discovered in nature to design and improve modern engineering systems and technologies. The two words were first coined in 1950s, and thrived ever since. However, it is estimated that there's only 12% overlap between biology and modern technology[13], which means

there’s still a lot new technologies waiting to be developed from biology. Many technologies nowadays we use come from imitating nature, and even some research areas such as fluid dynamic. It is even believed that the Hanging Garden of Ancient Babylon was inspired by nature.

Figure 1. 2: Biomimetic[14]

The pressure for lives to survive and evolve, drives almost all livings to develop into more efficient and optimized form in different functions. And this gives recent researchers perfect examples to study and imitate into modern technologies, as shown in Fig. 1.2. However, the history of bionic engineering studies and learnings is far beyond that. Leonardo Da Vinci’s drawings of his inventions are clearly showing the influence of nature on him. And modern

bionic engineering studies mainly focuses on imitating the natural method of manufacture, studying the mechanism found in nature, and understanding the organizational principles of social behaviours. And as an inter-disciplinary area, bionic engineering can be found in different industries. For example, the sonar and radar learning from bat, water proof material learning from lotus, and especially the artificial neural network in computer science. Other recent technologies like Velcro, designation of high speed rail coach, robotics and so on are also directly inspired by natural evolutionary results. In summary, bionic engineering is highly interesting to researchers in all engineering fields, and could apply to daily lives of human.

1.2 Research Objective

In order to study methods of enhancing heat transfer in complex fluid flow, the present work is trying to bring solutions to the two parts of research points in heat transfer of fluid flow:

Firstly, when using nanofluid as the working agent in the heat transfer process, it is widely recognized that the concentration of nanofluid could affect the performance of nanofluid in heat transfer. However, it is difficult to measure the concentration of nanofluid when it's flowing, and thus there's no method to see the concentration variation in fluid flow, which could therefore cause big difference in thermal conductivity and convective heat transfer

coefficient.

Secondly, the water migration system in plants has evolved into varied types amongst different families of plants. And the highly evolved function has been studied and shown to be very efficient. However, due to the microscale and complex structure inside, and different forces involved, little process was made previously in understanding the overall water transport mechanism in plants, especially stem. As applications of working agent flowing in porous structure and micro-channel are very critical issue to industrial heat transfer technology, such as heat pipe, and the forces involved are very similar, therefore, the study on plant water migration mechanism and involving forces becomes very essential to heat transfer in complex fluid flow.

Lastly, as both tasks are difficult to finish with previous equipment in lab, new technology is required to accomplish them. Nuclear Magnetic Resonance (NMR) is introduced into the experiment. And both nanofluid concentration and the flow velocity of water in plant stem in situ can be measured precisely with NMR. Fig. 1.3 illustrates the logic chart of this thesis. Therefore, in conclusion, the research aims to achieve the following goals:

- Measure the dynamic concentration of nanofluid flow and analyse the potential influence on thermal performance.
- Develop a novel mathematical model that suits for water migration process in plant stem, and compare with the experimental result.

- Exploring possibilities to use NMR from Physics/Medication into engineering research field, utilizing its advantages.

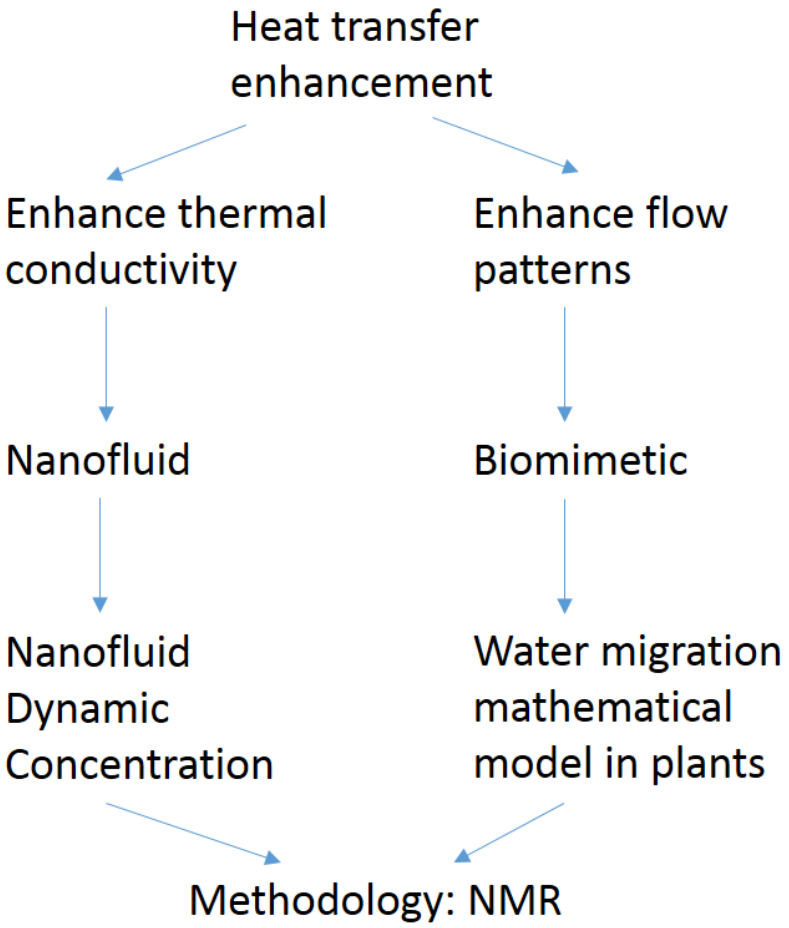

Figure 1. 3: Research logic chart

1.3 Thesis structure

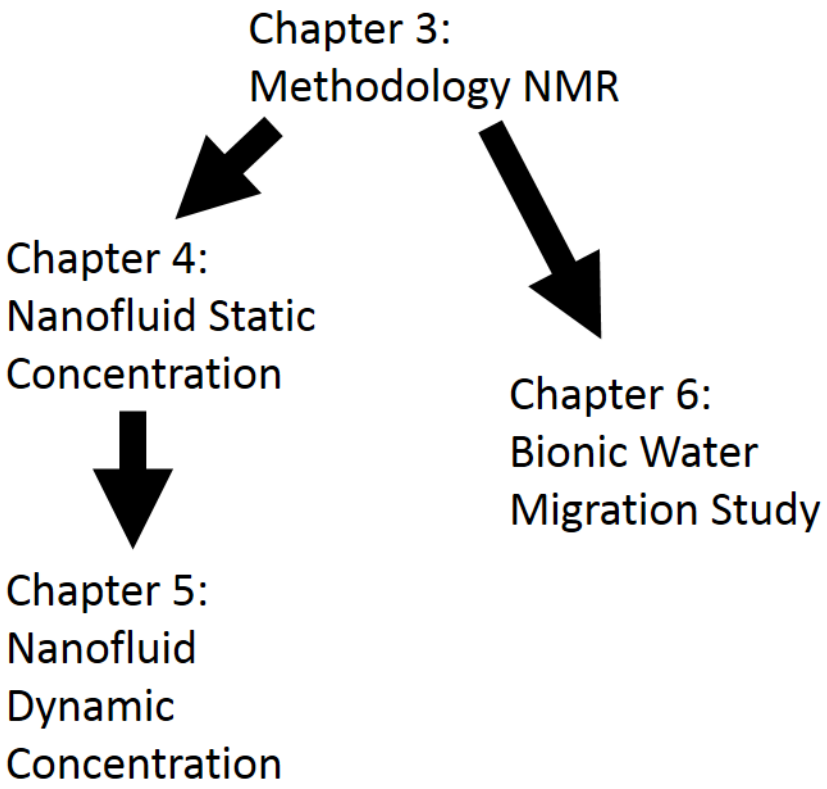

Figure 1. 4: Relationship between chapters

This dissertation has been divided into seven chapters, an outline of which is presented below, while the relationship between main chapters is shown in Fig. 1.4.

Chapter 1 Introduction about the background and research objectives

Chapter 2 Reviewing important information about the research carried out in the present work, including nanofluid heat transfer, concentration difference issue and bionic engineering in plant

water migration.

Chapter 3 The methodology of the research in the thesis is presented, especially on the function of NMR. Introducing a new technology to thermal engineering, the detailed NMR theory is listed, as well as its potential application in nanofluid research and plant imaging. The experimental idea and the test rig is illustrated as well.

Chapter 4 Nanofluid static experiment is presented. The whole nanofluid concentration experiment is divided into two parts, the static and the dynamic one. As in this chapter, the static experiment with NMR is presented, with all the results achieved. The empirical equation for nanofluid concentration calculation is also proposed. And all of these listed in chapter 4 is the preparation for the dynamic concentration measurement in chapter 5.

Chapter 5 A dynamic scan of nanofluid flow is carried out using NMR. And the empirical equation can be used here to calculate the accurate concentration in the nanofluid flow. And the potential influence on thermal conductivity and convective heat transfer coefficient is calculated as well. Furthermore, a brief analysis on the reasons causing the phenomenon is discussed.

Chapter 6 A detailed discussion about all forces that may involve in the

water migration system in plant stem is discussed. And major forces are hence listed and analysed. Then a novel overall mathematical model about the water transportation process is proposed, with a few parameters depending on different spices of plants, but can be easily tested or looked up in previous books. And this model can be used to calculate the mean velocity of water flow inside plant stem, which can also be scanned by NMR as well. Comparing the two results, the model for water transportation can be verified.

Chapter 7 Conclusion of all research work.

Chapter 2: Literature Review

In this chapter, the history of nanofluid heat transfer enhancement research is presented. The background of bionic engineering in water transportation process is also introduced.

2.1 Nanofluid heat transfer enhancement

2.1.1 General review: nanofluid history

Nanofluid is a kind of fluid that contains nano-sized particles in base fluid or carrier fluid. Currently nanofluids are mainly defined as stable suspensions with nanoparticles less than 100nm in diameter well disperse in the carrier fluid. And the sized of nanoparticles can be illustrated comparing with micrometres and millimetres, as is shown in Fig 2.1.

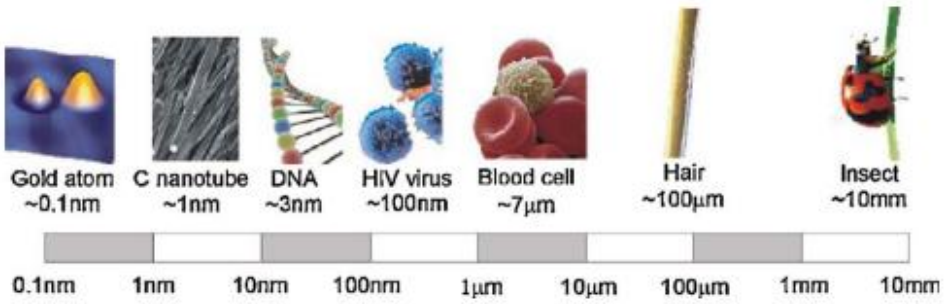

Figure 2. 1: Length scale examples[15]

Nanofluid is first proposed by Maxwell in 1873.[16] Since then,

nanofluids have attracted wide attention from industrial cooling[17], nuclear power generation[18], automotive[19, 20], fuel cell[21], drag delivery[22], cancer therapy[23], detergency [24], dynamic sealing[25] etc. Especially, some nanofluids with specific particles such as magnetic nanofluids, mainly known as ferrofluid, contain strong and unique properties, which may have wider usage in industry for being sensitive to external magnetic field. And even though it is primarily mentioned for its heat transfer enhancement properties, it is now used in many other aspects as well, while heat transfer problem with nanofluid will be introduced later in this chapter.

Nanofluid has been summaries in the following categories, heat transfer nanofluid, tribological nanofluid, surfactant and coating nanofluid, chemical nanofluid, process and extraction nanofluid, environmental nanofluid, bio and pharmaceutical nanofluid, and medical nanofluid. And they are attracting more and more attentions in industrial application, with a share increase in market volume, as shown in Fig 2.2.

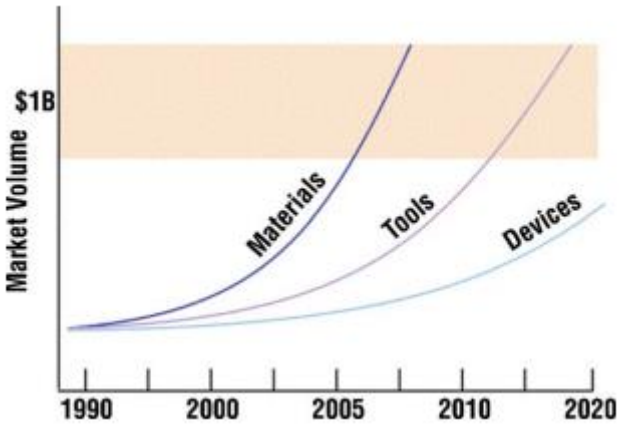

Figure 2. 2: Market volume of nanofluid and prediction[26]

Nanofluid consists of the technology of manufacturing materials into nanoscale, and thus has only been able to synthesis for the past few decades. And in modern nanofluid preparation, there're mainly two methods, two-step method and one-step method.

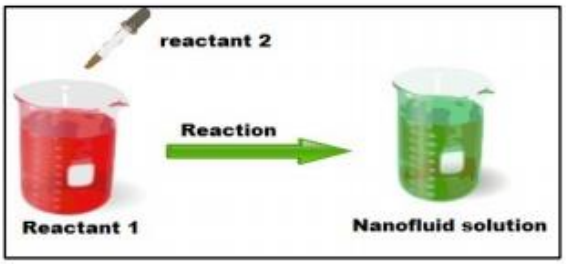

Figure 2. 3: one step synthesis method[27]

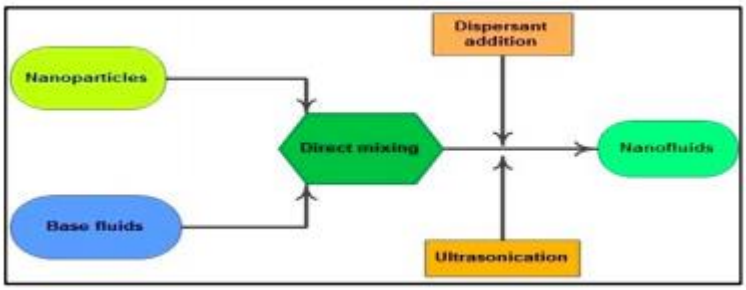

Figure 2. 4: two step synthesis method[27]

The two-step method is the most widely used way of preparing nanofluid, due to its advantages comparing with other methods, as in Fig. 2.4. In this method, the nanoparticles or nanotubes in nanofluid is firstly produced in dry powders. And then, they are dispersed in the carrier fluid, with some treatments that could help nanoparticles or nanotubes to disperse and stabilize, including magnetic force agitation, ultrasonic, high-shear mixing,

homogenizing and ball milling[28]. Even though these treatments are introduced, the synthesised nanofluid still lack of stability, therefore surfactants will be added normally. The two-step method is the most economical way of preparing nanofluid, because of its potential of large scale manufacture. However, the biggest disadvantage is the lack of stability, even after adding surfactant. The stability changes of nanofluid without stabilizer can be seen in Fig. 2.5. So other methods are proposed, including the one-step method.

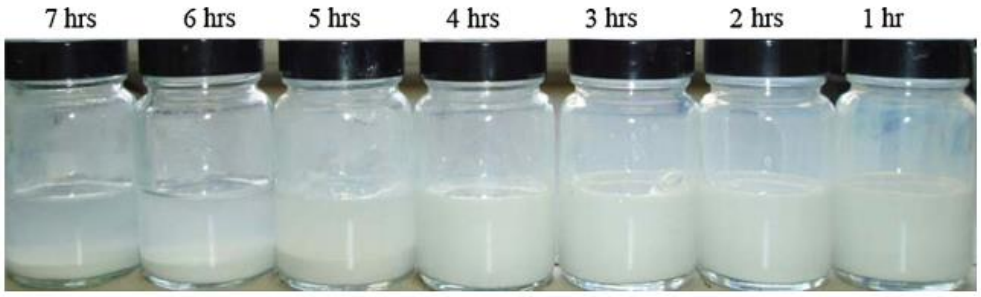

Figure 2. 5: Stability changes of Al_2O_3 nanofluid without stabilizer[29]

The one-step method is to prepare the nanoparticles or nanotubes directly inside the carrier fluid, and could then avoid the drying, dispersion process and so on, as is shown in Fig. 2.3. Since all reactions are carried out in the dispersed and stable solutions directly, this method can largely enhance the stability of nanofluid. However, this method also has obvious disadvantages. First, different from the two-step method, the one-step method preparation can't be conducted in large scale in industries. So the price for one-step method is very high, and the high stability nanofluids could only be used in

labs for now. Second, as the whole reaction is done within the carrier fluid, all the reactants are difficult to be taken out. Therefore, only very in few occasions would researchers use the one-step method, and two-step method is widely used recently. And because of this, stabilization become critical to nanofluid preparation.

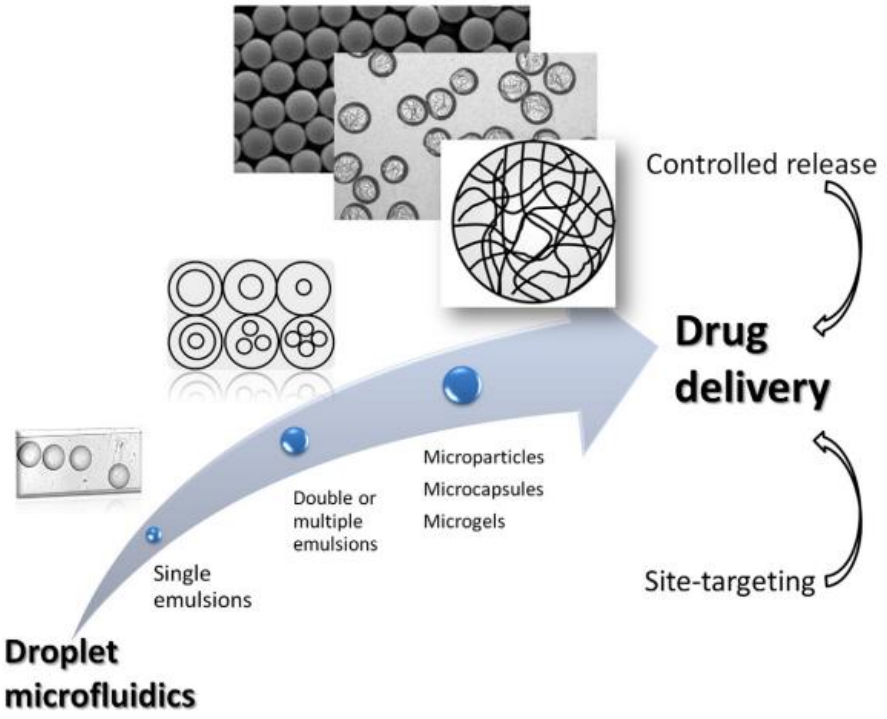

Figure 2. 6: Multiphase flow of nanofluid in drug delivery[30]

The most commonly used method, is adding surfactants, or dispersants. The reason for nanoparticles or nanotubes not being able to well suspend in carrier fluid is because of the interface between nanoparticles and carrier fluid molecules. Take metallic oxide nanoparticles in water for example, the particles are mainly hydrophobic, and have very low wettability in the contact

of water molecules. Thus it is necessary to add some surfactants inside. Typically, these surfactants have both hydrophobic heads that could be connected to the particle molecules and hydrophilic heads that could be connected to water or other carrier fluid molecules. Therefore, the wettability of the nanoparticles is increased, and the stability of nanofluids as well.

As one of the characteristics of nanofluid is the enhancement of thermal performance, it is most widely used in heat transfer enhancement industries nowadays. And the present thesis focus on the thermal performance of nanofluid as well, the heat transfer enhancement of nanofluid is listed individually in the following of this chapter. However, there still exists many areas where nanofluid is adapted beyond the only thermal character, such as friction reduction, drug delivery and so on. Researchers have found that solid nanoparticles dispersed in oil could largely reduce the friction in machinery, and enhancing the load capacity at the same time.[31] And drug delivery is another attractive area for nanofluid usage, as shown in Fig. 2.6. Scientists have always been trying to make medical components small enough to be absorbed, and delivered to the target as accurate as possible. And the small size and unique property shows a great advantage over other methods, including using magnetic field to attract nanoparticle based drug to the target position[22, 32-34]. At the same time, some researchers are trying to use nanofluid in fuel cells as well[35]. And it can be seen that the nanoscale of nanofluid opens the door to deeper and further researches for many different areas, and is gaining

more and more attractions from scientists and industries.

2.1.2 Heat transfer enhancement

Heat transfer process is critical to many different industries, from cooling of laptops at home to supercomputers in institutes, from radiators to power plants or nuclear reactors, or from airplanes to spaceships. And the heat transfer process in them plays important roles, as in vehicles for instance, if the cooling efficiency could be enhanced by just 1%, then a total of 5.5 million barrels of oil can be saved in US alone every year. Therefore, increasing heat transfer performance has become a major research area in modern engineering field. And the heat transfer process can be written on the basis of the following equation,

$$Q = hA\Delta T \tag{1}$$

From this equation, we know that the amount of energy or heat transferred in the process Q can be increased in the three aspects,

(1) Increasing heat transfer coefficient h;

(2) Increasing surface area A;

(3) Increasing temperature difference ΔT.

Increasing surface area and temperature difference do enhance the heat transfer process, however, they have serious limits. Increasing the surface area

is a very commonly used strategy in industries, such as radiators. It is already applied in many places of heat transfer devices, including micro-channels, complex surface structures and so on. However, when increasing the surface area, it could either increase the difficulty of manufacture which may exceed the technology or expenses limit, or simply increase the resistance from the surface to the flow, and affect the flow rate.

While on the other hand, increasing the temperature difference also has constrains. Take cooling of an engine for example, the hot end of heat transfer is determined by the combustion, and the cold end of heat transfer is determined by the circling coolant after going through the radiator. Therefore, reducing the cool end temperature is the only possible way in most cases. But reducing cool end temperature would need more power, no matter increasing flow rate, or cooling power, in the case of engine in Fig. 2.7. And that would make the whole system less efficient in the end.

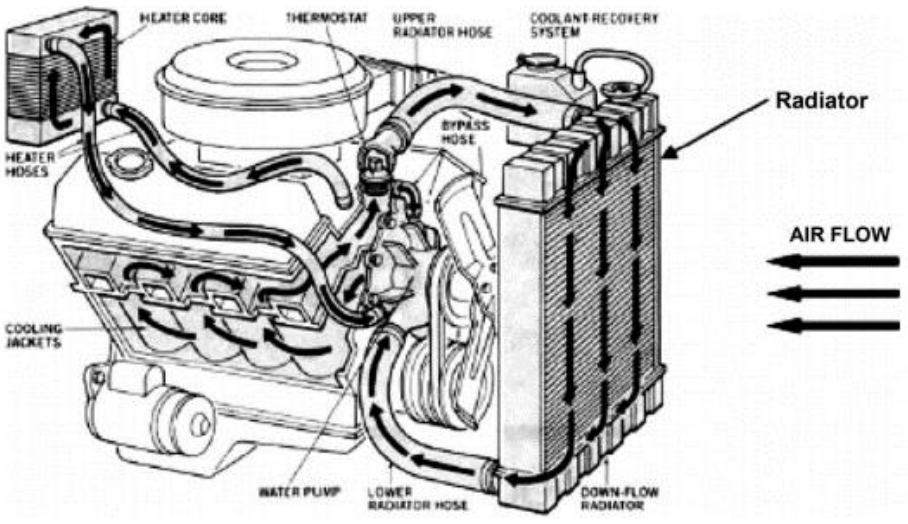

Figure 2. 7: Cooling of engine[26]

Therefore, increasing heat transfer coefficient is the main focus for researchers, and a lot of efforts have been taken, including testing different coolants and adding additives into coolants. And since the thermal performance of solid, especially metallic, is higher than normal liquid such as water in most cases, than adding solid particles in liquid could be possible to enhance the thermal performance of base liquid. And actually this is the beginning of the idea of nanofluid.[16] However, it was until 1995 that Chol tried to use nanofluids as working agents in heat transfer.[36] And this assumption by Maxwell was proved ever since.

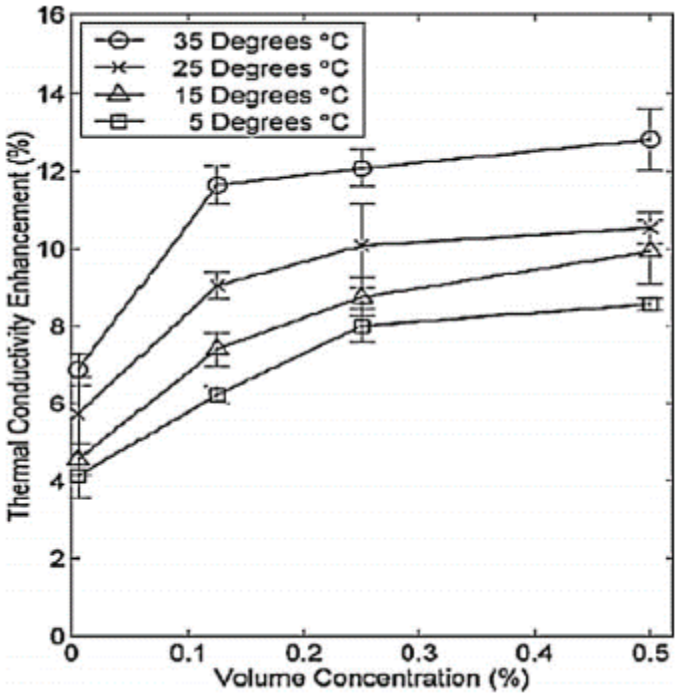

Figure 2. 8: Thermal conductivity enhancement of 2nm gold nanoparticles in water as concentration in volume fraction[37]

There have been many papers on the enhancement of nanofluid on the thermal performance of carrier fluid, as in Fig. 2.8. For example, Liu et al.

reported a 23.8% improvement at 0.1% volume fraction of copper nanoparticles in water[38]. While Choi et al. reported a much higher 150% improvement at 1% volume fraction of carbon nanotube in oil[39]. And the thermal performance enhancement of nanofluid is strongly connected to its properties. Most researches would compare the thermal performance of nanofluid at different concentrations, and there's no need to illustrate in detail. And of course, the thermal conductivity enhancement of nanofluid is influenced by the type of nanoparticles and base fluid, as carbon nanotubes perform better than SiO_2 nanoparticles in the same base fluid[40]. While the same copper nanoparticles at the same concentration performs much higher thermal conductivity enhancement in water than in ethylene glycol (EG).[41, 42] And the surface to volume ratio of nanoparticles also affect the thermal performance of nanofluid. As the more area of contact between liquid and solid interface, the higher thermal conductivity enhancement there will be, on that of nanofluid or base fluid, instead of the nanoparticle itself[43]. And there is also some reports on the influence from the pH value during preparation[44]. And temperature can affect the thermal performance as well, and nanofluid is reported to have a better performance under high temperature[45, 46]. A few selected papers reporting the enhancement observed is listed below in Table. 1.

And among different types of nanofluids, there is a special type with unique character, ferrofluid. As the nanofluid we use in the present work is

ferrofluid, because of its interesting properties, the performance and applications of ferrofluid will be introduced separately.

Table 1: Studies on thermal conductivity of nanofluid [6, 26, 47]

Particles	Size (nm)	Base fluid	Observation	Reference
CuO	33/36/18	Water	60%	Eastman et al.,[48]
Cu	10	EG	40%	Eastman et al.,[41]
Cu	100	Water	78%	Xuan et al,[49]
Fe	10	EG	18%	Hong et al.,[50]
Au/Ag	15/70	Water	21%/17%	Patel et al.,[51]
Al_2O_3	28	Water	12%	Wang et al.,[52]
SiC	26/600	Water	16%/23%	Xie et al.,[53, 54]
TiO_2	10×40/15	Water	33%/30%	Murshed et al.,[55]
SWNT	3×30	Epoxy	125%	Biercuk et al.,[56]
MWNT	25×50	Oil	150%	Choi et al.,[39]

Note: SWNT: Single Wall Nanotube; MWNT: Multiwall Nanotube

Ferrofluid is a colloidal nanofluid with ferromagnetic or ferromagnetic nanoparticles suspended in carrier fluid, normally water or oil. Ferrofluid would become strongly magnetized with the presence of external magnetic field, while on the other hand, would not retain magnetization with the absence of magnetic field in most cases, as shown in Fig. 2.9. And therefore usually

ferrofluid is considered as superparamagnetic instead of ferromagnetic. It is a major magnetic nanofluids (MNF). And there are other types of MNF as well, as long as the nanoparticles in MNF is ferromagnetic, such as cobalt and nickel. However, iron oxide is the most commonly used ferromagnetic material, so magnetic nanofluids mentioned in researches and industries are mainly ferrofluid.

Even though the magnetic forces within the nanoparticles are small enough for the Van der Waal's force to keep them separated and prevent aggregation, additive surfactants are still necessary for ferrofluid to keep stable for longer lifetime. And therefore oleic acid, tetramethylammonium hydroxide, citric acid and soy lecithin are commonly used to coat the nanoparticles[57, 58].

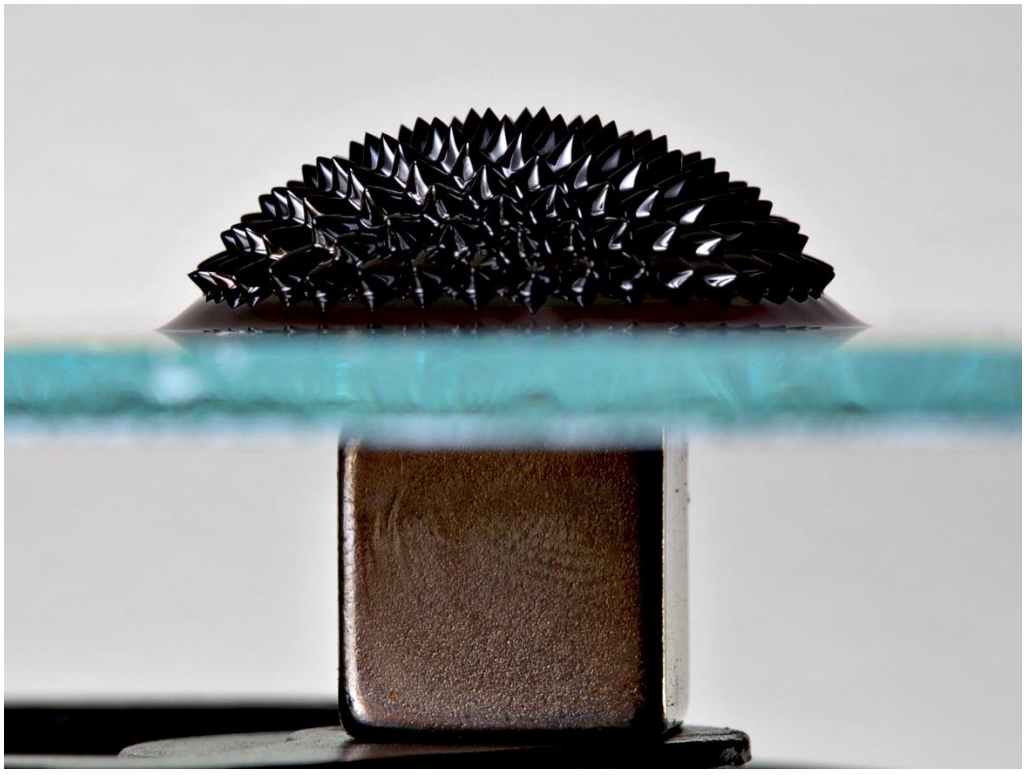

Figure 2. 9: Ferrofluid on glass, with a magnet underneath[59]

Due to its uniqueness in magnetic properties, ferrofluids have many applications other than normal nanofluids in electronic devices [60], mechanical engineering [61], materials science [62], analytical instrumentation [63], medical science [64], optics [65] and Art [66]. However, what matters most to researchers of ferrofluid is still its thermal properties and applications in heat transfer area, as ferrofluid could have obvious advantages over common nanofluid in heat transfer. First, ferrofluid guided by external magnetic field would large enhance the performance of normal nanofluid as the nanoparticles gathering to the hot end or cool end by magnetic force. Therefore, it is potentially used in places where flow is needed in certain direction. Second, the thermal magnetic convection can be more intensive than gravitation one[67]. And third, the thermal conductivity and viscosity can be changed under external magnetic field[68, 69].

Nkurikiyimfura et al. [7] introduced the recent developments on heat transfer enhancement using magnetic nanofluids, and also emphasized on the mechanisms of thermal conductivity enhancement and thermomagnetic convection at the same time. Yamaguchi et al. [70] investigated both experimentally and numerically the natural convections of a magnetic fluid in a cubic cavity under uniformed magnetic field. All the results obtained from experiments and numerical simulations revealed that the magnetic field and magnetization are influenced by temperature. With the magnetic field imposed,

the heat transfer inside the cavity is enhanced significantly compared to that without the magnetic field.

Ghofrani et al [71] presented their experimental work on investigation in forced convection heat transfer of ferrofluid flow passing through circular copper tube under alternating magnetic field. It is believed that the mechanisms behind the heat transfer enhancement of ferrofluids are particle migration, viscosity gradient, Brownian motion, the disturbance of the thermal boundary layer and the increase of the effective thermal conductivity of nanofluids. Maryamalsadat et al [72] carried out an experimental work on the convective heat transfer of ferrofluid flowing through a heated copper tube in the laminar regime in the presence of magnetic field. They concluded that the main reason for the enhancement of heat transfer coefficient is the remarkable changes on thermal-physical properties of ferrofluid in the presence of the influence of external magnetic field.

Li and Xuan[73] conducted an experimental investigation on convective heat transfer features of magnetic nanofluid flow over a wire under the influence of an external magnetic field. The sample magnetic nanofluid is water based ferrofluid using Fe_3O_4 nanoparticles, prepared by the chemical precipitation method. The average particle diameter for the Fe_3O_4 nanoparticles is about 10 nm, and the volume fraction of the ferrofluid is about 1.0%. It is found that the heat transfer between the magnetic fluid and the wire surface is weakened under a uniform magnetic field. This should be because of

the increase in the viscosity of magnetic fluid. When a magnetic field gradient is applied along with the flow direction, the heat transfer process is remarkably enhanced between the magnetic fluid and the heated wire surface, because the auxiliary Kelvin force accelerates the magnetic fluid flow. On the contrary, a magnetic field gradient in the opposite direction of the main stream will suppress the heat transfer process. Some other researches on the thermal conductivity of ferrofluid is conducted as well without magnetic field, as shown in Fig. 2.10.

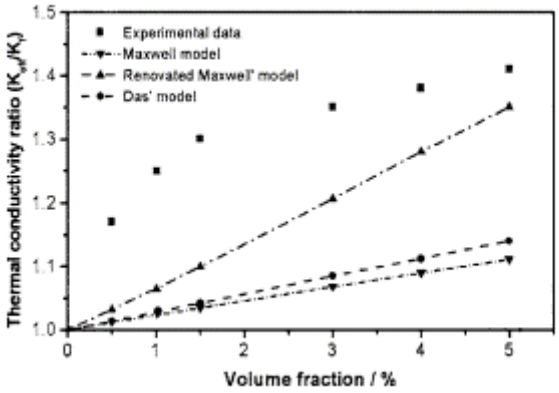

Figure 2. 10: Thermal conductivity of Fe_3O_4 nanofluid[74]

Liu et al[75] carried out a pool boiling heat transfer comparison among water-based magnetic fluids, with its carrier liquid water made, in the absence and presence of a magnetic field. The experimental results indicate that the boiling heat transfer of magnetic fluid largely enhanced in the absence of a magnetic field, and the applied magnetic field would enhance the boiling heat transfer of magnetic fluid even more than without the magnetic field. It is

believed that boiling heat transfer enhancement of a magnetic fluid in the absence of a magnetic field is due to the nanoparticles and surfactants. And the boiling heat transfer enhancement of a magnetic fluid in the presence of a magnetic field is mainly the result of the strong influence of magnetic field on the bubbles. Şeşen et al [76] experimentally investigated the two-phase heat transfer characteristics of nanofluids, using the designed system with magnetic actuation, and then compared to the results without magnetic actuation. Two -phase average heat transfer enhancement observed by Şeşen et al using the suggested system was 17%. While the average single-phase enhancement is measured as 29% with magnetic actuation. Magnetically actuated nanoparticles neither precipitate nor form any clusters in the experiments. The reasons for the thermal enhancement mechanism by the utilization of nanoparticles as heat transport agent for heat transfer from the surface of the pool to the bulk fluid along with the circulation created within the pool by magnetic field is explained in their work as well.

Kamiyama and Ishimoto [77] introduced the effects of magnetic field on the characteristics of boiling two-phase pipe flow using temperature-sensitive magnetic ferrofluid in detail both theoretically and experimentally. The effect of magnetic force in boiling two-phase flow on the increasing of the driving force of magnetic fluid flow in a non-uniform magnetic field is very obvious, and the two-phase flow characteristics are strongly influenced by the magnetic field. Shuchi et al [78] presented a new type of binary magnetic fluid, which is

considering ferrofluid as a mixture of base magnetic fluid with an organic secondary fluid, with the new overall saturation temperature lower than that of the previous base magnetic fluid. Basic thermal characteristics of the binary magnetic fluid were measured for boiling two-phase flow in a partly heated pipe. It indicates that the continuous boiling could be achieved without any deterioration in magnetic properties of the ferrofluid and the heat transfer flux of the flow was remarkably improved by applying magnetic field at higher flow rate.

Taslimifar et al [79] also conducted an experimental investigation on the start-up and steady thermal performances of open loop pulsating heat pipes (OLPHPs). Effects of working fluid, heat input, non-condensable gases, ferrofluid concentration, magnets location, and inclination angle on the thermal performance of OLPHPs are considered. It is found that start-up and steady state thermal performances of ferrofluid OLPHPs could be enhanced in the presence of external magnetic field. Furthermore, thermomagnetic convection also has a critical role on this thermal performance enhancement. The best inclination angle is around 67.5° relative to horizontal axis for the steady state thermal performance for various working fluids and heat inputs.

From the discussed above, magnetic nanofluids play an important role in different heat transfer phenomena, such as natural convection, forced convection, pool boiling, flow boiling, and that in pulsating heat pipes. But different authors may have different explanations on the heat transfer

enhancement mechanisms. And all the conclusions are drawn on the base of static magnetic nanofluids characteristics. However, the characteristics are dynamic in the real heat transfer process, especially the concentrations of magnetic nanofluids will change along with the time and position, which may have great influence on the heat transfer. The dynamic concentration of magnetic nanofluids is very difficult to measure. A new method is put forward based on the Nuclear Magnetic Resonance (NMR), as will be introduced in detail in Chapter 3.

2.2 Bionic study of plant water migration

2.2.1 History of Bionic engineering in different areas

In the past few decades, more and more researchers start to believe that nature is a good source of inspiration, and start to imitate and study from nature to design produces and scientific output.[80] With the help of modern technologies, scientists from different area all learn a lot from nature, and present more and more industrial product in human's daily lives. Besides, it is not just physical products that is learnt from nature, even algorithm can be proposed based on bionic studies, such as the Ant Colony Optimization (ACO) and Bees Algorithm (BA)[81].

Figure 2. 11: Hydrophobic surface of lotus[14]

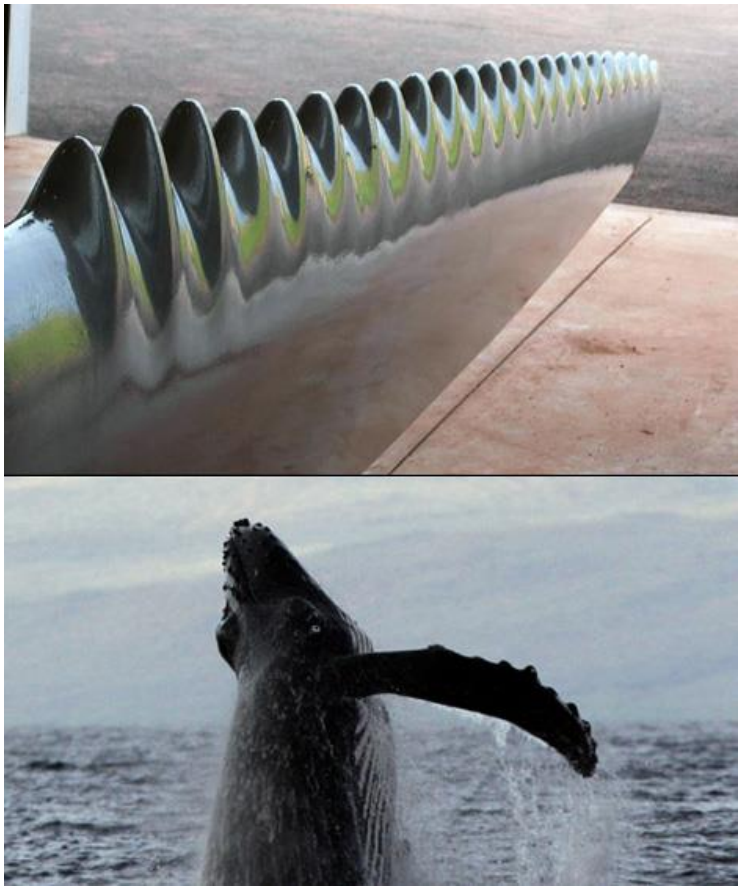

Figure 2. 12: Under water turbine blade learning from fin of whale[14]

Mankind has a long history of learning from nature, and we have no idea which invention of human beings is the first example of bionic engineering,

but as least far earlier than people start to build a flying machine inspired by birds. However, with the help of modern technologies, more and more previous guess and assumptions on nature become reality and are now able to manufacture, such sonar and radar learning from bats, or solar cells learning from the photosynthesis effect in plant leaf. And nowadays, there are many products we use in daily lives that we take for granted come from bionic engineering, apart from planes.

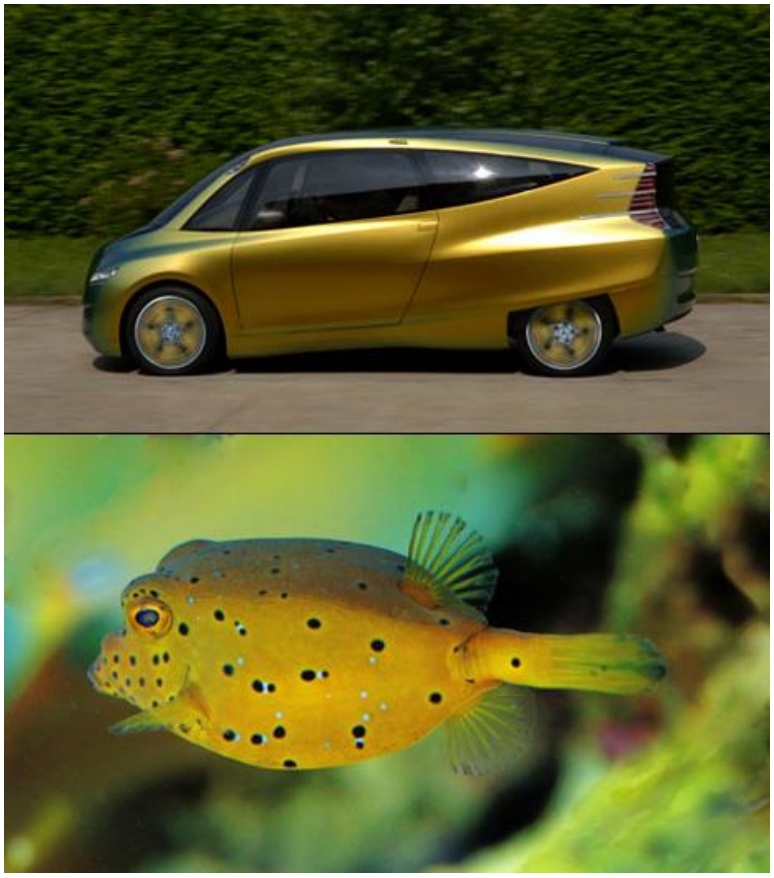

Figure 2. 13: Swim fin imitated from fish[14]

For example, the hydrophobic surface of lotus keeps the surface from wetted by raindrops in Fig. 2.11. So the droplets fall onto the surface go

directly downward without wetting or sinking into the lotus leaf. This function is studied and then give birth to the water-proof materials on clothes. And the fin of whale is very efficient in generating power to move huge weight of whale forward in Fig. 2.12. This character attracted scientists, and thus proposed the uneven boundary of blades in under water turbine, which enhance the output power. And not to mention the swim fin that is widely used today by divers and swimmers, which is imitated from fish. They all uses the advantages of nature, a well evolved fluid dynamic. Further application of it also includes the design of vehicles, even the high speed rail system, which is believed to come from swordfish, as shown in Fig. 2.13. And also the well-known phrases to the public, artificial intelligence and robotic.

2.2.2 Bionic study of plant-water relationship

Researchers from different research backgrounds would learn differently from nature, even with same object in nature. And in thermal engineering, how to enhance the heat transfer performance of heat exchanger is a major part of the present work. And besides the ideas mentioned previously in this chapter on enhancing thermal conductivity h of fluid flow, another part is to enhance the surface area of the interface between walls and fluids. And that requires the flow channel to be manufactured as small as possible, which would relatively enhance the surface volume ratio of working agent. However, when narrowing

the flow channel into extremely small size of microscale or even nanoscale, forces would become much more difficult to analyse than previously in macroscale. What's more, the designing of the micro-channel would also become a critical issue, which could strongly affect the thermal performance. Therefore, researchers start to look outside into nature for inspiration, something that also involves liquid or mainly water flow efficiently. And the answer is plants. And this bionic study of the relationship between plant and water is called Hydraulic Architecture (HA), and become especially well known for researchers in relevant fields in the past few decades, shown in Fig. 2.14.

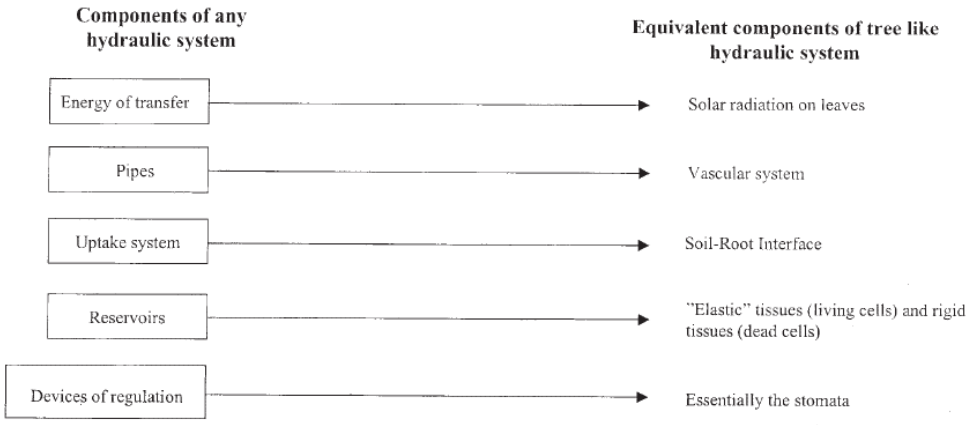

Figure 2. 14: Bionic application from hydraulic architecture of trees[82]

The idea of Hydraulic Architecture is believed to be firstly proposed by Zimmerman in 1978[83]. However, he didn't give out a clear definition of it, and it is now widely defined that, HA is the structure of the water conducting

system, which describes the relationship of the hydraulic conductance of the xylem in various parts of a tree and the amount of leaves it must supply, governing frictional resistance and flow capacity of plants[84-86].

It is estimated that over 70% of the water fall onto soil is returned to atmosphere through transpiration effect in plants. And most of the water absorbed by plants is evaporated instead of used by cells on an overall basis. Scientists have been interested in the water migration within plants for a long time, and various theories were proposed to explain the mechanism. However, researchers start to focus on this interesting phenomenon again recently because of the development of bionic engineering.[87-89]

The water as we know it in plant stems moves under the determination of water potential. Water potential, especially in botany studies, is the difference in intramolecular pressure exerted in a given specimen with reference to the intramolecular pressure exerted between molecules of pure free water at atmospheric pressure and the same temperature[90]. And the unit is J/m^3, as is energy per unit volume. The water potential of water is therefore raised by the external positive pressure, and is lowered by the external negative pressure. Water potential can be influenced by solute as well. Adding additives into water can reduce the water potential, and therefore the higher the concentration is, the lower the water potential would be. Therefore, for water transport within plants, the water potential gradient is easily illustrated in Fig 2.15,

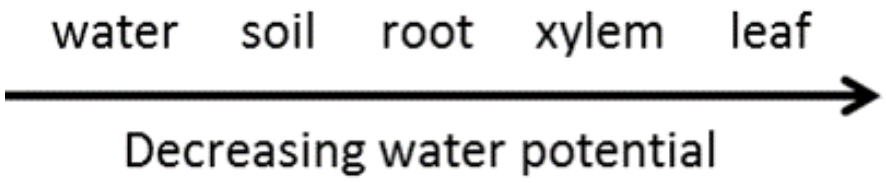

Figure 2. 15: Water potential gradient

And water potential becomes a critical part of botany studies, as when studying about the water transport between soil and root, then the water potential is mainly generated by the difference of ion concentrations between root cells and soil, while the water potential difference in stem comes from pressure, as the concentration would remain the same. Previously, there are mainly two different equations to describe the flow pattern of water transport in plant stems, the Darcy's Law and the Hagen-Poiseuille Equation, in a modern botany research form.

$$Q = L\frac{\Delta \emptyset_p}{x} \tag{2}$$

$$Q = \frac{r^2}{8\gamma}\frac{\Delta \emptyset_p}{x} \tag{3}$$

The ΔΦp indicates the pressure potential difference, and x is the length. Comparing the two equations, it can be concluded that in a capillary, the hydraulic conductivity L can be written in the form of viscosity γ and tube radius r as below in capillaries.

$$L = \frac{r^2}{8\gamma} \tag{4}$$

However, there are never enough to study the complex structure and function in stem, and more researches need to be carried out.

As we know today, water transports in plants through the vascular system, xylem and phloem, from root to leaf. Xylem and phloem are formed by a brunch of dead-cell rings, in vast number of shapes, through evolution. Xylem is believed to be the conduit that moves water upward from root to leaf, while phloem is the one that moves nutrients.

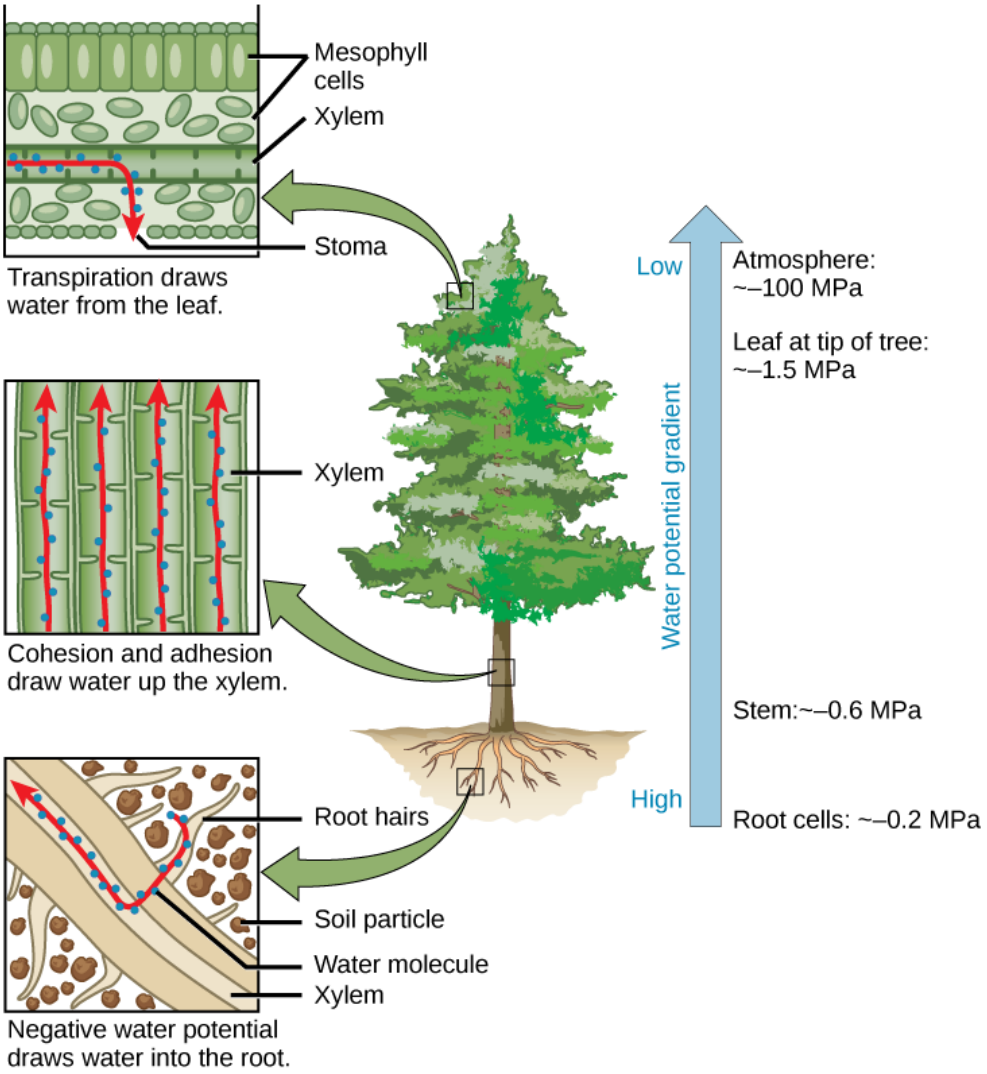

Figure 2. 16: Water transport in plants[91]

Generally, xylem pathways are diffused in roots, while aggregated in stem as perfect conduit vessels, and then back ramify again in leaves among leaf cells, as shown in Fig. 2.16. Therefore, it is possible to consider the xylem conduits as a capillary tube when studying xylem water transport only. With the growth of plant, the stem gets wider, and forms annual rings. These annual rings are the previously formed vascular conduits, and the outermost are new-borns. And the water transported in stem moves from the outermost xylems in stem. This is because water is expected to flow in the least resistance path, and flow from outermost part in new-born xylems.

And with the clear knowledge of the xylem structure where water migration happens, it is still not clear what is driving it. And the whole history of studies on water transportation theory in plants, is a story of vitalistic theories (water pumped up by living cells) overtaken by physical mechanism theories gradually, especially under the proposed Cohesion and Tension theory[92], with more and more researches proving it in the last century. And it is not widely believed that the water migration process is almost wholly physical, except for a few occasions such as freezing or cavitation, which is still unknown yet. However, there is already no evidence showing that living cells participate directly in the water migration process at all. The development of plant water migration theories with important papers is listed below in Table. 2.

Table 2: Brief history of plant water migration theories[90]

Year	Name	Work
1669	Ray	Sap circulates in plants like blood in animals
1717	Hales	Quantitative approach to sap transport in plants (and animals)
1840	Boucherie	Sap ascent continues despite poisons
1887	Sachs	Vessels empty; therefore water moves physically through imbibed walls
1894	Dixon and Joly	Cohesion theory propounded for ascent of sap
1935	Priestly	Doubted cohesion mechanism: xylem air-filled
1939	Handley	Cooling of stems above freezing point causes wilting
1964	Zimmermann	Handley's experiments disproved by improved techniques

And Cohesion and Tension theory is now widely accepted as the explanation of water migration process among most scientists. However, the inner mechanism and forces is still unclear[93].

2.3 Summary

In this chapter, a detailed literature review is carried out on nanofluid heat transfer and bionic engineering. The basic principles of heat transfer are analysed to clear the methods in heat transfer enhancement. And thus nanofluid

is adapted. The characters and applications of nanofluid are specified. And then, a special type of nanofluid, ferrofluid, is introduced, as this is what is used in the present work. And the unique magnetic and thermal properties are discussed as well.

Later in this chapter, the history of bionic engineering is presented. Bionic engineering can be applied in various research backgrounds, such as mechanical engineering, computation, mathematics and medication. Researchers from many areas are trying to innovate by learning from nature nowadays. And in heat transfer enhancement, methods to improve liquid flow can be inspired by the study of plant water migration system in plant stems, or xylem conduits as we know it today, which is the flow path of water in woody plants. And the basic ideas of water migration in plants is introduced. Further details on the forces and structures in plant xylem is specified in Chapter 6.

Chapter 3: NMR and Methodology

In the previous chapter, the history of heat transfer and bionic engineering is briefly reviewed. There are still more details which need to pay special attention when doing experiment and analysis. And they will be discussed in this chapter. To study the nanofluid concentration issue, and the bionic water migration problem, NMR technologies are introduced. NMR can be applied into many areas, while in the present work, both nanofluid concentration measurement and bionic engineering research are connected with NMR. Background of the present work is introduced, and the experimental theory is proposed as well, together with the test rig introduction.

3.1 The basic NMR theory

Nuclear magnetic resonance was first described by Isidor Rabi in 1938[94], and won the 1944 Nobel Price. Later in 1945, first NMR signals were observed by Bloch and Purcell independently[95], and were jointly awarded 1952 Nobel Price. And the development of NMR was very rapid ever since, as the first commercial NMR spectrometer was produced in 1953, etc.[96] And therefore more and more potential applications of NMR are proposed, and is now widely used in medication, biology, chemistry, non-destructive testing, petroleum industry and so on.[97-101] And for the public, the NMR is mostly encountered in hospital, as a clinical tool. The NMR has been developed to

measure various organs systems, including brain, spine, musculoskeletal, liver, heart and so on.[95, 102-104]

Most people who don’t know much about NMR may think at first thought that the NMR is very much similar to Computed Tomography (CT), especially when comparing the output images. However, there're a lot of differences, with NMR highly advanced than CT, except for the expenses in commercial usage.[105] CT is a two dimensional slice of the sample, using X-ray photons absorption to image the sample, NMR is a three dimensional measurement, and works well on soft tissues. What’s more, the data in NMR is temporally stored in four dimensional form, and could be than adapted in Fourier integral to transfer between time domain and space domain. Besides, the strength of signals and fields are fixed in CT, while in NMR they can be defined by the user to control the interaction with the sample. Therefore, NMR has many advantages over CT in measurements, with Fig. 3.1 giving a rough comparison.

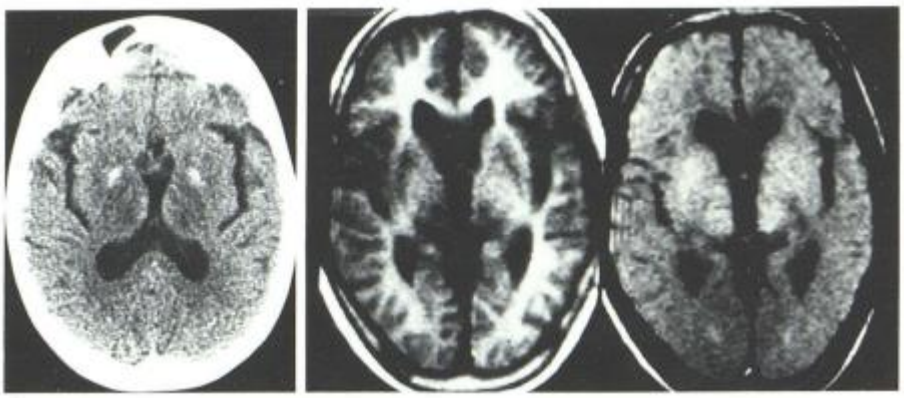

Figure 3. 1: Comparison of CT (left) and NMR (right)

NMR performances experiment on the nuclei of atoms and molecules, not the electrons. And it is based on the interaction between an applied magnetic field and a particle that possesses spin[106]. The NMR technology is based on an external magnetic field B_0, and the dipoles of atoms are aligned with the magnetic field. And the next step is the application of a pulse, also known as radio frequency (RF) energy. The energy of the RF signals will be absorbed by the atoms, and later slowly reemitted to the environment. And the NMR technology is to place a receiver outside to observe the signals reemitted from the sample. Therefore, take hydrogen for example, the more hydrogen atoms there are in the test region, the more energy will be absorbed and reemitted. Therefore, together with other aspects that may affect the observation, the output could clearly illustrate the performance of the sample in the desired way. And there is a particular frequency that will be absorbed by the atoms, which is proportional to the magnetic field B_0. And this follows the Larmor equation,

$$\Delta E = hw_0 = \frac{h\gamma B_0}{2\pi} \tag{5}$$

where h is Planck's constant, γ is a constant for nucleus, also known as gyromagnetic ratio, w_0 is the frequency of RF which is absorbed, and ΔE is the energy of the absorbed RF.

Longitudinal (or spin-lattice) relaxation time T_1 and transverse (or spin-spin) relaxation time T_2 are the two basic parameters in NMR, which is the time needed for a value to return to 63% of its original value or decay to 37% of its original value. T_1 is the decay constant for the recovery of the z

component of the nuclear spin magnetization towards its thermal equilibrium value, and T_2 is the decay constant for the component of perpendicular magnetization field.[107] As with the hydrogen atoms in water, they would be firstly magnetized by the RF, and later release signals after its magnetization process, which would decay away when it goes back to equilibrium distribution, as is shown in Fig. 3.2. So T_1 and T_2 become the most important relaxation times in the progress with different tissues or fluid situations. In general,

$$M_z(t) = M_{z,eq} - \left[M_{z,eq} - M_z(0)\right]e^{-t/T_1} \tag{6}$$

$$M_{xy} = M_{xy}(0)e^{-t/T_2} \tag{7}$$

where M is affected by external magnetic field.

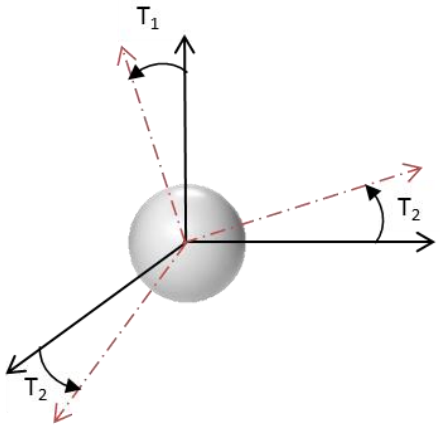

Figure 3. 2: Relaxation time of resonance signals from nuclei

So when the nuclei are going back to equilibrium, the signals it releases will be detected by NMR machine, recorded as the signal intensity *S*.

3.2 Nanofluid as NMR contrast agent

In NMR medical scanning there is always something called contrast agent, which can reduce the relaxation time, so that the scanning can be done as fast as possible when doing research, especially on patients. The contrast agents are widely used in scanning, including CT as well. However, the contrast agents in CT is directly visualized under X-ray, and create shadows, while the contrast agents in NMR is only affecting the signals of other atoms, hydrogen for example. And that means only a small fractions of the contrast agents, in low concentration, could greatly affect the performance of samples in NMR, and thus enhance the NMR measurements.

Contrast agents for T_1 and T_2 are separately categorized, according to their primary effect in shortening the relaxation times, on T_1 or T_2. However, contrast agents for T_1 for example, could shorten T_2 as well to some degree, which is also influenced by concentration. When concentrated, T_1 agents will shorten T_2, and when diluted, T_2 agents will reduce T_1 relaxation times as well[106]. And since the relaxation time T_1 is for signals going up to 63% of previous value, the T_1 contrast agent could help the signals to increase faster than normal; while the relaxation time T_2 is for signals going down to 37% of initial value, the T_2 contrast agent could help the signals to decrease faster than normal. In this case, the T_1 contrast agents are also defined as positive contrast agent, and the T_2 contrast agents are defined as negative contrast agent. As is shown in Fig. 3.3, the TR indicating T_1 goes higher than normal, while TE

indicating T_2 goes down lower than normal.

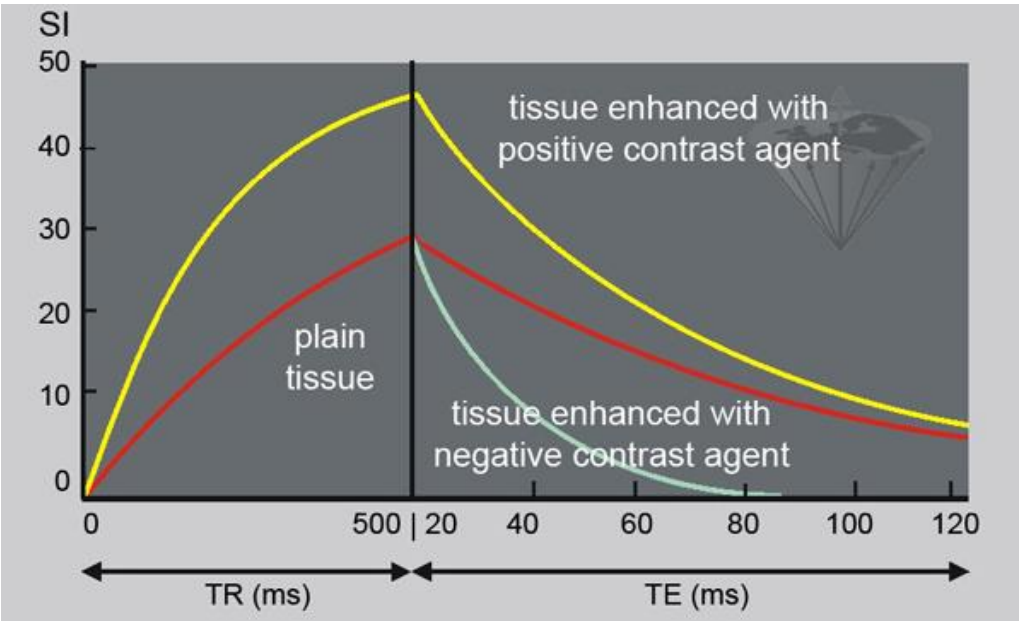

Figure 3. 3: Positive and Negative contrast agents affecting relaxation times[108]

As NMR technology recently is mainly used in clinical treatments, so most researches are carried out in this purpose. The application of NMR is mainly known to public is magnetic resonance imaging for medical diagnosis and magnetic resonance microscopy. And most clinical used contrast agents are T_1 relaxation agents. Most researchers would use solutions with metal ions to achieve that goal. In which Mn^{2+}, Cu^{2+} and Fe^{2+}, Fe^{3+} are the most widely used metal ions[109], especially gadolinium-based agents. While the other type, T_2 contrast agents, are typically macromolecules containing several iron atoms. The magnetic properties of these atoms could distort local magnetic field, and cause a significant signal loss in T_2 signals. Therefore, T_2 contrast agents are

mainly iron oxide based particulate molecules. It has already been proved by some researchers that in nanofluid, such as Fe_3O_4 can still give a very good performance as a T_2 contrast agent, which means that it could strongly affect the T_2.[110, 111] And most commonly known T_2 contrast agents recently are nanofluids, including two types, superparamagnetic iron oxides (SPIO) and ultrasmall superparamagnetic iron oxides (USPIO)[112]. There are the nanofluids or ferrofluids previously mentioned, and are widely used in industries. Therefore, using nanofluid or ferrofluid as contrast agents is proved to be workable, and is the prerequisite of the nanofluid dynamic concentration measurement work.

3.3 NMR scanning in botany researches

Most recent techniques studying plant functions are destructive, and could cause inaccuracy when cutting and making into samples. While NMR provides a very unique method in measurement in situ without all the labours required in making samples, and could see real situations in live plants. And this become a great advantage of NMR over other techniques, and make NMR a key method in plant analysis, [113-120] including metabolomics, structural analysis, etc. And there has been some researches on water distribution in plants as well with NMR [121-125]. Structural researches are carried out using NMR in botany,[126] such as the imaging of water distribution in

vegetables[127, 128], water distribution in seeds or roots[121, 129], and water flow in plant stem as well[130, 131], as shown in Fig. 3.4. While on the other hand, metabolomics researches with NMR focuses on various functions inside plants, including growth condition, stresses, infection, storage, water balance and so on.

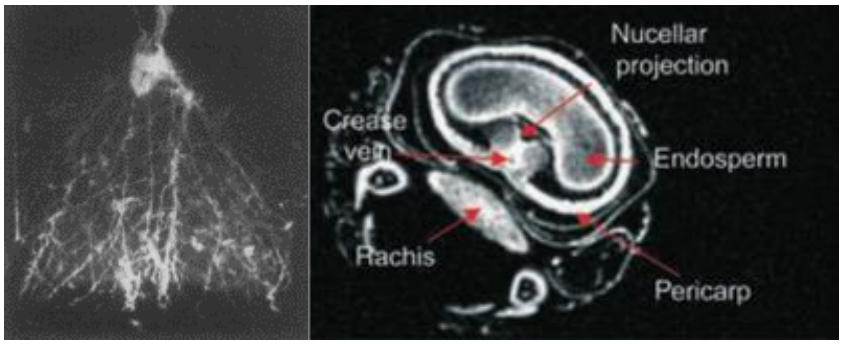

Figure 3. 4: NMR image of plant root (left) and seed (right) [121, 132]

Details of a few selected publications on the application of NMR on plant science is listed below in Table 3.

Table 3: Applications of NMR on plant science[126]

Subjects	Plant	Reference
Watercore formation	Apple fruit	Wang et al.,1988,[133]
Change of water status	Mangrove	Koizumi et al,1992,[134]
Distribution of water and oil	Coconut	Jagannathan et al,1995,[135]
Vitrification	Gypsophila	Gribble et al,1998,[136]

Subjects	Plant	Reference
Stimulation	Mimoza plant	Tamiya et al,1988,[137]
Freezing	Wheat crown	Millard et al, 1996,[138]
High temperature	Tomato fruit	Iwahashi et al,1999,[139]
Root nodule, oxygen evolution	Peanut & Soybean root	Chudek et al,1997,[140]
Chilling injury	Zucchini Squash	Wang and Wang,1992,[141]
Sugars and oils	Grape berry	Pope et al,1993,
Distant transport in root	Broad bean	Bottomley et al,1986,
Water flow in stem	Castor bean seedling	Xia et al,1992,
Water flow in xylem and phloem	Castor bean seedling	Koeckenberger et al, 1997,[142]
Anatomy	Geranium stem	Brown et al,1988,[143]
Structure, air space	Mushroom	Donker et al,1997,[144]

And all these researches, as well as the present work, is focused on the water distribution and flow situation in plants. As water molecules contain two hydrogen atoms and one oxygen atom, one type of NMR measurement, the H-NMR is applied, which is designed to use RF signals to affect hydrogen atom, and then receive the signals reemitted from hydrogen. This type of NMR technique can track the presence of water, and thus become very popular in botany researches.

NMR can measure the flow velocity as well, besides water distribution. It is proved that linear flow can be measured when flowing in a magnetic field of

NMR technique[145]. As when flowing, the nuclei inside experiences a shift in magnetic field strength, and therefore causes change in Larmor equation as in Eq. 5[146, 147]. And that could be told from the signals received by the machine. This method has been used in botany studies for several decades[131]. And in this thesis, we are using NMR to measure the flow rate of water migration in xylem conduits.

3.4 Methodology

3.4.1 Nanofluid dynamic concentration measurement

In order to further understand the heat transfer enhancement mechanism of magnetic nanofluids, the dynamic concentration of magnetic nanofluids is experimentally investigated using NMR method in present study.

As explained previously in Chapter 2, the concentration of nanofluid is one of the most important factors that determine the characteristics of nanofluid. For the high surface to volume ratio, nanoparticles suffer from a non-ignorable Van der Waals force and surface tension, leads to a tendency of gathering together in nanofluid.[148] This makes it even worse in flowing nanofluid for the boundaries could generate a strong gathering tendency within the nanoparticles. And nanoparticle is so small in size that it will be affected by Brownian movement itself and the fluid clusters around it.[149]

The uneven dynamic concentration will affect the behaviours of nanofluids especially heat transfer. The concentration of nanofluid is always assumed as equal in these researches for the lack of measurement methods, which is measured in static state using particle sizes observed from machines such as Transmission Electron Microscopy (TEM) before the experiment as in Fig. 3.5, or calculated from the size distribution of nanoparticles.[44, 150-152] However, the heat transfer behavior is closely related to the specific heat and conductivity of nanofluid, which is decided by the nanoparticle concentration of nanofluid. The conductivity always has optimized concentration where conductivities reach maximum, while the specific heat considered always going down as concentration increases.[153]

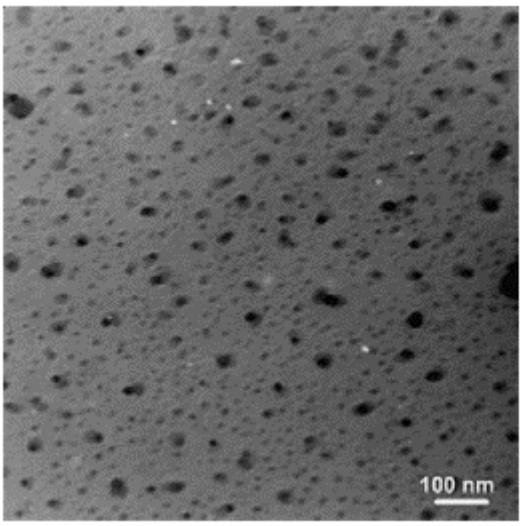

Figure 3. 5: TEM micrograph of $Al_{70}Cu_{30}$ nanoparticles in ethylene glycol

Even though the heat transfer performance of nanofluid can be treated as a whole, it may still be possible that circumstances may be different and affect

the gradient and cause different performance under the same concentration, which makes the real concentration in dynamic very different from the one observed and calculated in static. And also the heat transfer efficiency of nanofluid is decided by the conductivity of nanofluid near the boundary surface. So, the concentration of nanofluids cannot be assumed as equal under flowing condition.

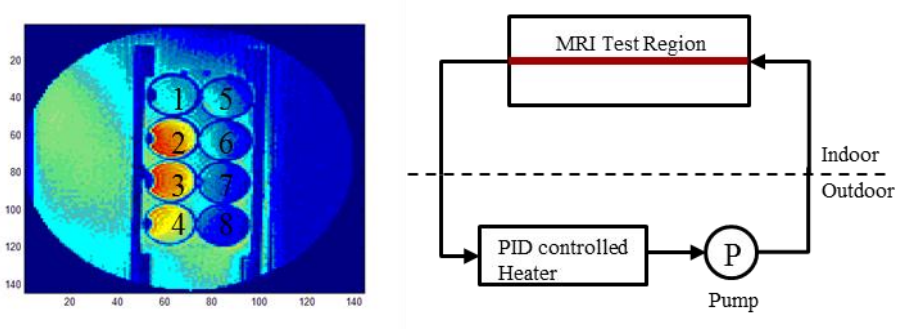

Fig. 3.6a: Static Experiment Fig. 3.6b: Dynamic Experiment

Figure 3. 6: Static and Dynamic Experiment

Therefore, the dynamic concentration of cross section along the flow channel is necessary for analysing the performance of nanofluid. A new method for dynamic concentration measurement, Nuclear Magnetic Resonance (NMR), is introduced to measure the dynamic concentration distribution of cross section of flow channel. A new overall parameter from NMR, which is easily detected and has a unique relation with concentration, temperature and velocity etc., is firstly introduced in the measurement of dynamic nanoparticle concentration with NMR in this work. Then a method to calculate the dynamic

concentration distribution of cross section with this parameter is developed. The experiments are carried out with ferrofluid (a magnetic nanofluid using Fe_3O_4) in the pipe under different concentration and temperature. The dynamic concentration of nanoparticles is calculated with the method developed in the present work. The thermal conductivity of ferrofluid flowing in the pipe is also studied with the dynamic concentration obtained with the method in this thesis. And the test rig in the dynamic concentration measurement study is presented as Fig. 3.6. Fig. 3.7 illustrates the NMR machine in the present work, and also the thermal insulated pipe that goes through the test region of the machine.

Since Fe_3O_4 can affect T_2, the T_2 is very suitable for dynamic concentration measurement, as will be explained later in Chapter 4. So ferrofluid is chosen as the working substance in the experiments.

The ferrofluid used in the experiments is composed of pure water as carried fluid, Fe_3O_4 as nanoparticles and oleic acid as its surfactant, with the final size within the range of 9-10nm and hydraulic diameter of 12nm. The experiments were carried out with Philip 3T Achieva NMR machine, with 3 Tesla magnetic field and 128MHz Radio Frequency.

Figure 3. 7: Pipe in NMR machine

The experiments were carried out in three parts. First, the T_2^* was measured in static measurement at different temperature and nanofluid volume

concentration. The ferrofluid was in the tube with a diameter of 18mm, and scanning was carried out on certain section of tube. Eight test tubes were tied between two boards and put into the scanning, with water bath around to heat them up from 20°C to 69°C with a proportional-integral-derivative (PID) controller, as can be seen in Fig. 3.6a. The Fe_3O_4 nanoparticles are dispersed in Sodium Dodecyl Sulphate (SDS) to be diluted into the desired concentration. The fluids measured in static experiments include pure water, SDS water solution with volume percentage of 0.01%, 0.03%, 0.05%, 0.07%, 0.09%, 0.1%, 0.11%, 0.2%, 0.3%, 0.4% and 0.5%. The experiments were carried out with these 7 concentrations at 10 different temperatures from20°C to 69°C.

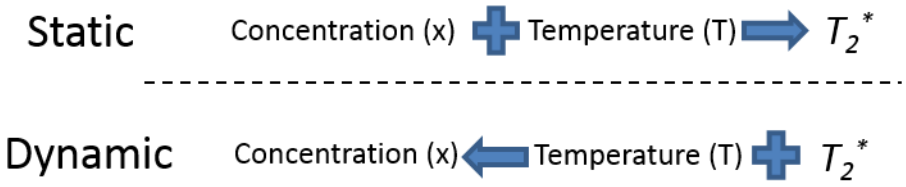

Figure 3. 8: Experiment chart

Second, the results from static experiments were analysed to obtain the nanofluid concentration. The resolution of NMR in our experiment is around 1mm, which means there are several T_2^* Signals at the section of tube. By taking average value of each T_2^*, the overall T_2^* of every concentration were calculated at different temperatures. All the data including T_2^*, temperature and concentration from these 70 tests were put into empirical equation to obtain the relationship between these parameters. The equation will be later used to

analyse the concentration gradient in dynamic flow scanning. The logic chart is as in Fig. 3.8.

As mentioned before, the nanofluid we chose to use is a special type, ferrofluid, which is also a T_2 contrast agent in medical use. And what's more, by taking logarithm of the T_2 signals intensity S in Eq. 7, the equations are as below,

$$\log(S) = -t / T_2 + \log(M) \tag{8}$$

The slope is,

$$k = -1 / T_2 \tag{9}$$

The *log(S)* has a linear relation with time t in Eq. 8, for T_2 is a decay constant related to the fluid characteristics. So the T_2 performs much better than T_1 based on this point, which is much easier to calculate. So we are using T_2 as the parameter in dynamic concentration measurement experiment.

In real case, the distribution of resonance frequency can lead to a loss of signal intensity, which causes the signals decaying faster than theory, then a smaller T_2 is measured, which is T_2^*,

$$\frac{1}{T_2^*} = \frac{1}{T_2} + \frac{1}{T_{in\,\mathrm{hom}}} = \frac{1}{T_2} + \gamma \Delta B_0 \tag{10}$$

Then T_2^* is used to instead T_2 in the following discussion. So the concentration ϕ measured by NMR are related to T_2^*, T and v,

$$f(\phi, T_2^*, T, v) = 0 \tag{11}$$

where ϕ is volume concentration, meaning ϕ=0.1 refers when 0.1% volume for example.

It is hard to analyse the effects induced by velocity on dynamic concentration directly from the data provided by NMR. At the same time, T_2^* is seriously affected by velocity, the effects of velocity can be compensated manually when analysing T_2^* from the signal, and Eq.11 can then be written as,

$$\phi = g\left(T_2^*, T\right) \tag{12}$$

And this empirical equation is the key part of the experiment, and is also the critical link between static and dynamic experiment.

Then the dynamic concentration measurements were carried out with 5L ferrofluid with a volume concentration of 0.05% in tank. The ferrofluid was pumped into the NMR machine from the tank, and then flowed back to the tank, the temperature is controlled with PID controller, as can be seen in Fig. 3.6b. The size of the pipe used is 22mm diameter with thermal insulation. The pump used here must be a DC pump, as AC pump with alternating current could generate magnetic field, which could result in an unnecessary force on the ferrofluid flow. The red line indicates the part of the pipe going through the NMR machine and being scanned, as can also be seen in Fig. 3.7. When temperature reached at some certain points, the scans were carried out with flowing ferrofluid and the state immediately after the pump shut off, respectively. The profile of the flow was scanned to achieve a group of T_2^* (each pixel has a T_2^*) data in flow and stable condition. And the concentration at each pixel of the dynamic concentration scanning will be calculated separately using the empirical equation obtained previously.

And at last, the concentration distribution can be plotted and analysed, together with a calculation of the thermal performance in nanofluid flow. The forces affecting the nanoparticles distribution can be discussed based on the experiment results.

3.4.2 Bionic engineering in water migration system

Plant can take water from soil up to several metres high. Learning from the water migration process in plants has been attracting interests from scientist for over a hundred years. The water migration in plant stem, especially xylem, involves various driving forces including capillary effect, osmosis effect, Marangoni effect and transpiration effect, etc. However, the mechanism by which water rises against gravity occurs are still controversially discussed despite many water migration mechanisms that have been proposed by different researchers. And also, there still lacks of a critical transportation model because of the diversity and complex xylem structure of plants.

The present work mainly focuses on the water transport process within xylem. As xylem system is simplified as micro channel, a mathematic model is presented based on micro channel theory, with critical analysis and simplification. With a simplified micro channel from xylem structure and the calculation using the model of water migration in xylem, the relationship between various forces and water migration velocity is identified.

The main work in the bionic water migration study of the present work is to propose an overall mathematical model that could roughly include all major forces involved in the water transport process in woody plants, and helping following researches to predict the flow pattern in plants and other similar structures in engineering and industries, such as the heat pipe.

First, all possible forces are considered and analysed to see if they contribute to the water migration in plants. And second, these major forces are quantized into equations with simple parameters that are easy to calculate or test, and then put together into an overall equation. Third, use one plant as an example, to check the parameters needed in calculation, and obtain the mean velocity of water migration in the particular plant. And at last, test the plant with NMR to check the flow velocity in situ and compare with the mathematical model calculation result. And that will finally prove whether the mathematical model is right or wrong, as in Fig. 3.9.

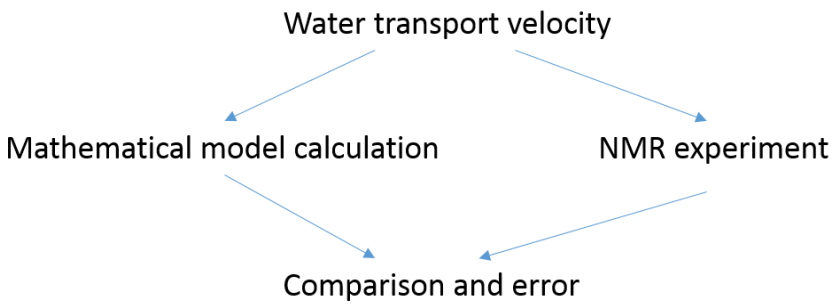

Figure 3. 9: Flow chart

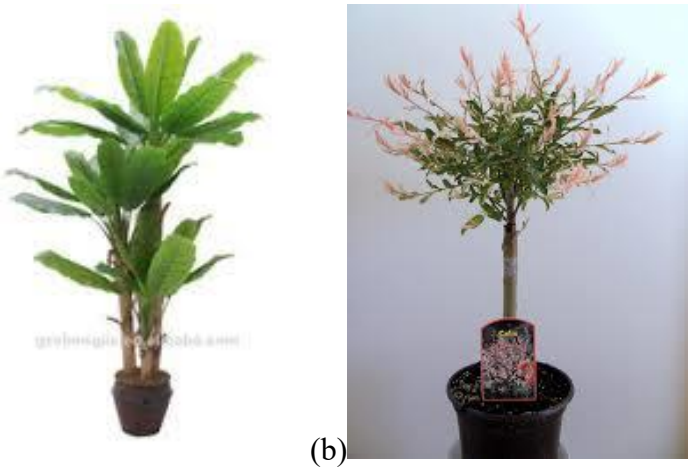

(a) (b)

Figure 3. 10: a) Musa × Paradisiaca; b) Salix Flamingo.

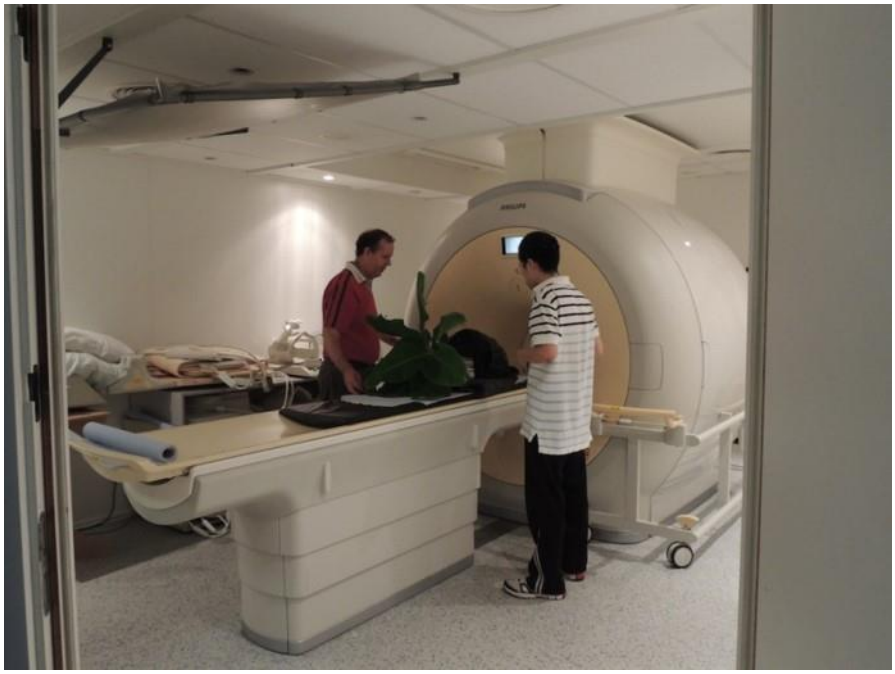

Figure 3. 11: NMR and plant

The NMR machine we use here is still Philip 3T Achieva NMR machine, with 3 Tesla magnetic field and 128MHz Radio Frequency. The scanning has a resolution of 0.22×0.22mm, and 3mm gap within layers. Since our bionic

study is based on plants, we use two different types of plant to monitor the water transport. One is called Musa × Paradisiaca, a small size plantain as shown in Fi. 3.10a. And the other is called Salix Integra Flamingo, a woody plant also known as Dappled Willow, as shown in Fig. 3.10b. And between which Salix Integra Flamingo is chosen to be the plant used for later calculation, because of its woody plant property, with obvious xylem structure in stem.

As is presented above, we can make scans in 2D images, but achieve dozens of layers with the gap set as 3mm in our experiment. With the millions of data received, we can analyse the flow velocity and water distribution.[121] Even though the flow rate can be very low and affect the accuracy of our result, and the noise would also increase with the high resolution, by taking several scans each time and get average can largely increase the accuracy as well. Ferrofluid can also be added inside as tracer as well under NMR by dripping into the plant like intravenous injection. This would be useful after we can get a database of ferrofluid under different concentration and temperature.

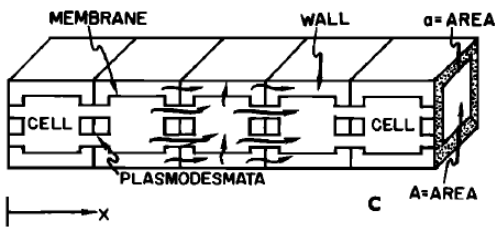

Figure 3. 12: Structure of Plasmodesmata in plant cells[154]

In this study, we use plants as a bionic model of porous structure, which definitely has a lot in common. We previously believe that plant cells are lines of regular bricks, with membrane and fibre cell walls surrounding the cells outside.[155] And that means, water need to saturate and then sink out of cell and back in to the next cell again during the water transport. However, that is not the case. As shown in Fig. 3.12, with the discovery of plasmodesmata, we can see that cells are connected together by a lot of micro channels between the neighbour cells, and the plasmodesmata can be as big as 50-60nm in diameter, and there could be 1-10 plasmodesmata per square micrometre. By transporting water through plasmodesmata, water in xylem doesn't have to go through membrane and cell walls. This could also explain why previous researches use Darcy's Law to simplify the water transport in plants, which should be the classic law in fluid flow through porous media.[156]

By studying water transport in plant, pressure and velocity gradient, distribution and movement of nanoparticles, we may be able to find better solutions to enhance fluid flow and heat transfer in porous structure,[157] and achieve data to support numerical simulation methods as well.

3.5 Summary

In this chapter, the Nuclear Magnetic Resonance (NMR) technology has been introduced. First, the basic theory and principles of NMR is presented, including the T_1 and T_2 relaxation time. And since some researchers have found the ferrofluid can be used as contrast agents in NMR imaging, thus it can be assumed that NMR may be a reasonable method of measuring nanofluid flow. And biology analysis using NMR is also introduced, as there has been a great number of botanic researchers using it to study the performance of plants.

And finally, the experimental theories and the research logics of the presented work are illustrated. The whole procedures of the experiments together with the test rigs are introduces. As TEM can only see the nanofluid concentration at static, but can't represent the dynamic concentration distribution as well while flowing, there is a critical demand in confirming the dynamic concentration. And the present work is trying to observe the NMR parameter T_2^* of ferrofluid, which should be affected by temperature and concentration. And then an empirical equation will be calculated on the relationship between temperature, concentration and T_2^*. And then, when temperature and the T_2^* is measured when the ferrofluid is flowing, the concentration gradient of ferrofluid flow can thus be calculated using the empirical equation.

And in plant water migration study, the structure of xylem is studied. And

all potential forces that may contribute to the water lifting up process are analysed and discussed. After quantizing all these major forces, an overall mathematical equation should be able to be proposed, covering all parameters that may affect the water migration, which should be easy to measure as well. And then this mathematical result can be compared to the experimental result from NMR, to prove its accuracy. And both parts of the present work will be explained in detail in the following chapters.

Chapter 4: Nanofluid static concentration

4.1 Introduction

In this chapter, a novel method of measuring concentration of nanofluid or ferrofluid has been developed to investigate statically. Different concentrations of ferrofluid perform differently under NMR, and are connected to the temperature as well. Therefore, the performance of ferrofluid, as is T_2 in this experiment, forms an equation with temperature and concentration. And when knowing the temperature, the concentration of nanofluid can thus be calculated from the equation, using NMR technique.

4.2 Problem description

As reviewed in Chapter 2 and Chapter 3, the concentration of nanofluid is measured mainly by TEM and calculated from size distribution, which although accurate, but must be carried out statically. However, no one could be sure of the concentration distribution of flowing nanofluid, especially when most application of nanofluid in engineering involves flow. Therefore, there could be a great gap between the theoretical assumption of fixed concentration and dynamic nanofluid concentration in reality. And the present work proposed a novel method to solve the problem. Using this method, we can clearly observe the dynamic concentration distribution of nanofluid flow, and start to analyse the forces behind the phenomenon in future work.

4.3 NMR measurement and results

We firstly carried out a test scan on different concentration of ferrofluid as discussed before. As mentioned, ferrofluid is mainly used in our lab, and thus is diluted into different concentrations, namely 1%, 0.1%, 0.01%, 0.001% and 0.0001% in volume percentage. As we put these five test tubes into the NMR machine, together with a bottle of copper sulphate water solution, scanning image can be seen as in Fig. 4.1. Even though it may not be very clearly shown in this figure, we can still see there's a little difference within the signals in different test tubes, which is caused by the concentration difference. But there is one test tube cannot be seen under NMRI, which refers to the 1% volume percentage ferrofluid.

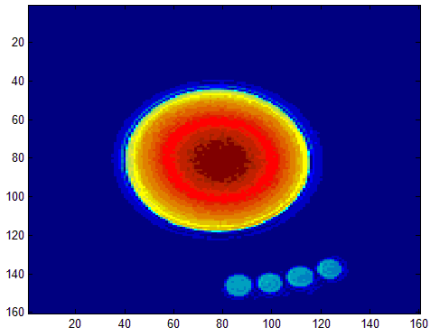

Figure 4. 1: Signals of ferrofluid under NMR

This is because the ferrofluid has a property of blocking signals from hydrogen atoms, and thus the signals would be totally lost at higher concentrations. Therefore, in the present research of ferrofluid under NMR, the

concentration can't exceed 1% volume concentration. And this is also a part of reason that ferrofluid is chosen here, as although every kind of nanofluid has the same property, ferrofluid is one of the strongest. And other nanofluids' upper concentration limit in NMR would be much higher than as in the present work.

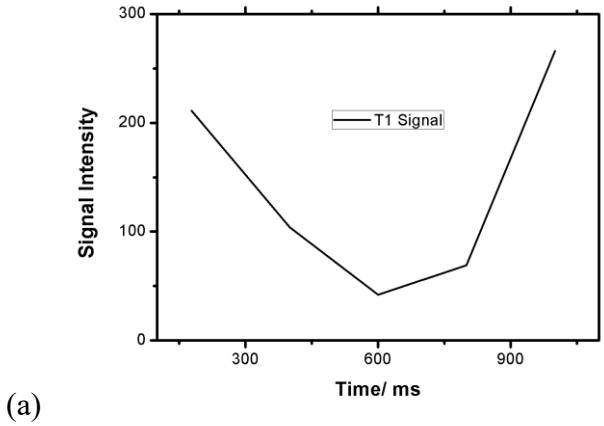

(a)

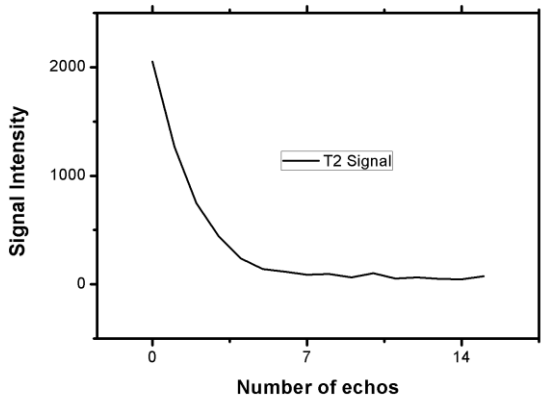

(b)

Figure 4. 2: The decaying trend in NMR (0.01% volume) in T_1 signals (a) and T_2 signals (b)

Also, we can plot two lines as in Fig. 4.2, which represent the reaction of received signals with different T_1 and T_2 value. These two lines are unique with the fixed concentration, which comes from the data we achieved in 0.01%

ferrofluid test tube.

Fig. 4.2 gives out the trend of T_1 signals and T_2 signals during a scanning process of a nanofluid sample. The T_1 signal gets weaker and weaker at first, and then goes up after 600ms, this is because negative value cannot be plot under NMR data, and is shown in positive value. While the T_2 signal just gets weaker during the scanning. The two lines perfectly match with NMR theory.

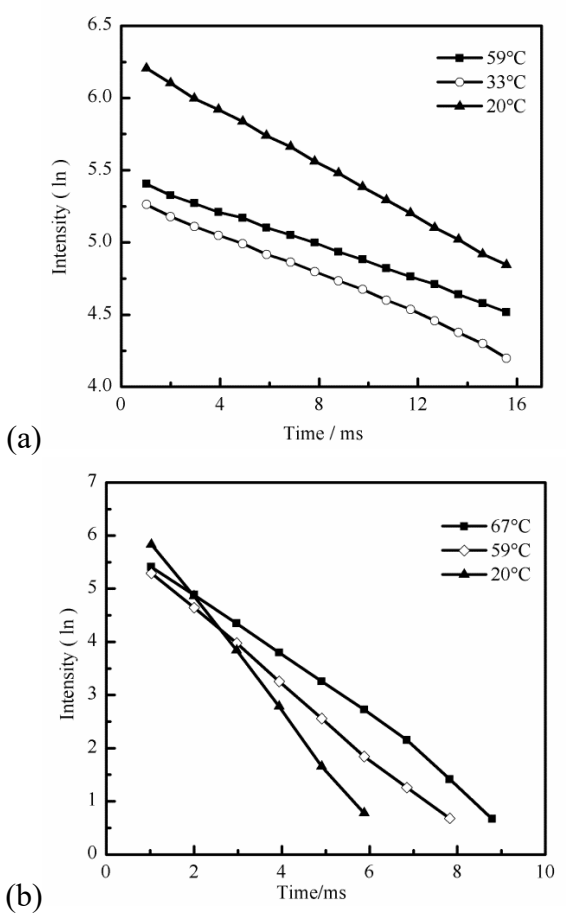

Figure 4. 3: The decaying of log intensity at different temperature, using 0.01% (a) and 0.1% (b) volume concentration

The data from NMR scanning are a 3D database with huge numbers of signal values. These data were analysed and calculated into the decaying line

using Matlab. Then the decaying trend of signal intensity, the slope *k*, was used for further calculation, from which we can directly know T_2.

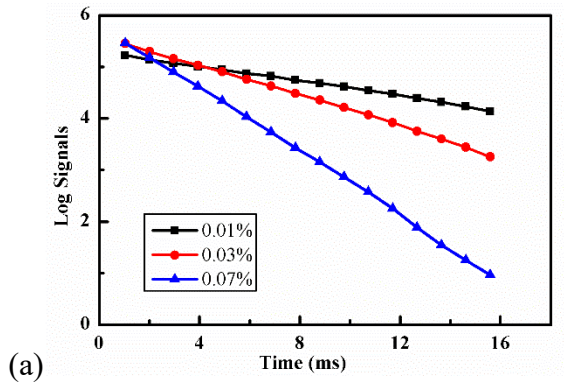

(a)

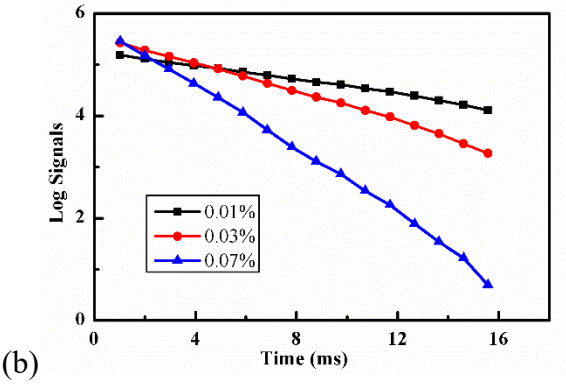

(b)

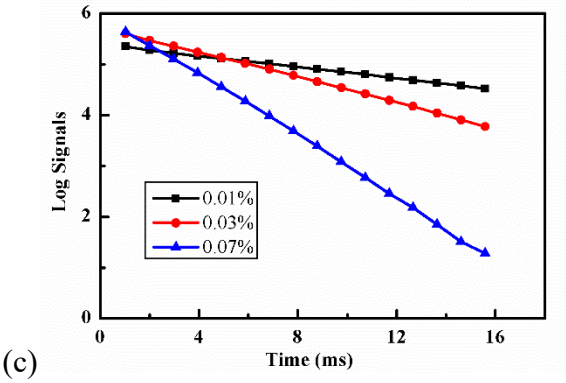

(c)

Fig. 4.4a 29ºC Fig. 4.4b 43ºC Fig. 4.4c 67ºC

Figure 4. 4: The decaying of log intensity at different concentration

The slopes of curve of logarithm *S* against time were calculated for the 70 experiments, which equals to $1/T_2^*$, as in Eq. 9. Fig. 4.3a gives out the three

typical curves of the *ln(S)* against time of 0.01% volume concentration, and Fig. 4.3b gives out the three typical curves of 0.1% volume concentration.

The curve of 20°C is on the top, the 59°C is in the middle, and the 33°C is at the bottom for 0.01% concentration, as can be seen in Fig. 4.3a. While the curve of 20°C is at the bottom, the 33°C is in the middle, and the 59°C is on the top for 0.1% concentration, as can be seen in Fig.4.3b. The lowest temperature curve decays faster, while the highest temperature decays relatively slow.

And if we take another comparison on different concentrations of ferrofluid affecting the signals' decaying pattern at a certain temperature, the data from NMR can also be plotted as Fig. 4.4. A few selected concentrations are plotted, and a clear pattern can obviously be seen. The curve of 0.01% volume fraction is on the top, the 0.03% volume fraction is in the middle, and the 0.07% volume fraction is at the bottom for 0.01% concentration, as can be seen in Fig. 4.4. And the three figures are showing the same pattern, at different temperatures. The highest concentration curve decays faster, while the lowest concentration decays relatively slow. However, the value for the signal intensity or the logarithm of it doesn't matter the most. The parameter we are focusing on is the relaxation time T_2, which is related to the decaying speed of signals, as is the slope of the linear lines plotted.

The slope k decreases when temperature rises for each concentration. These curves show almost linear relation between *ln(S)* and temperature, so

this concentration measurement method can be proved to be acceptable and accurate.

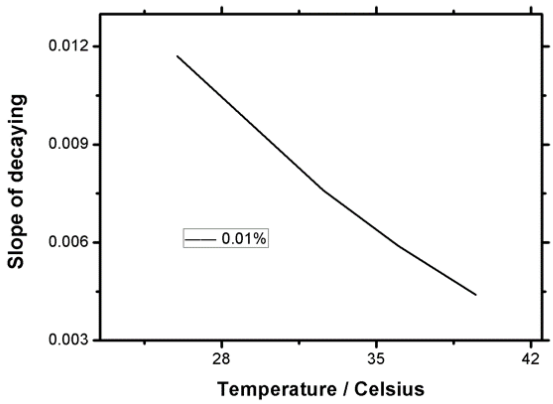

Figure 4. 5: Decaying slope with different temperature

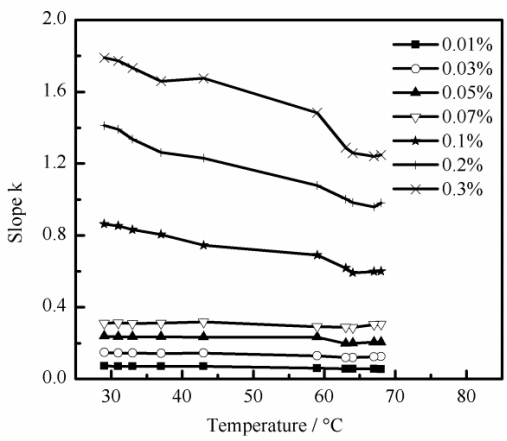

Figure 4. 6: Slope *k* against temperature under different concentration

The slope *k* the 70 experiments were calculated, as can be seen in Fig.4.6. It can be found out that the signal of pure water does decay very slowly for pure water, which means a very high T_2. So the slope *k* is very small which is very close to 0 and decay very slowly. The differences of the slopes *k* at different temperatures are very small for pure water.

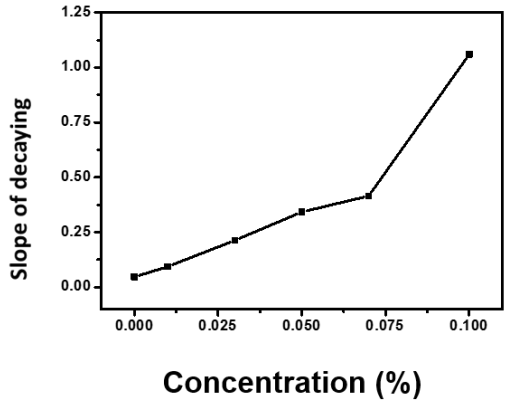

Figure 4. 7: Change of decaying slope with different concentration

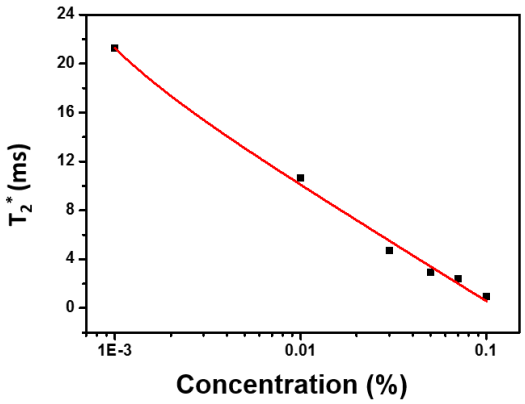

Figure 4. 8: Change of T_2 with different concentration in logarithm

It has been observed that the ferrofluid with 0.01% volume concentration looks like as transparent as pure water, while the ferrofluid with 1% volume concentration is pretty dark. The slopes k of low concentration ferrofluid are small and decay slowly, as can be seen in Fig.4.6. As the concentration increase, the decaying speed of slope k increases. The slope line of 0.3% concentration is no longer linear, because the nanoparticles in ferrofluid affect

the signals when the concentration is high. The NMR scanning cannot be carried out with high concentration ferrofluid.

The signals obtained from NMR scanning are T_2^*, but the T_2^* equals to -1/k, according Eq. 9. So, T_2^* is used in Fig. 4.8 instead of the k in Fig.4.7, then the curves of T_2^* against concentration were plotted in Fig. 4.9 as well. The T_2^* increases with the decrease of concentration under certain temperature. It can be found out that temperature, T_2^* and concentration have a clear relationship. So, with temperature and T_2^* measured by NMR, the concentration can be easily obtained.

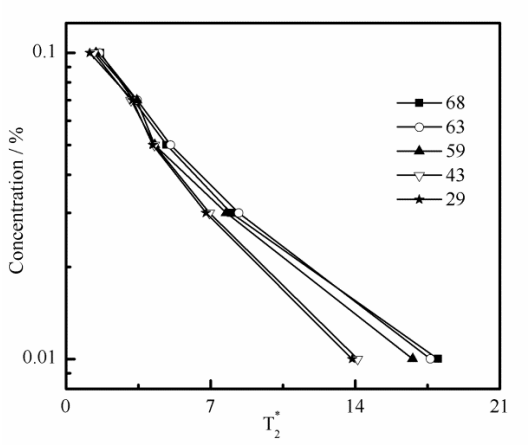

Figure 4. 9: Concentration against T_2^* under different temperature

In the experiment condition, the linear region of T_2^* with logarithm concentration is only within the range below 0.1% volume, as can be seen in Fig. 4.9. Because when the concentration is higher than 0.1%, the T_2^* signals will be affected by the Fe_3O_4 nanoparticles in ferrofluid. And actually, it would go beyond the previous patterns because of the limitation from the NMR

machine.

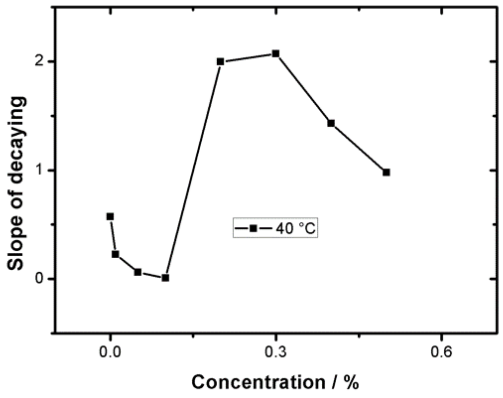

Figure 4. 10: Slope of decaying with concentration over 0.1% volume

4.4 Empirical equation

Now since the T_2^* can be calculated from temperature T and volume concentration, a figure can be plotted using these data, and then the concentration at different temperature can be found in Fig. 4.11, as long as the T_2^* is measured from NMR.

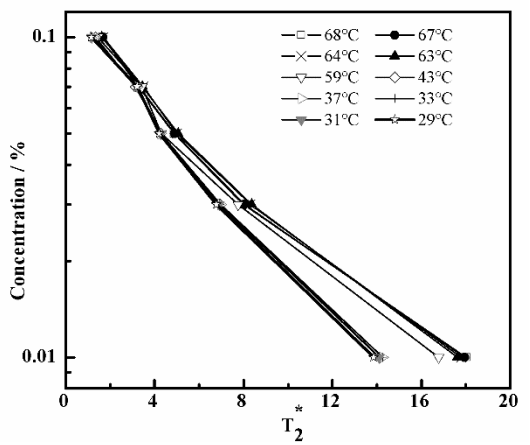

Figure 4. 11: Concentration of ferrofluid at different T_2^* and temperature

And all T_2^* values at different temperatures and concentrations are listed

below in Table 4.

Table 4: T_2^* values at different temperatures and concentrations

T \ ϕ	0.01%	0.03%	0.05%	0.07%	0.1%
68	18.02	7.99	4.87	3.27	1.67
67	17.95	8.05	4.88	3.29	1.67
64	17.79	8.30	5.00	3.48	1.69
63	17.64	8.36	5.06	3.45	1.45
59	16.78	7.75	4.30	3.44	1.45
43	14.12	6.94	4.28	3.14	1.34
37	14.27	6.98	4.28	3.24	1.20
33	14.27	6.94	4.27	3.24	1.20
31	14.10	6.90	4.27	3.20	1.17
29	13.85	6.77	4.21	3.22	1.16

Then the empirical equation was solved with T_2^*, temperature and concentration based on Eq.7, as is demonstrated before, that the T_2^* is linear to temperature and the logarithm of concentration. And based on these, the equation should be written in the form of,

$$T_2^* = a + b \cdot log(\emptyset + c) \tag{13}$$

where *a, b* and *c* are factors depending on temperature *T*, as T_2^* is linear to the logarithm of concentration.

Or,

$$T_2^* = \frac{1}{a \cdot T + b} \tag{14}$$

where a and b are factors depending on concentration ϕ, as the slope k is linear to temperature T, and is the inverse reciprocal of T_2^*.

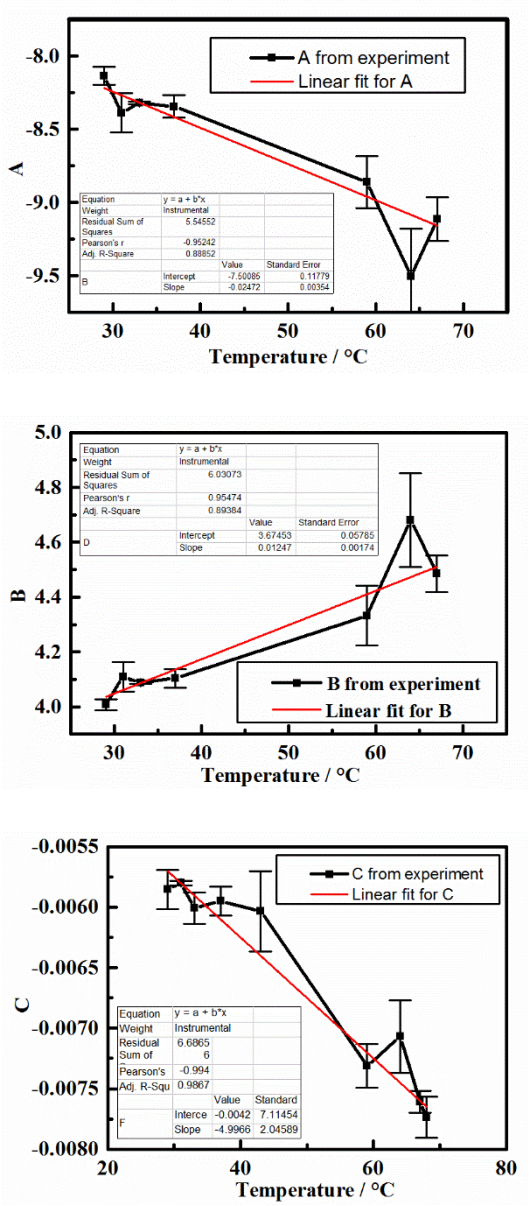

Figure 4. 12: Fitting of parameters A, B and C in Eq. 13

And by fitting the data into the form of Eq. 13, the parameters *A*, *B* and *C* in the empirical equation will be fitted into Fig. 4.12, while the empirical equation will be then written as,

$$\begin{aligned} \phi &= e^{\left(A-T_2^*\right)/B} - C \\ A &= -7.38 - 0.028 * T \\ B &= 3.63 + 0.014 * T \\ C &= -0.0043 - 0.000048 * T \end{aligned} \tag{15}$$

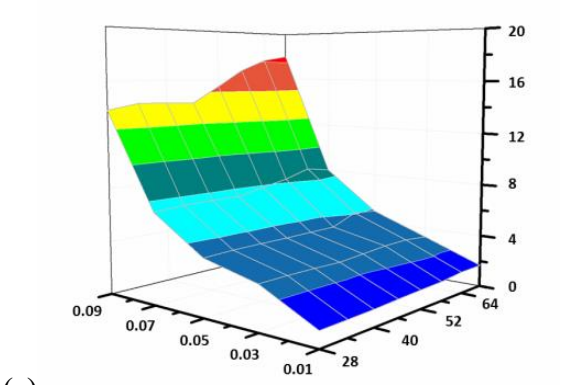

(a)

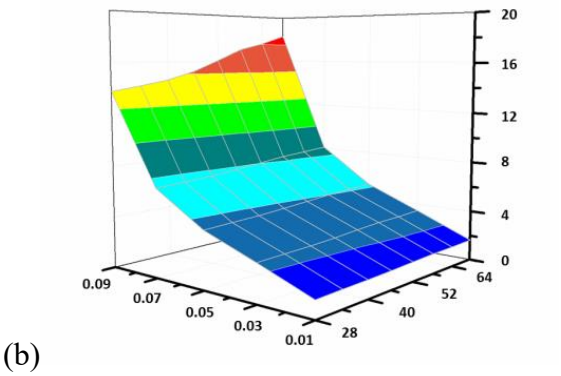

(b)

Fig. 4.13a Experiment Fig. 4.13b Equation

Figure 4. 13: Contour of T_2^* distribution in experiment and equation with bottom axis concentration and temperature

The *R* square for the linear fitting is 0.95. And the standard error of Eq.15 is 0.0046, while the relative error is 8.25% on average. The result from

experiment and Eq. 15 were compared at the range of T_2^* ranging from 0 to 20, volume concentration from 0.01% to 0.1% and temperature from 28°C to 70°C. It can be seen that the difference between experiment and the result from Eq. 15 is very small. The Eq. 15 has a high accuracy.

And by taking these fittings into the equation, the data calculated from the empirical equation and measured experimentally from NMR can be plotted in a 3D contour as Fig. 4.13. And it can be seen that they match very well.

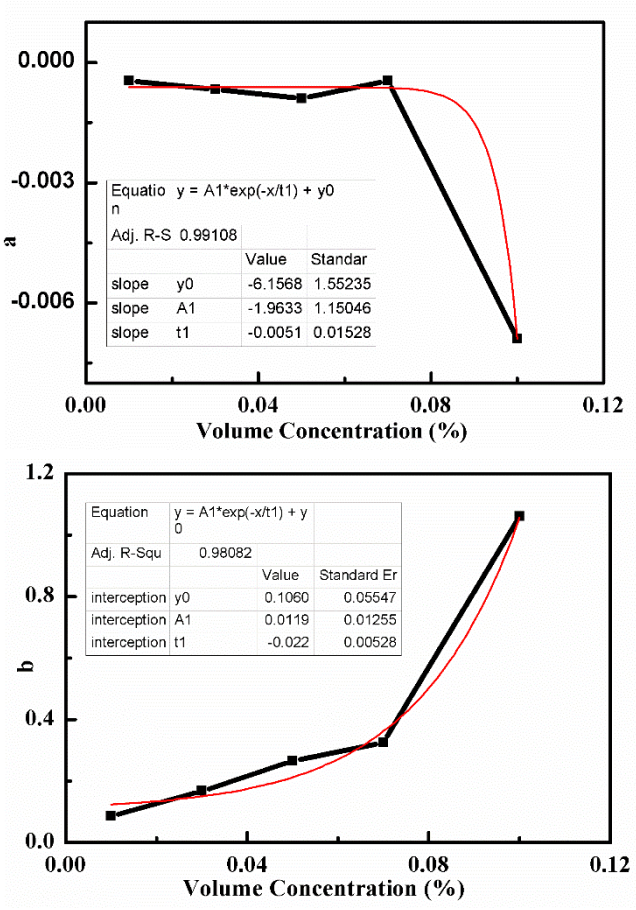

Figure 4. 14: Fitting of parameters *a* and *b* in Eq. 14

And at the same time, the data can also be fitted in the form of Eq. 14. However, *a* and *b* in different concentrations are uneasy to fit, as in Fig. 4.14, and thus has no possibility in expressing concentration in the form of Eq. 12, even though they themselves form a very good linear relationship in Eq. 14, with a *R* square of 0.95. And therefore, Eq. 15 should be used as the empirical equation in the following chapter in nanofluid dynamic concentration measurement and calculation.

4.5 Summary

The novel method of nanofluid concentration measurement is investigated, and proved to be workable. The static results have shown a good linear relationship between the concentration, temperature and T_2. Therefore, the empirical equation can be based either on that the T_2^* goes linear with the logarithm of concentration, or on that the slope k goes linear with the temperature, which also equals to $1/T_2^*$. And by comparing the two methods, it is found that only one of them is good enough to be summarised.

And this empirical equation is proposed based on the static results. It is presented that the error between experimental results and empirical equation calculation results is very small, and therefore should be ready to use in dynamic concentration measurement in the next chapter.

Chapter 5: Nanofluid dynamic concentration

5.1 Introduction

In this chapter, the dynamic concentration of ferrofluid flow is measured. And the signals of the ferrofluid flow is put into analysis to calculate their T_2. Then the empirical equation achieved previously in Chapter 4 is adapted. The final result of ferrofluid flow dynamic concentration distribution is plotted. And the effect of this phenomenon is then discussed, together with the potential forces and reasons for this.

5.2 Dynamic concentration distribution

The two curves in Fig. 5.1 are the relationship between logarithm intensity and time of under flow and static condition in the pipe. It can be found out that the signals of flow condition decay faster than static condition. Because the signals obtained by the NMR scanning are from the certain atoms in the fluid, those atoms will move away with the fluid. The decay speeds of initial part of these two curves are almost the same, for the velocity of the fluid is very small in the experiment condition. The signal loss caused by velocity is below the sensitivity of signal receiver. As the scanning carried on, the signal sources move away as well, and cause a loss in signal. And the curve decay speed faster with the increase of flow velocity. So the effects of velocity on concentration can be included in T_2^*.

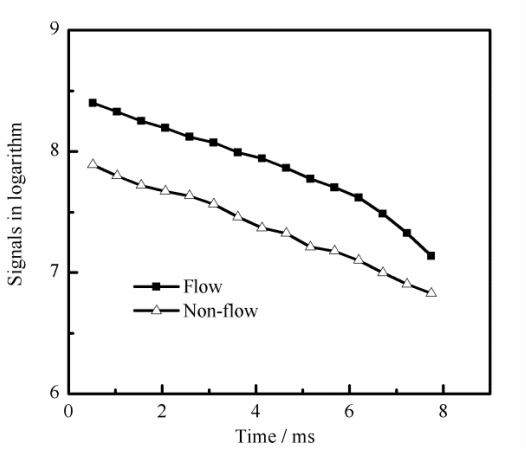

Figure 5. 1: The relationship between logarithm intensity and time of nanofluid under flow and static condition

The 0.05% volume concentration ferrofluid is adopted in dynamic scanning. The ferrofluid is circled around in the pipe using a pump, during the scanning. The flow in the pipe is laminar flow during experiment. The diameter of the tube used in the experiments is about 8 pixels, and the cross section is divided into 72 pixels (8×9 pixels), as can be seen in Fig. 5.2. Each pixel gives a group of individual T_2^* signals, which means there are 72 groups of T_2^* signals. The 72 groups of T_2^* signals are seriously analysed, and then put into Eq. 8 with temperature to calculate the concentration of each pixel, separately. Then the dynamic concentration distribution of the cross section is obtained with the concentrations of 72 pixels, as can be seen in Fig.5.2b.

It is clear that the dynamic concentration distribution of the cross section under flow condition is closely related to the velocity distribution of the cross section. The highest concentration appears near the wall of the tube, which is about 0.06% volume, and the concentration at the centre of the cross section is

about 0.03% volume. The concentration decreases from wall to the centre of tube along the radiation, as can be seen in Fig. 5.3. At the central area, where proportion to radius is 0, the concentration is the lowest; while at the boundary area, where proportion to radius is 1, the concentration is the highest.

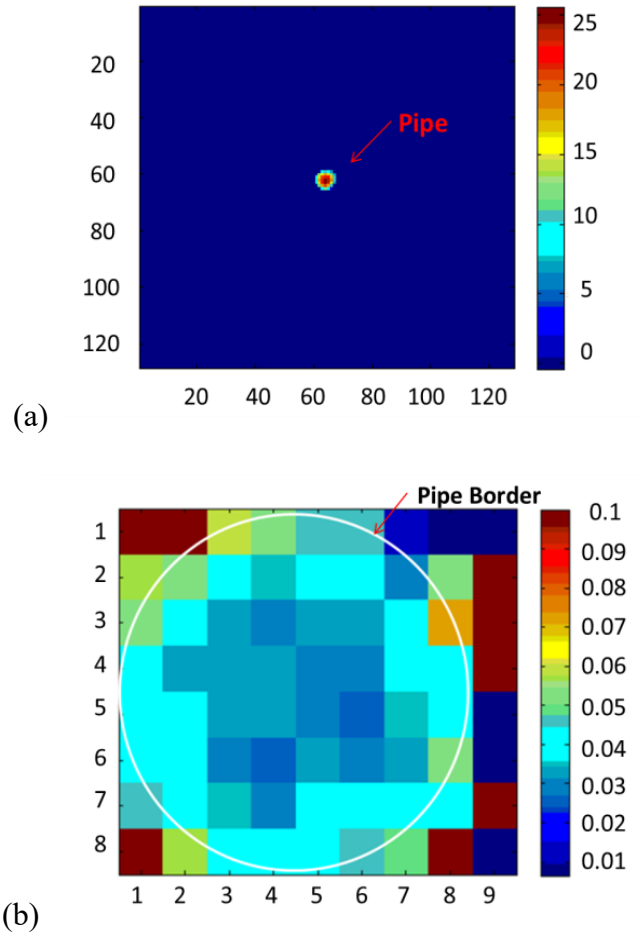

(a)

(b)

Figure 5. 2: Velocity distribution in mm/s (a) and concentration distribution in % (b) across the tube

At the same time, the velocity near the wall is relatively small compare to the centre and the flow is stable under laminar flow condition, which may also contribute to the aggregation of nanoparticles near the wall. So as long as the flow state is laminar flow in pipe, the cross section of pipe will have almost the

same concentration distribution like Fig. 5.2b and Fig. 5.3.

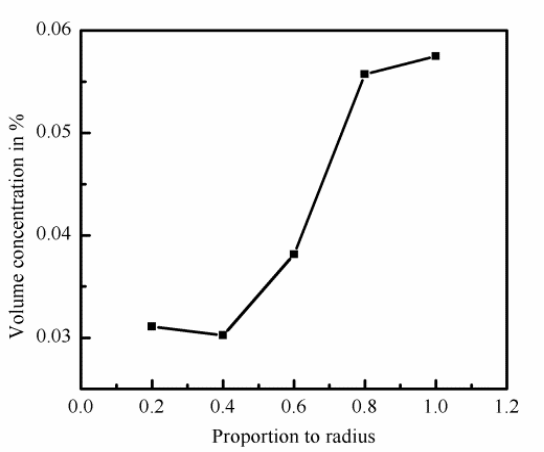

Figure 5. 3: The concentration gradient along the radius

The average concentration of the cross section measured in the experiment is 0.046% calculated with Eq.15, which is about 0.004% less than that in the tank. This is because the distribution of nanoparticles isn't uniform in the tank. And the pump induces a serious turbulence around the pump, which also affect the nanoparticle concentration in the tank. Then the concentration of the nanofluid that pumped into the tube may have a small difference with that in tank. So the dynamic concentration measured by NMR with Eq. 15 is acceptable.

5.3 Influence on fluid flow heat transfer

The heat transfer behavior of nanofluid in the pipe is closely related to the thermal conductivity of the nanofluid. The conductivity near the wall is the

main factor that decides the convective heat transfer speed between the wall and water in tube. For the non-uniform concentration distribution, the thermal conductivity in the tube isn't uniform. One of the most conmen used thermal conductivity calculating method for nanofluid is,

$$\lambda_{ef} = \phi \cdot \lambda_p + (1-\phi) \cdot \lambda_f \tag{16}$$

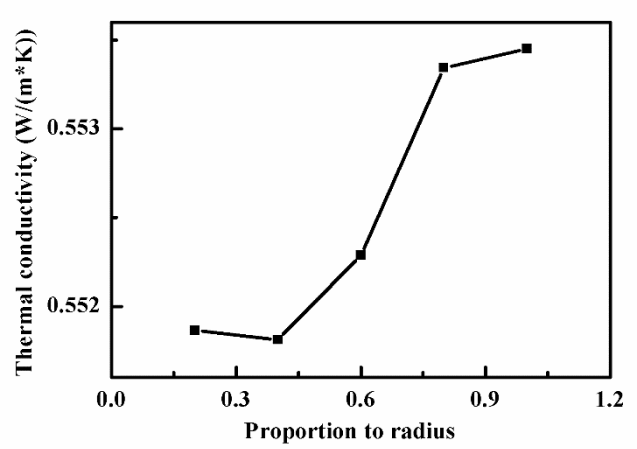

Figure 5. 4: Thermal conductivity gradient along the radius of tube

The thermal conductivity of Fe_3O_4 nanoparticles is considered the same as that of Fe_3O_4 powders, which is 6W/(m·K), and water 0.55 W/(m·K).[158] Thermal conductivity of the nanofluid with average concentration in tube is 0.5525 W/(m·K), 0.5529 W/(m·K) with dynamic concentration, and 0.5532 W/(m·K) near the wall. The difference of dynamic conductivity and conductivity near wall with the average conductivity will increase when the concentration increases. The conductivity near the wall will be around 5% higher than the average conductivity at 1% concentration with Eq. 15. And

along with the concentration gradient across the tube, the thermal conductivity would also follow the same pattern, as is in Fig 5.4.

5.4 Forces analysis

In our experiment, we focus on the concentration distribution of ferrofluid when it's flowing. And it is now proved that the ferrofluid flow does have significant concentration distribution in the process which can't be ignored. While in the previous studies of nanofluid, several papers are trying to illustrate and explain the convective heat and mass transport of nanofluid, mainly in two models[159].

- Homogeneous flow model, mainly adapted by Choi previously and a few other researchers[36, 160]. This model considers nanofluid as a simple form of single phase flow, and can be used in all previous pure fluid equations. And the thermal performance only comes from the characters of the fluid.
- Dispersion model, firstly proposed by Xuan and Roetzel[161]. This model believes that the thermal performance of nanofluid comes from not only the high thermal conductivity itself, but also the dispersion and distribution of nanoparticles in base fluid. As there could be a relative velocity or slip between nanoparticles and base fluid molecules. And this perturbation should be put into energy calculation equations.

Therefore, our experiment directly unveiled the disadvantage of the homogeneous flow model, and there are many forces that could lead to a slip between nanoparticles and local base fluid molecules. And this slip velocity is the relative movement of nanoparticles to the base fluid, and thus generates a non-uniform concentration distribution.

1. Inertia

Particle movements with inertia could cause a relative slip between nanoparticles and base fluid. And the motion due to inertia can be written as,

$$\frac{\pi}{6} d_p^3 \rho_p \frac{dV_e}{dt} = -3\pi d_p \mu V_e \quad (17)$$

where d_p is the diameter of nanoparticles, ρ_p is the density of nanoparticles, V_e is the slip velocity due to turbulent eddies, and μ is the viscosity of nanofluid.

The stopping distance can thus be conducted from Eq. 17, and it is much smaller than the length of eddies and the thickness of boundary sublayers[159]. Therefore, the inertia's role in contributing to the concentration distribution is very limited.

2. Brownian motion

Brownian motion is the random motion of particles suspended in a fluid resulting from their collision with the fast-moving atoms or molecules of the fluid[162], and a very important force contributing to the particle movement. The nanoparticles can be seen as larger molecules in the fluid, and thus with lower velocity than around. The Brownian motion is given by the

Einstein-Stokes equation in the form of Brownian diffusion coefficient, D_B,

$$D_B = \frac{k_B T}{3\pi\mu d_p} \tag{18}$$

where k_B is the Boltzmann constant, T is the temperature of nanofluid and ϕ is the concentration of nanofluid. Therefore, the mass flux in Brownian diffusion, J, is calculated as,

$$J = -\rho_p D_B \nabla\emptyset \tag{19}$$

3. Thermophoresis

Thermophoresis is an effect that mixture of particles with different types perform differently under the force of a temperature gradient. It is also known as Soret effect in normal fluid mixtures. And the thermophoresis velocity V_T can be written as follow, with a factor β which is linked to the thermal conductivity of fluid, k, and that of nanoparticles, k_p.[163-165]

$$V_T = -\beta \frac{\mu}{\rho} \cdot \frac{\nabla T}{T} \tag{20}$$

$$\beta = 0.26 \frac{k}{2k + k_p} \tag{21}$$

Thus the nanoparticle mass flux J due to thermophoresis effect can be calculated as below, with the thermal diffusion coefficient D_T.

$$J = \rho_p \emptyset V_T = -\rho_p \frac{\nabla T}{T} \tag{22}$$

$$D_T \equiv \beta \frac{\mu}{\rho} \emptyset \tag{23}$$

Malvandi and Ganji proposed a mathematical model to calculate the

concentration, temperature and velocity gradient of nanofluid flow in heated tube[167]. Even though the thermophoresis effect is very significant in particle movement, it is not contributing to the present work. As the nanofluid flow in experiment is conducted in thermal insulated pipe, and the temperature difference between the nanofluid and surrounding area is also very small, the temperature difference and heat transfer can be ignored. Therefore, it would not be considered in the present work.

4. Gravity and buoyancy

The movement of nanoparticles vertically should also be affected by the balance between gravity, buoyancy and viscous. And the equation can also be written according to Stokes Law,

$$\frac{\pi}{6} d_p^3 (\rho_p - \rho) g = 3\pi d_p \mu V_g \tag{24}$$

$$V_g = \frac{d_p^2 (\rho_p - \rho) g}{18\mu} \tag{25}$$

And for nanoparticles with diameter smaller than 100nm, the V_g is very small and thus can be neglected.

5. Hydrophobic effect

Nanoparticles have an intrinsic property of self-assembly at interfaces[166]. As all kinds of nanofluid are more or less hydrophobic, when dispersing in water, the thermodynamic free energy of nanoparticles would be higher than gathering towards other hydrophobic boundaries, such as the tube

wall. And the gathering of nanoparticles on the interface can also reduce the interface energy, forming extra force to attract nanoparticles over the boundary, and therefore creates a concentration gradient. In the present work, as we use Fe_3O_4 nanoparticles in water as our ferrofluid in experiments, the hydrophobic effect is even stronger, which is why oleic acid is added as surfactant. However, the hydrophobic effect of nanoparticles still exists. And that makes the nanoparticles much easier to gather around the boundaries of the tube, instead of uniformly dispersed in water. However, this effect is not quantified yet. But it is for sure that this effect would cause the nanoparticles to aggregate around the wall of tube.

According to the analysis of different forces and effects contributing to the dispersion and aggregation of nanoparticles in base fluid, the major causes of the phenomenon observed in our experiment are Brownian motion and hydrophobic effect.

5.5 Summary

The ferrofluid flow is measured with NMR, and the velocity and T_2^* distribution is observed. And using the empirical equation from Chapter 4, the concentration can be calculated from the T_2^*, when the temperature is achieved. And by assuming the temperature is uniform across the tube after the flow is

stabled, concentration gradient is plotted, with a clear view of concentration gradient, highest at boundary region, and lowest at core region.

The nanoparticles, molecules and clusters can't be seen directly under NMR, bus instead is calculated from T_2^* relaxation time. And nor can we see the precise layer of velocity, due to the limit of resolution around 1mm. Only a roughly plotted vague image of the concentration gradient layers and velocity can be achieved. However, these should already enough for forces analysis. Brownian motion and hydrophobic effect are the main reason for nanoparticles' distribution. And previous models on the concentration gradient mathematical model is presented, and could also be proved by the present work.

Chapter 6: Bionic water migration in plants

6.1 Introduction

In this chapter, the second part of the present work is introduced, which is the bionic engineering study and analysis of forces involved in water migration system in plant xylem.

Tree hydraulics is not a familiar research field for decades because it contains very complex mechanism with many influential parameters from its microscale inner structure. To analyse the water migration in detail, various factors need to be considered, such as gravity, resistance, C-T (cohesion & tension) theory, capillary effect, transpiration effect, root pressure and so on. And in this thesis, we will simplify the xylem as a cylinder vessel without any water passing through conduit walls. Despite most researches so far that would simplify the conduit as smooth surface,[168] we will put drag force due to surface friction into consideration, and prove that friction force is not negligible. And then all forces will be put into one water migration mathematic equation, with basic parameters that could be measured, so that the water transport velocity and be calculated, and compared with experimental measurements.

The structure of water migration system in plant stem and the forces involved are discussed, together with novel analysis and simplifications that previous researches seldom mentioned. And by putting all discussed forces

together, a mathematical model is proposed to explain the inner mechanism of water migration in plant xylem. Using this mathematical model, the velocity of one selected plant can be calculated, while on the other hand, the water flow velocity in the plant xylem can be measured with NMR technique. By comparing the two results, the mathematical model's accuracy is proved by matching experimental result. And the mathematical model therefore can be used to explain and predict many situations in engineering and industries, such as the heat pipe.

6.2 Water migration theory

Currently, it is mainly believed that the sap rising in plants should be explained by the Cohesion & Tension theory. It doesn't illustrate a novel force that drives the water in plants upward, but instead explains how forces from different part of the plant can work together, as in the negative pressure and tension within water takes water up, while the cohesion force keeps water continuous.

The Cohesion and Tension theory is first proposed by Dixon and Joly in 1895,[92] and then developed into modern forms.[90] And according to it, there are a few previous assumptions for researches afterward. The liquid water in plant xylem system is considered as a continuous single phase flow, while the narrow conduit wall could enable evaporation from transpiration, but

resist the entry of air at the same time. And water is closely contacted to the conduit wall because of the cohesion of water molecules and tension with the wall. And above all, the Cohesion and Tension theory allows forces to provide energy for water to move within xylem, using capillary effect, root pressure (osmosis effect), transpiration effect and also friction.

6.3 Forces involved analysis

6.3.1 Root pressure

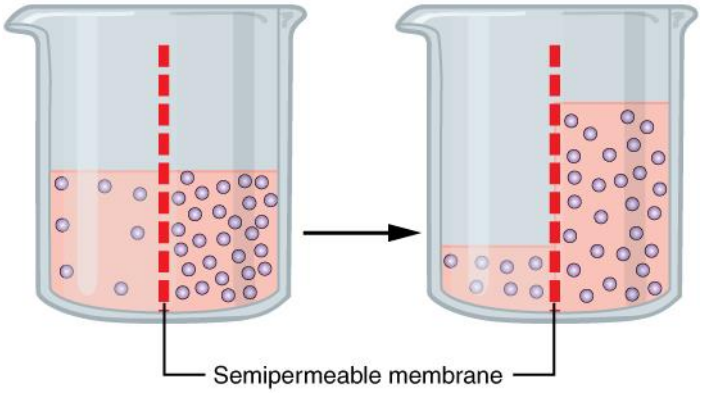

Figure 6. 1: Osmosis effect

Root pressure is also known as osmosis effect in plant researches, shown in Fig. 6.1. As water moves in the direction of a decreasing water potential, this effect generates a force along the decreasing water potential from pure water, soil, root, xylem, leaf to atmosphere. Mineral ions in soil can be absorbed by the root cells, which would cause the accumulation of ions on the other side of

root cell membranes in the cells, with higher concentration comparing with soil environment outside. And this would drive the water to flow into the root cells as well. While due to its limitation, it only accounts for the major water migration when transpiration effect is low, such as during the night. Root pressure is a main reason for guttation, as well as the absorption of minerals by root cells[93]. It would also contribute to the water refill in xylem, as some plants' xylem conduits are empty during winter, even though not always the case[169, 170]. However, it is now considered as a positive but relatively unimportant force in water migration in xylem, instead of a major one. Therefore, it is not discussed and analysed in detail in the present work.

6.3.2 Capillary effect and gravity

Capillary effect and gravity are the two most frequently discussed forces in xylem studies. Most researches would consider a xylem conduit as one capillary tube, and analyse the two forces only. Capillary force generates from the inter-molecule forces between liquid and solid walls, which would be more significant when the size of tube is small enough, while on the other hand, gravity has no need to specify. And we are putting the two forces together because they are already well studied and easy to present in mathematical model. Normally, the xylem system of plant is around 10 to 100μm, even at the smallest size, the xylem structure can only lift the water up to 3m using

capillary effect only. It is a big contributing force in water migration, but not the most important one, especially for those tall plants over 10 metres in height. The commonly used equation for capillary force is as follow,

$$p_c = \frac{2\gamma \cdot \cos\theta}{r} \tag{27}$$

$$p_g = \rho g h \tag{28}$$

where γ is surface tension of water in plant xylem conduit, θ is the contact angle, and r is radius of xylem conduit.

6.3.3 Transpiration effect

Transpiration effect is caused by the water evaporation from plants, mainly in leaves. This is widely believed to be the critical mechanism for long distance water transportation in xylem system, especially in tall trees of over ten metres height. As water evaporates, negative pressure appears in xylem, and force water to move up with the cohesion and tension within water molecules.

The simplification of transpiration effect is very difficult, and the most famous solution one proposed by Van den Honert in 1948,[171] that consider the water flow in xylem as an analogue of the Ohm's Law. This means the pressure gradient is linear along the xylem, and the pressure is linked to the water flux in evaporation, together with a parameter, hydraulic conductivity as the resistance in Ohm's Law.

Imagine the xylem conduit as a cylinder, with radius r, or diameter d, and height h. P_x is the transpiration pressure. Q is volume flow rate. Then the pressure gradient generated through transpiration effect is as follow,

$$-dP_x / dx = EA / K_h \tag{29}$$

$$P_x = \rho Q h / K_h \tag{30}$$

where E is evaporation flux density, while A is the surface of leaves, K_h is the hydraulic conductivity. Since flux density multiplies surface is the flow rate, then it is written as volume flow rate Q instead. This can be analysed from Hagen – Poiseuille equation, then all depends on the value of hydraulic conductivity of stem, which can be determined by experiment.[172]

6.3.4 Friction

In most researches, friction is not considered, as the extremely complex inner structure of xylem in microscale. However, there are various remarkable structures inside the xylem conduit that could be believed to be strongly affecting the friction force within the sap flow. The inner structure of xylem is seen as helical structure in capillary conduit, with resistance higher than ideal, as can be seen in Fig. 6.2. These structure details could determine the friction factor of the xylem walls in fluid flow, as we are using the Darcy – Weisbach Equation to calculate the pressure loss in the water migration process due to friction.

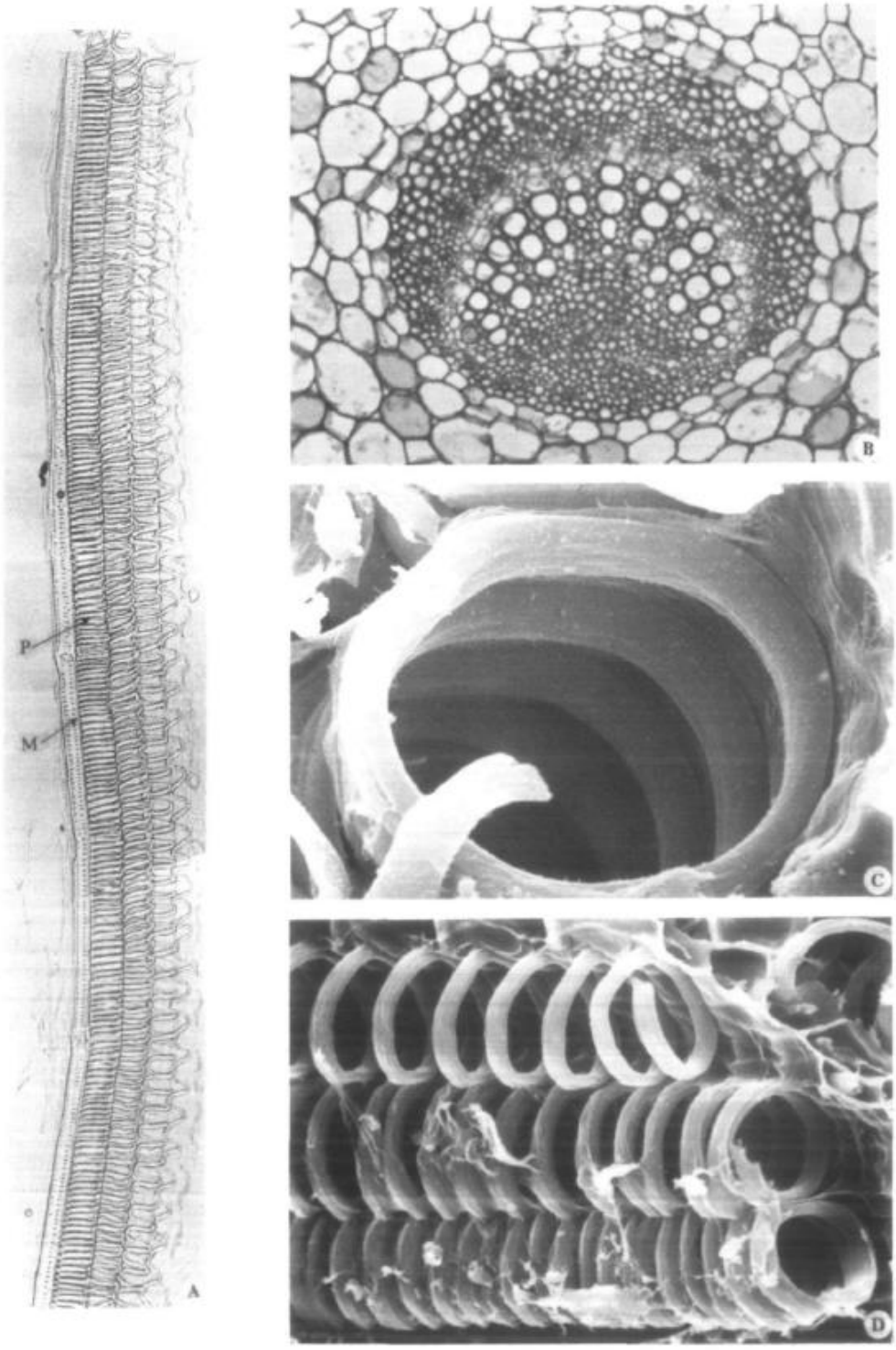

Figure 6. 2: Microscope image of xylem inner structure[173]

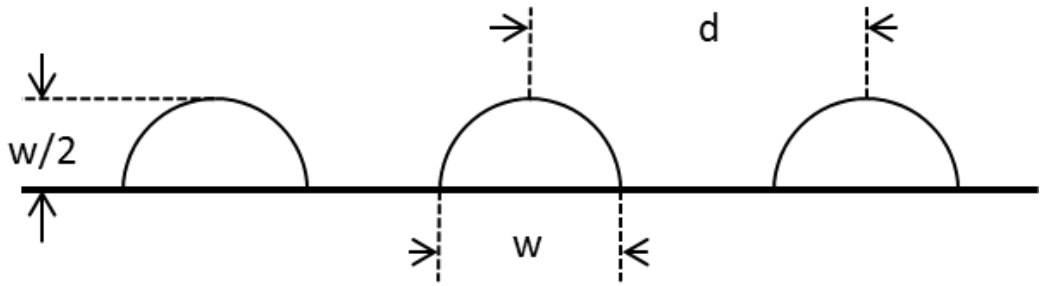

(a)

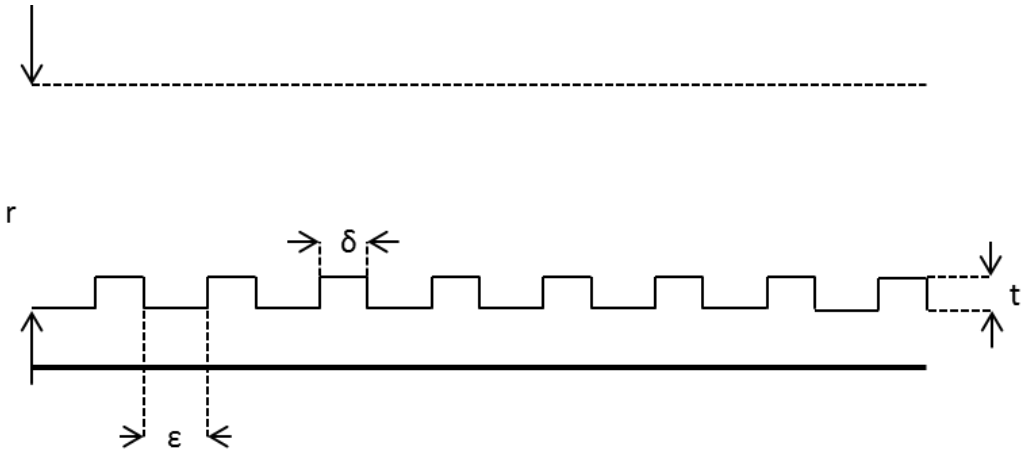

(b)

Figure 6. 3: (a) xylem conduit wall structure in 2D; (b) simplified wall structure

Thus if we turn the three dimensional helical structure into two dimension so as to simplify the calculation, we can get the structure as in Fig. 6.3.

So if we turn the half circle in Fig. 6.3(a) into the form of Fig. 6.3(b) at $\delta \times t$, then the relationship among these parameters of xylem wall structure can be written as,

$$\varepsilon = d - \delta \tag{31}$$

$$\delta = \sqrt{\frac{\pi}{4}} w \tag{32}$$

$$t = \sqrt{\frac{\pi}{4}} \frac{w}{2} \tag{33}$$

And the following calculation of friction force will be based on these simplifications, and will be discussed in detail in the calculation result section.

6.4 Mathematical model

As discussed previously, the main forces that contribute to the sap rising from root to leaf through xylem in plants are capillary effect, transpiration effect, friction and gravity.

Most researches on the water transport would focus on pressure gradient, and write forces in the form of pressure as well.[83, 174, 175] And since in well hydrated plants, the tension is reflected in velocity and volume flow.[176] So the overall equation can be simply written as below, and within which, flow velocity will be mentioned and listed out as an independent factor to calculate in the following work, and be measured as well in NMR test.

$$p_f + p_c + p_g + p_t = 0 \tag{34}$$

where friction force p_f, capillary force p_c, gravity p_g and transpiration force p_t add together should be equilibrium. And the next step is to describe each pressure in detail. And it would be easy to find that for capillary force and gravity, since capillary pressure is already listed in Eq. 27, and gravity in Eq.

28.

And the transpiration effect can also be found in Eq. 30, and then all that's left is friction factor, which is ignored in most cases for its complication. The friction factor is taken out as a parameter, so the pressure loss due to friction can be written as Darcy – Weisbach Equation,

$$p_f = \rho \cdot g \cdot h_f = \rho \cdot f \cdot \frac{h}{d} \cdot \frac{u^2}{2} \tag{35}$$

where ρ is sap density, f is friction factor, h is height, d is diameter of xylem conduit, and u is flow velocity. And all that's left is to determine the friction factor. As this is in Fanning's friction equation, so normally, the friction factor f should be

$$f = \frac{16}{\mathrm{Re}} \tag{36}$$

However, as with the complex structure and surface of xylem conduit, we have to find the exact number over Reynold Number, instead of 16. But in here, we will simply use f to illustrate it first, and the final mathematical model for water migration in plant xylem system can be written as,

$$-\rho \cdot f \cdot \frac{h}{d} \cdot \frac{u^2}{2} + \frac{2\gamma \cdot \cos\theta}{r} - \rho g h + \frac{\rho Q h}{K_h} = 0 \tag{37}$$

Since density, viscosity, and surface tension of sap is very easy to measure, together with the height and diameter of xylem, most parameters are easy to find. The only difficulties remains in friction factor and hydraulic conductivity, which can be measured as well.[173, 177] Therefore, we can get to calculate the mean velocity in xylem.

6.5 Results and comparison

6.5.1 Water distribution test

Figure 6. 4: Three plants, banana plant, cactus and willow from left to right

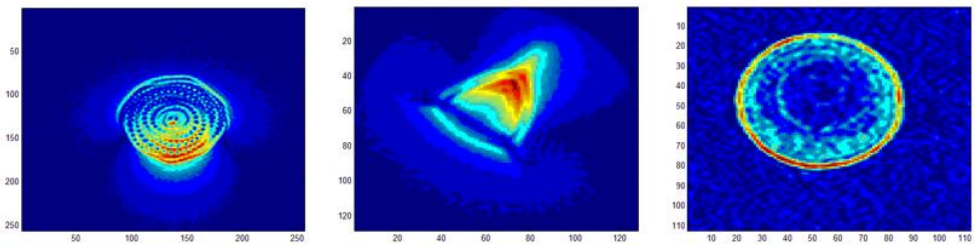

Figure 6. 5: NMR image of banana plant, cactus and willow from left to right, with pixels referring to resolution

First of all, we carried out a set of NMRI scanning of plants, with dozens of layers. An initial scan is first taken on three different type of plants, a tropical banana plant, a cactus and a small willow in Fig. 6.4. They were put into NMR for a scan at first to see their performance, as in Fig. 6.5.

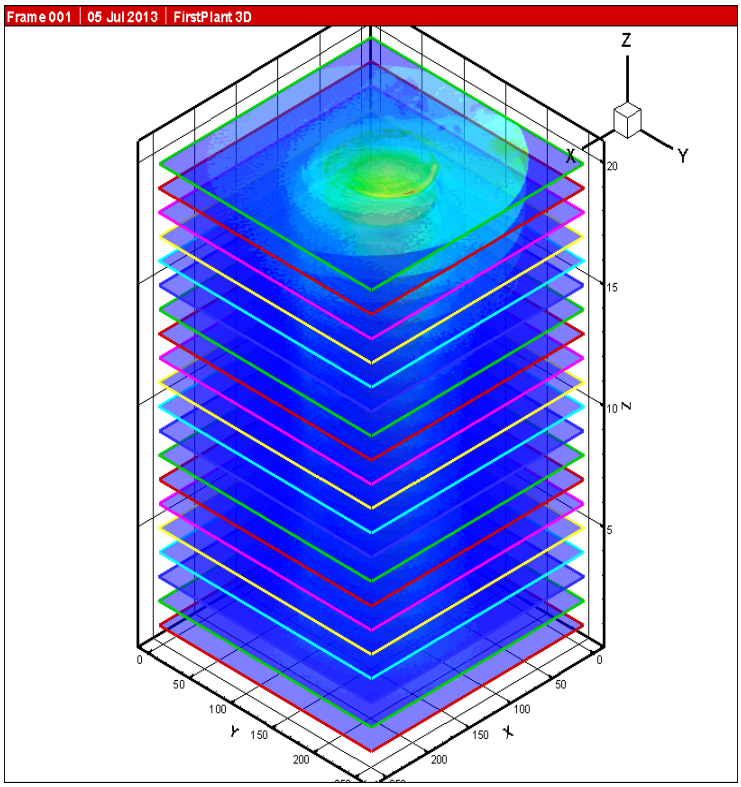

Figure 6. 6: Layers of plants

And we can see that the brighter part in Fig. means more water distributed, and therefore means the flow path of water in plant. However, the water distribution of cactus is very vague, and would cause additional difficulties in later analysis. So only the other two plants, Musa× Paradisiaca and Salix Integra Flamingo are proceeded into the following experiments.

As shown below in Fig. 6.7, different plants have different water flow paths. With the difference between woody and herbaceous plant, we can see clearly from the two image, Musa× Paradisiaca plant and Salix Flamingo. The woody plants have a highly evolved vascular system which lies on the outer

side of the stem, while the stem of Musa × Paradisiaca plant is the base of leaf stalks, as water transport conduits all around the stem. It is also shown that the water gathers within the xylem, and mainly concentrated in the lower part. This is because of gravity, since we have to lay the plant down when doing NMRI.

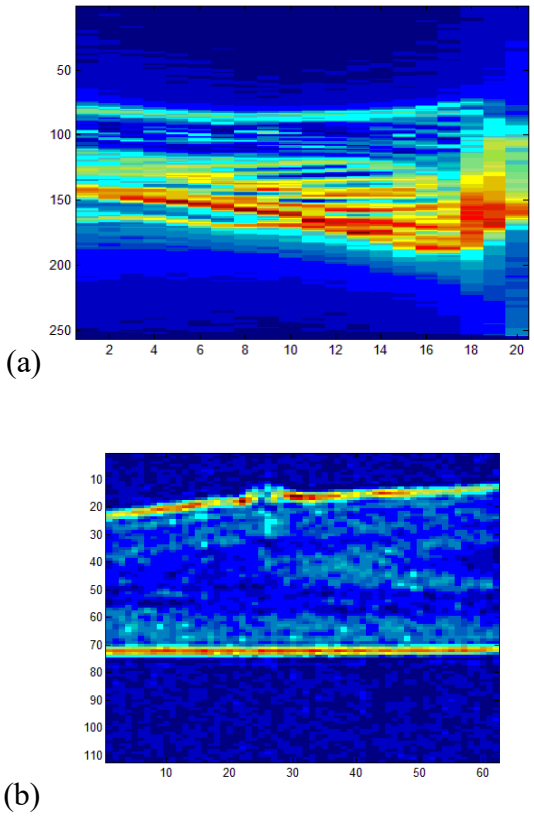

Figure 6. 7: a) NMR profile of Musa × Paradisiaca; b) NMR profile of Salix Flamingo

As NMR is a three dimensional technology, we can have vast numbers of layers along the stem, and put them together to form a profile of the plant stem, as in our experiment, the distance between each layer is 3mm, as shown in Fig 6.6 and Fig. 6.7, with pixels referring to resolution.

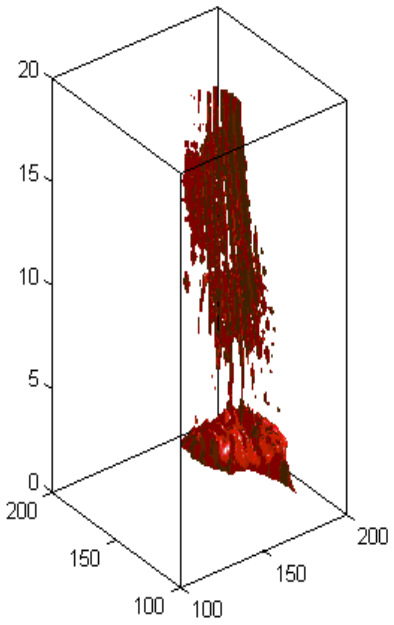

(a)

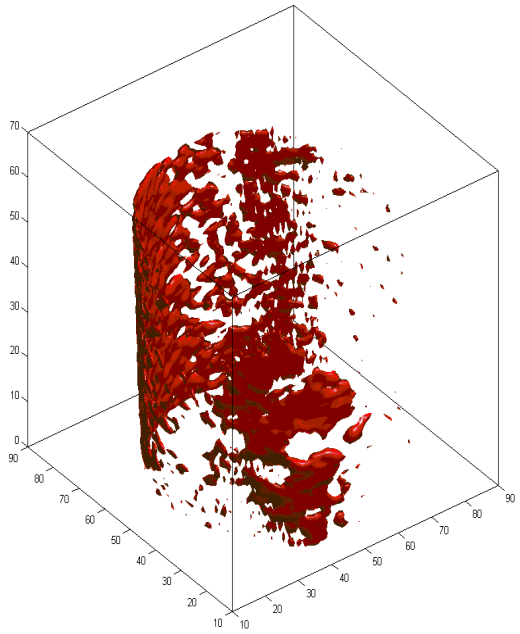

(b)

Figure 6. 8: Water distribution in three dimensional,

a) Musa × Paradisiaca; b) Salix Integra Flamingo

And by putting these layers together, we can see the water distribution in plants along the stem in Fig 6.7. Also, if we plot them in a three dimensional model and try to illustrate the water in plants, we can also have images in Fig. 6.8. From these images, we can clearly observe the water distribution in different plants, and obviously, woody plants as Salix Integra Flamingo, has a branch of xylem vascular structures which are easy to find. While on the other hand, water flow path would be relatively more difficult to illustrate in the images of Musa × Paradisiaca. Therefore, the Salix Integra Flamingo would be the examples of the following experiments, and would be simply called Flamingo for short in the followings.

6.5.2 Water transport velocity using NMR

NMR can measure the velocity in one direction. And if we consider the water flow within different xylem conduits to be extremely few and slow, and that all water in plant stem flow within the xylem in the same direction, from root to leaf. The velocity of water flow in plant stem is measured, and then comparing with the previous image of the water distribution in stem. And by putting the two images together, the velocity which falls on the same pixels with higher water distributions, would be the real velocity of flow in plants.

When leaving the velocity values at high water distributions in the image, and deleting other values where no water is detected, the velocity map in plant stem is plotted as below in Fig. 6.9, with each pixel referring to the resolution of 0.22mm. This should be the case as plant xylem in woody plants mainly

distributed in the outer part of the stem, especially the new-born ones, and most water transport happens in this region. So water flow velocity forms a circle at the very edge area of stem is very reasonable.

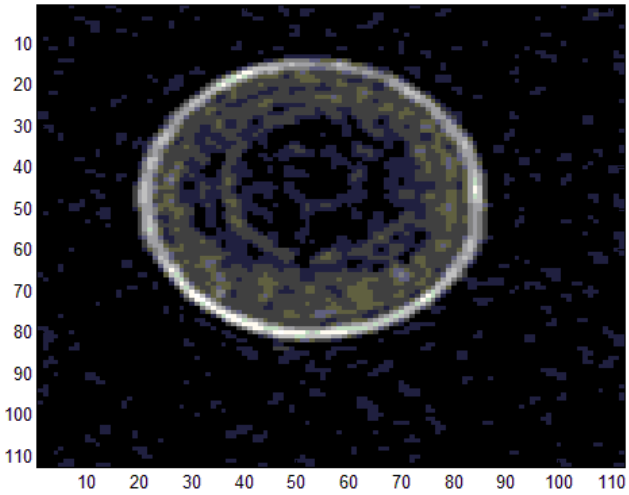

(a)

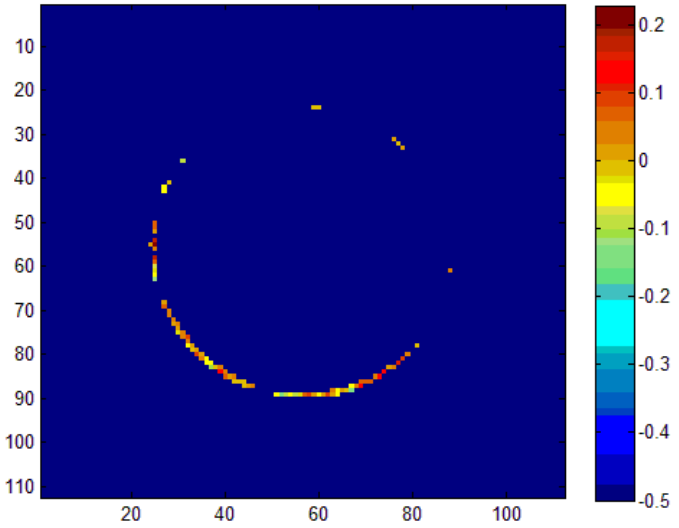

(b)

Figure 6. 9: Xylem water distribution in stem (a) and the flow velocity in plant stem (b)

If we take averages of all the velocity points in the xylem, the average velocity would be calculated as 0.11mm/s. Even though it is only an average

velocity, instead of a precise value in individual xylem conduits, it would still be helpful and be compared with the result from mathematical model.

6.5.3 Water transport velocity using mathematical model

Normally, the xylem system of plant is around 100μm, even at the smallest size. And this structure is mainly considered as a cylinder, with diameter d, and height h,[168] and Q is volume flow rate, as in Fig. 6.10.

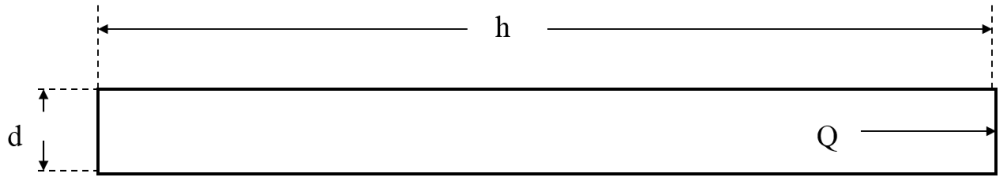

Figure 6. 10: Xylem conduit

The xylem structure can only lift the water up to 3m using capillary effect only, even though most researches consider this force the main contribution to water lift. And obviously it may not be the case for taller trees. For capillary effect, the force can be written as in Eq. 27,

$$p_c = \frac{2\gamma \cdot \cos\theta}{r} \tag{27}$$

And as the radius of the conduit is relatively easy to measure, together with the surface tension as well. And therefore, the key factor is to determine the contact angle of water to the conduit wall. This should be measured carefully, since the surface structure is very complex. Previous measurements

of contact angle between water and xylem conduits can be found on different kinds of plants,[178] and even though that of Flamingo is not listed or measured in the previous researches, it is closest to Melia azedarach. Flamingo and Melia azedarach are not in the same order or family, however, they all belong to Rosids. Plants of the same order or family shares very similar characters in such parameters, as is proved in previous researches, as is shown in Table. 5. And a simple comparison between two different types of Rosids from the researches is carried out as well, and it is found that parameters among the same order are close enough and the error is very limited[178]. Although this may still not be convincing enough, but another research also mentioned that the contact angle times surface tension in $2\gamma \cdot cos\theta$ is 0.1, which is the same result.[179] And therefore, the capillary pressure in the Flamingo xylem conduits should be,

$$p_c = \frac{0.1}{r} \tag{38}$$

While on the measurement of the radius, microscope is usually used. And the radius of xylem conduit for Flamingo is measured in Fig 6.11. As can be seen in Fig. 6.11, the upper image shows the cross section of the stem, with outermost parts barks of the stem, and inner part the regular xylems, which is the small circular shapes in the lower image, with a diameter of around 10μm. And this would be the average value for xylem conduit diameter in the following calculations.

Table 5: Contact angle of different species of Callitris[178]

Species	$\theta/°$
Drummondi	51
Endlicheri	50
Oblonga	59
Roei	49
Glaucophylla	50
Canescens	49
Rhomboidea	54
Baileyi	52
Columellaris	52
Preissii	47
Monticola	53
Muelleri	54

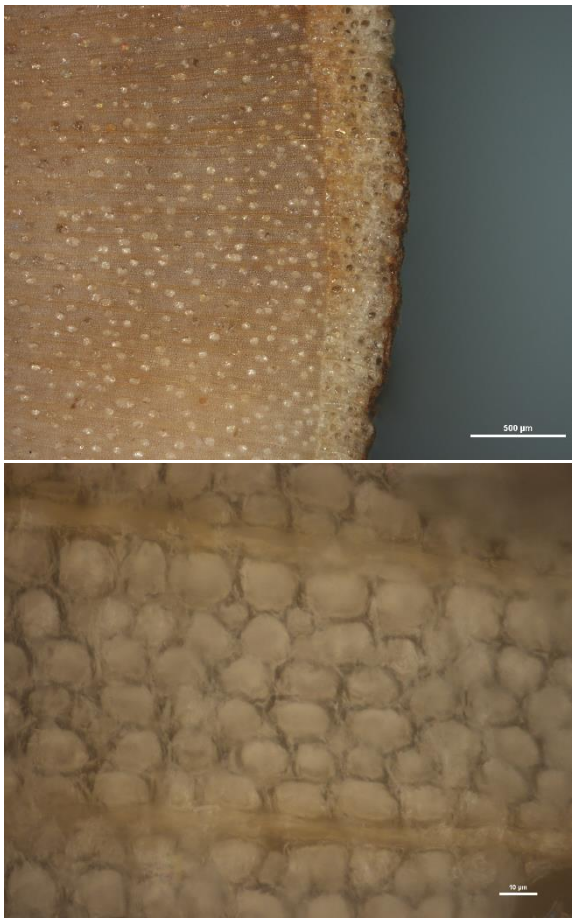

Figure 6. 11: Microscopic image of Flamingo's xylem conduits under microscope

As with transpiration effect, as is mentioned before, the pressure gradient generated by transpiration effect is difficult to analysis theoretically, and therefore an empirical theory is proposed to solve this issue, an analogue of the Ohm's Law[177], as is in Eq. 29 and Eq. 30.

$$-dP_x / dx = EA / K_h \tag{29}$$

$$P_x = \rho Q h / K_h \tag{30}$$

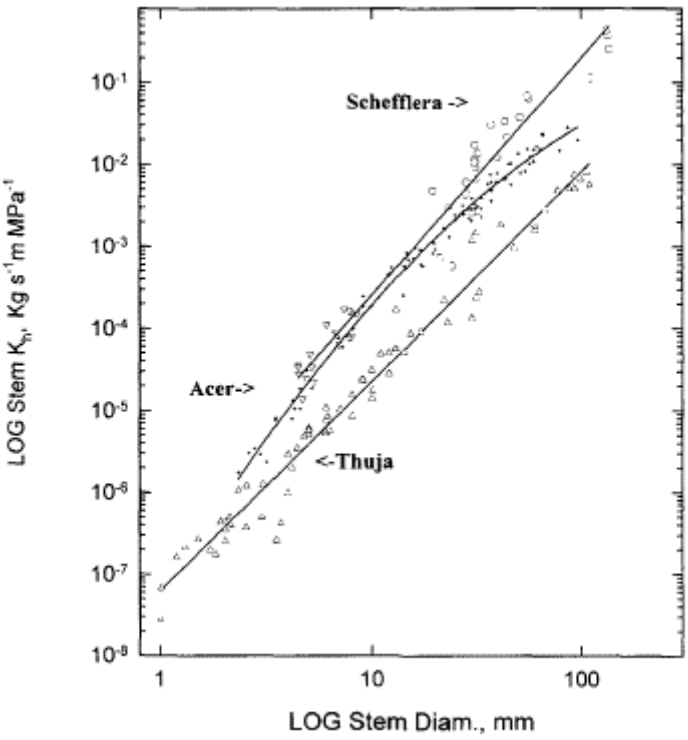

Figure 6. 12: Hydraulic conductivity of different species

with different stem diameter[177]

And in this equation, the density of water ρ, and the height of the xylem conduit *h*, are easy to achieve. As in this simplification of overall mathematical model, the water flowing up is mainly water solutions, and the density, viscosity and surface tension can be considered the same as water, which is a common simplification in previous researches. And since the velocity is what we want to achieve from the calculation of mathematical model, then the only parameter that needs to be measured is K_h, which is the hydraulic conductivity of Flamingo. Still, this parameter needs to be looked up in previous researches, which has been done for many times [180-182]. However, no data on Flamingo is found, and thus the K_h used here should be that of Acer (Maple). They are

very similar to each other in scientific classification, which is the same order Sapindales, though not in the same family. And the stem we use is 10mm, indicating the K_h of the xylem should be 7*10-4kg·m/(s·MPa).

The friction force is seen as the result of the helical structure in xylem conduits, with resistance higher than ideal. And there has only been a few papers working on the resistance of water flow in xylem[173, 178].

As is mentioned before, the resistance of water flow in xylem is written in the form of Darcy-Weisbach Equation, as is Eq. 35,

$$p_f = \rho \cdot f \cdot \frac{h}{d} \cdot \frac{u^2}{2} \tag{35}$$

If this is to present the friction force in water transport process in xylem, the density ρ, height or length of xylem conduits h, and conduit diameter d are all known. And the flow velocity u, which is to be calculated, should be kept in the equation as unknown. Therefore, the key problem is to determine the friction factor f.

In typical laminar flow, the friction factor should be as follow in Fanning's Law,

$$f = \frac{16}{\mathrm{Re}} = \frac{16\mu}{\rho u d} \tag{39}$$

Or four times higher in Darcy's Law.

$$f = \frac{64}{\mathrm{Re}} = \frac{64\mu}{\rho u d} \tag{40}$$

And at this time, it would become known as the Hagen-Poiseuille Equation in laminar flow,

$$\Delta P = \frac{8\mu LQ}{\pi r^2} \tag{41}$$

However, the water migration in xylem can't be simply considered as a laminar flow, even though the Reynold Number calculated from the experimental result as a reference is less than 1, due to the extremely low velocity in xylem.[183] As this seems different in plant xylem since researches shown that friction factors at different *ε/D* are much higher than ideal conduits.[177]

And therefore, the main work is to find the friction factor in xylem, or the number which is divided by Reynold Number, instead of 16 or 64 in laminar flow. And to discuss this, we have to define the boundary structure of the xylem conduit first.

In the simplification of the present work, if we turn the helical structure from three dimension down to two dimension, we will get the figure in Fig. 6.3a. And if we then convey the half cylinder into a *2a*a* form as in Fig. 6.3b, and the parameters of helical surface is,

$$\begin{aligned} \varepsilon &= d - \delta \\ \delta &= \sqrt{\frac{\pi}{4}} w \\ t &= \sqrt{\frac{\pi}{4}} \frac{w}{2} \end{aligned} \tag{42}$$

Table 6: Parameters of surface structure in Fig.3 [178]

Species	$d/\mu m$	$w/\mu m$
H. populnea	6.3	2.4
P. betulinus	7.3	1.4
M. azedarach	6.7	3.5
I. aquifolia	5.1	1.5
H. angustifolia	8.7	2.7
O. numularifolia	4.0	0.9
S. microphylla	3.8	1.6
S. tetraptera	2.7	1.3
P. edgerleyi	6.2	1.6

And here, as different types of plants have different parameters of the helical structure, thus the parameters of ε, d, δ, w and t should be borrowed from previous researches on other plants as well. And we also employ Melia azedarach here, and the structure can therefore be simplified, as listed in Table. 6.

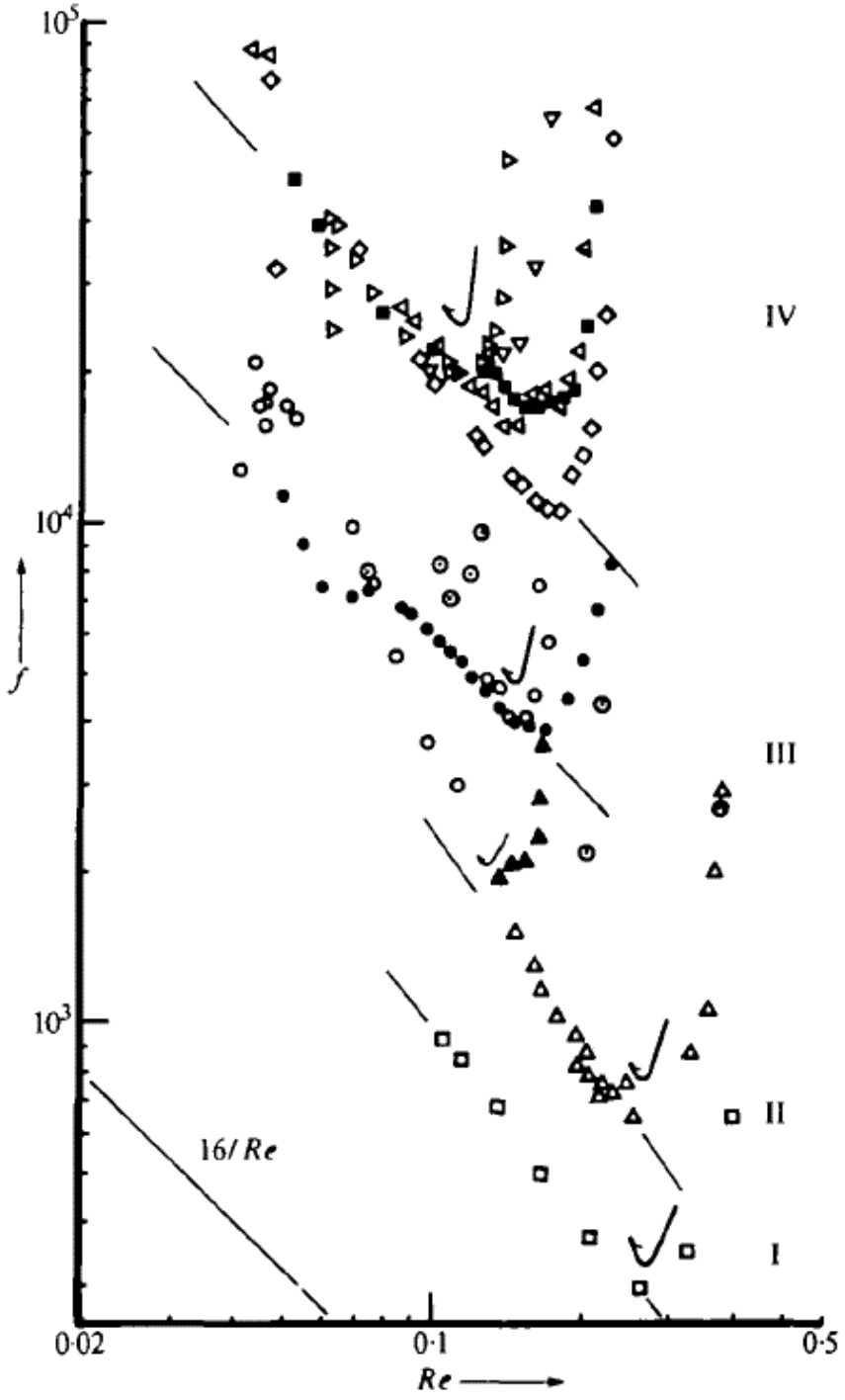

Figure 6. 13: Friction factor f versus Reynold number for water flow in xylem[173]

According to Jeje and Zimmermann's work[173], the friction factor of water flow in xylem falls into four different groups of surface roughness. And

they're calculated and tested in their work.

And different groups of data are listed below in Table. 7.

Table 7: Parameters of different groups[173]

Group	δ/d	t/D	$\delta(\mu m)$
I	0.45	0.19	2.3
II	0.25	0.18	2.3
III	NA	NA	NA
IV	0.6	0.1	8

Take the data into calculation, and

$$\begin{aligned} \delta / d &= 0.463 \\ t &= 1.551 \end{aligned} \tag{43}$$

So δ/d falls in group I. Then take the $D=10\mu m$,

$$t / D = 0.155 \tag{44}$$

which also roughly matches the group I in Jeje and Zimmermann's work. And then the friction factor can be seen. According to group I, the friction factor should be

$$f = \frac{90}{\mathrm{Re}} \tag{45}$$

in Fanning equation, or

$$f = \frac{360}{\mathrm{Re}} \tag{46}$$

in Darcy's equation.

By putting these forces together, the overall equation for all forces

involved in the mathematical model can be written as,

$$p_f + p_c + p_g + p_t = 0 \tag{47}$$

$$\rho f \frac{h}{d}\frac{u^2}{2} + \frac{0.1}{r} + \rho g h + \frac{\rho \pi r^2 u h}{K_h} = 0 \tag{48}$$

This would be the overall equation for all plants, and then put this equation into the Flamingo case in our experiment, by bringing in the parameters we mentioned before in this chapter. At the same time, in order to compare this mathematical model with the NMR experiment result, gravity has to be taken out, since the plant is lied down when doing NMR scan, which means water is moving horizontal, with all other forces. Even though the result may be higher than normal as previous research indicates without gravity affecting the water migration[184], the result would still be meaningful as to be examined whether it's accurate or not. And the result could be easily calculated, with all other parameters known already, which is 0.13mm/s.

It is only the average velocity in xylem, as water flows in different xylem conduits have different situations, at least in different diameters, which, the 10μm, is also an average value. And not to mention that in real cases, the volume flow rate in xylem is not equal, with some water may be absorbed by plant cells to be utilized, and also penetrate outward into other conduits, or inward from other conduits, as water can flow through the xylem walls as well. However, the relative flow within conduits would be ignored in an overall basis, and the amount used instead of vaporized is relatively small, so in our assumption and simplification, the conduit is considered as one solid wall tube

without water loss in any form.

6.5.4 Error discussion

From previous introductions in this chapter, now we have two velocities of water flow in plant xylems. The experimental measured velocity is 0.11mm/s using NMR, while the calculated velocity from mathematical model is 0.13mm/s. It is already not easy for numerical equations like this to match the experimental result in the same scale, and not to mention that the relative error is only 18.2%. And this result strongly proved the accuracy of the mathematical model, and the potential for the model to be adapted into further fields in engineering, such as micro-channel flow and heat pipes.

However, there still exists some error, which could be cause by some reasons.

(1) Some minor forces such as the root pressure are ignored, even though they may still more or less contribute to the water migration process

(2) The simplification of wall structures in friction calculation could cause some error

(3) The plant used in the present work is not tested for all the parameters used in the mathematical model, thus we use values for other plants of the same order or family instead. Some error may come from here, even though we have checked previously that plants of some order share almost the same value for those parameters.

6.6 Summary

In the present work, a novel mathematical model is proposed covering all major forces involved in the water migration process in plant xylem conduits. All forces are quantized and written in the form of pressure, including capillary force, gravity, transpiration effect and friction. The inner structure of xylem conduit is mentioned and simplified to calculate the friction factor.

To verify the mathematical model, a NMR experiment is carried out to compare with the result calculated from the mathematical model. And the two value match very well, indicating the model to be correct. And the error should be contributed by the ignorance of several minor forces such as root pressure, simplification in the calculation of friction, and the lack of direct values of the Salix Integra Flamingo's parameters such as hydraulic conductivity. And basing on these assumptions for the error analysis, further improvement on the accuracy of this model is needed.

Chapter 7: Conclusions and future work

7.1 Major accomplishments

In this dissertation, the NMR technology is employed to investigate several complex fluid dynamics and heat transfer issues, including nanofluid dynamic concentration measurement and bionic water migration system in plants. The following is a summary of our major accomplishments.

1. Investigation of nanofluid dynamic concentration

A novel method of nanofluid dynamic concentration measurement was developed to investigate the dynamic concentration gradient of nanofluid, and analyse the nanoparticle distribution when nanofluid is flowing in a pipe. A special type of nanofluid, ferrofluid, is tested. And the performance of ferrofluid under NMR is recorded, at different concentration and temperature.

A new parameter T_2^* is proposed in the present work. The concentration is closely relating to T_2^*, velocity and temperature. And the effects of velocity on dynamic concentration are considered in T_2^* in this work. An empirical equation for the performance of ferrofluid is proposed, using which dynamic concentration of ferrofluid can be traced back. Under dynamic experiment, temperature and T_2^* is measured, using thermocouple/thermometer and NMR. Then the concentration gradient across the pipe is calculated with the empirical equation. It is shown clearly that the concentration of ferrofluid when flowing

has a gradient across the radius, forming layers of concentration along the radius.

The nanoparticles of ferrofluid have a tendency of gathering around the boundary, together with other forces involved. The dynamic concentration shows that the highest concentration appears near the wall, and then the concentration decrease along the radius to the centre of the pipe. Thus with this special distribution of ferrofluid particles, the thermal conductivity and convective heat transfer coefficient of dynamic nanofluid flow is different from measured before in static condition. It is calculated to be a slightly enhancement of the thermal conductivity and convective heat transfer coefficient in the nanofluid flow, and that proves the needs to measure the concentration of nanofluid dynamically, instead of statically under TEM. And the result also indicates that our measuring method with NMR is workable. Even though the test concentration and temperature range is limited, that somehow is caused by the special properties of ferro and ferri oxide particles in ferrofluid. Therefore, this method is believed to be capable of applying onto other kinds nanofluids as well.

2. Investigation of water migration process in plants

All possible forces that may contribute to the water migration system in woody plants are considered and discussed in the present work. And a novel

methematical model is proposed based on the analysis of different forces in the water transport process within xylem conduits in woody plant stem. Finally, capillary force, gravity, transpiration force and friction force are listed out in the model, connected together in the xylem conduit under the Cohesion and Tension theory. And by simplifying the vessel's wall structure, we are able to find a way to put resistance into consideration as well.

And finally, a new mathematical model is proposed to calculate and predict the mean velocity of plants. And that velocity can be measured by the NMR as well, which is then campared with the calculated value. The results match each other very well, and only a small error occurs. This indicates that the mathematical model should be right and could be work on other similar cases in not just plants, but also engineering industries such as heat pipe and other divices that contains complex fluid flow.

3. Investigation of potential usage of NMR technology in engineering

We have developed two different ways of using NMR into engineering field, one in thermal engineering when measuring the concentration of nanofluid, the other measuring the pressure and flow velocity in living plants in situ for bionic engineering. Even though there exists many limits when using NMR, the technology still holds many advantages that previous measuring methods and technologies don't have.

First, NMR can measure the distribution of water inside livings such as plants without cutting them, especially with its high resolution, we can see details previously only in microscopy, and definitely not when plants are alive. This non-destructive property of NMR is very attracting to many researchers in various areas.

Second, NMR measures the signal of objects under magnetic pauses, which could pass through most materials. And as we confirmed previously in the experiment, the signals have relationship with temperature, type of solutions or nanofluids ,and concentration. And there could still be other aspects that could influence the signals. Thus it provides a new method to measure complex stuctures, such as fluid flow in complex situation. With signals detected from outside, many parameters that previously difficult to measure, can now be calculated from the signals in NMR, as long as it has relationship with signals.

And last,as NMR already has a long history of being used in biology science, it is a would be a very relavant technique for bionic engineering studies as well. Even though measurement in engineering studies and industy applications are far more complex, some basic phenomenon can be found in nature. And by studying the machanism of plants, animals or insects, we are able to find modern solutions to industrial questions. And in that process, NMR is proved to be a useful tool.

Therefore, using NMR in engineering field would be very interesting, and may have many further applications in other research fields.

7.2 Recommendations for future work

There are several possible further directions regarding the nanofluid dynamic concentration study and bionic engineering research in plant water migration, which are summarized as follows.

1. Further exploration in NMR nanofluid scanning

Although we have confirmed the possibility to use NMR in nanofluid dynamic concentration measurement, there still lies some problems. First, the temperature range of NMR machine is limited under boiling point, and the concentration of ferrofluid is limited under a low value as well. Signals of ferrofluid is totally invisible at over 1% volume concentration, while useful T_2^* values can only be achieved under 0.1% volume concentration. Even though other nanofluids beside ferrofluid can have higher concentration limits, but would still face the limitations as well.

Further research can be focused on how to broaden the limits from the NMR machine, by having deeper understandings of the NMR technology. What's more, in the current calculation, the compensation of the influence

from velocity on signals is carried out manually, it is hoped that an automatic program can be written by analysing the patterns of velocity influence with more experiments.

2. Theoretical analysis of concentration distribution and quantization

For the dynamic concentration, we have proved the existence of concentration gradient when nanofluid is flowing. However, it is now only able to explain the phenomenon with a few known forces and theories, without quantization. More research is hoped to be focused on the forces involved in the concentration layers.

Bringing Brownian movement, interface forces, friction forces and so on together, an overall theory and mathematical model will be proposed later to explain in detail the forces in the nanofluid flow. And with the concentration gradient measured in the experiment, numerical simulation should be drawn using the mathematical model to compare with the experimental result.

And for numerical simulation, microscale simulation method Molecular Dynamic (MD) or mesoscale simulation method Lattice Boltzmann Modelling (LBM) should be introduced and compared. It would be very promising if a mathematical model that could contain microscale forces and be proved and examined under numerical simulation will be proposed later in our work.

3. Improvement of mathematical model and parameter measurement

Even though the results from calculation and experiment matches each other very well, there still exists many errors potentially.

First, the mathematical model mainly focuses on the friction force, which previously seldom mentioned by researchers. And the present work simplifies the complex inner structure into 2D shape, and thus making it able to calculate. More detail of the helical structure can be discussed under Transmission Electron Microscopy (TEM), and put into the simplified model.

Second, many parameters in the calculation result comes from previous measurements by other researchers. However, the parameters of the plant we use in our experiment are not measured or mentioned in previous researches. So we are using parameters of other plants within the same family or order of the plant we use. Although it is examined previously that the same family or order share very similar values of those parameters, there still may have some error in this process. Further tests are required to measure accurate parameters of the exact plant we use, and others in further experiments.

And last, the NMR test in the present work contains huge numbers of averages during the scanning, and therefore creates much noise in the image. And these noise may generate some error in the calculation of fluid flow velocity, and thus cause uncertainty in the accurate velocity of fluid flow in

xylem conduit. Further step is required eliminate the noise in scanning process of NMR.

Appendix A: NMR performance of ferrofluid concentrations

A.1 Signals of SDS at different temperature

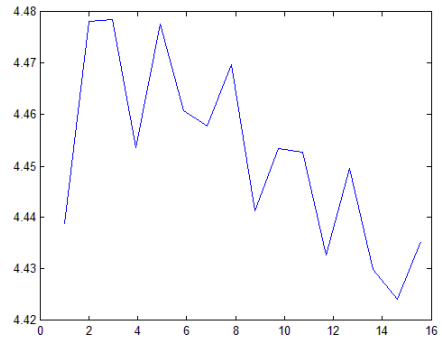

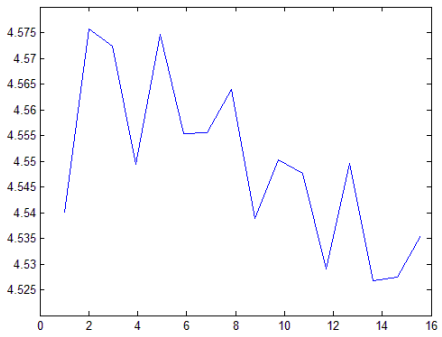

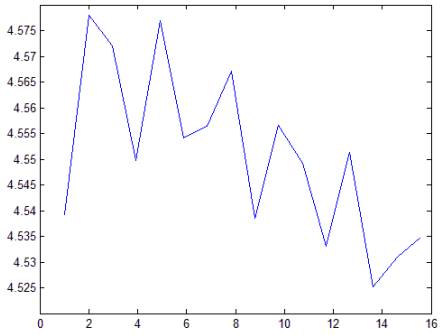

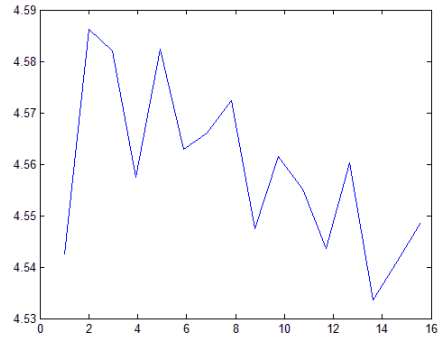

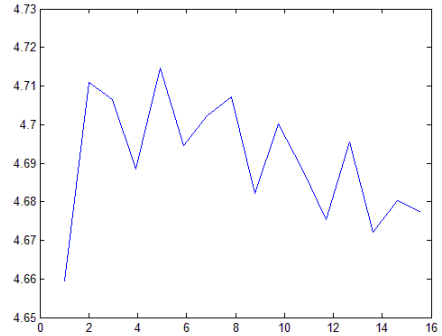

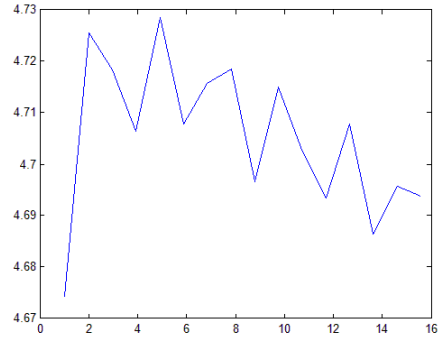

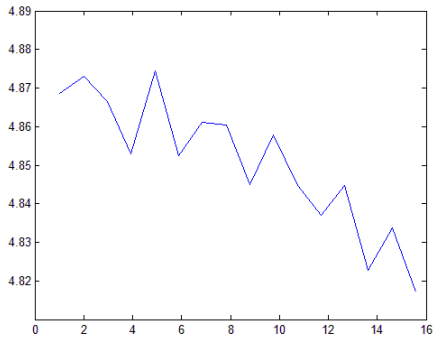
4.89
4.88
4.87
4.86
4.85
4.84
4.83
4.82
0 2 4 6 8 10 12 14 16

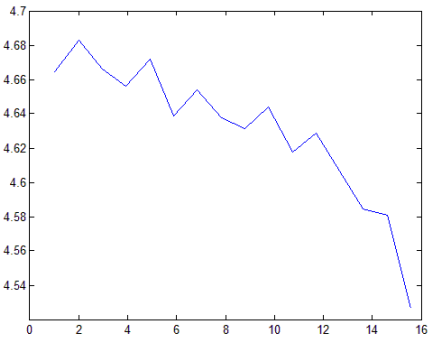
4.7
4.68
4.66
4.64
4.62
4.6
4.58
4.56
4.54
0 2 4 6 8 10 12 14 16

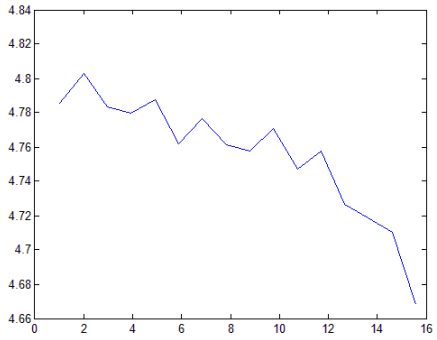
4.84
4.82
4.8
4.78
4.76
4.74
4.72
4.7
4.68
4.66
0 2 4 6 8 10 12 14 16

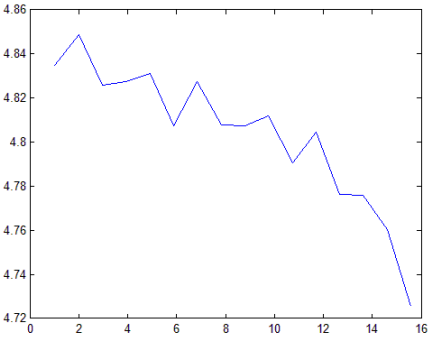
4.86
4.84
4.82
4.8
4.78
4.76
4.74
4.72
0 2 4 6 8 10 12 14 16

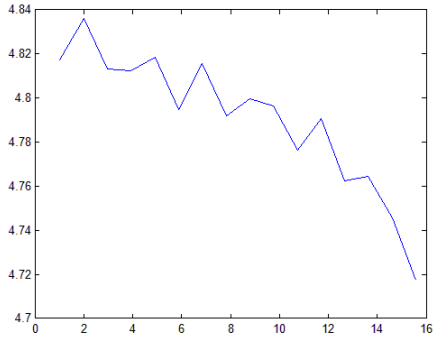
4.84
4.82
4.8
4.78
4.76
4.74
4.72
4.7
0 2 4 6 8 10 12 14 16

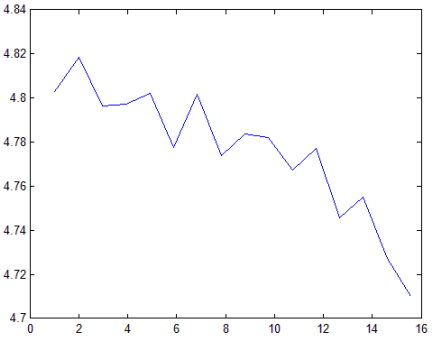
4.84
4.82
4.8
4.78
4.76
4.74
4.72
4.7
0 2 4 6 8 10 12 14 16

A.2 Signals of 0.01% volume concentration at different temperature

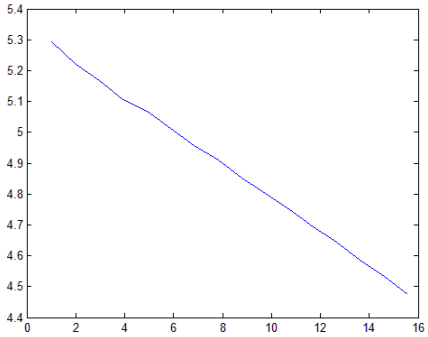
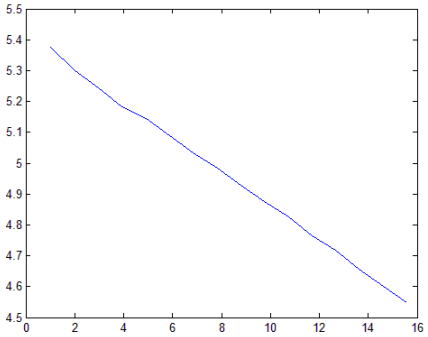
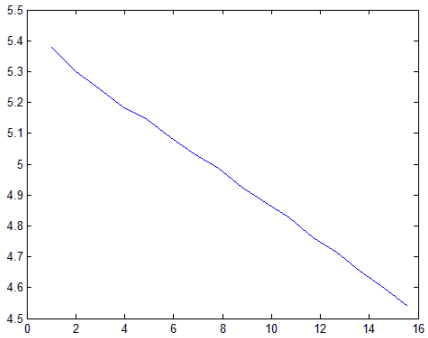
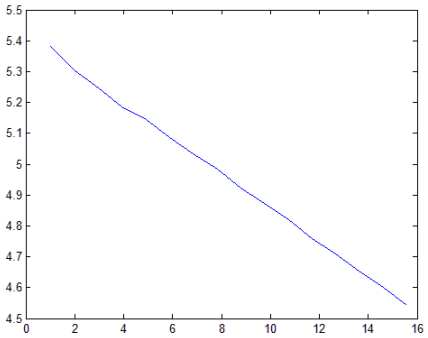
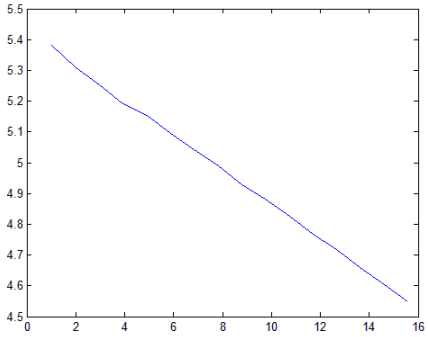
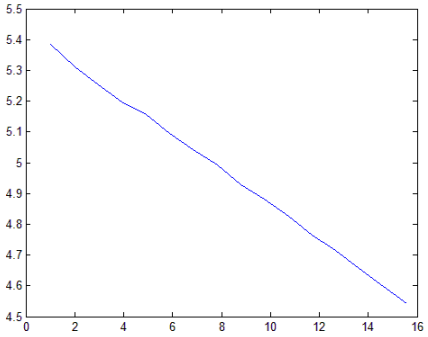
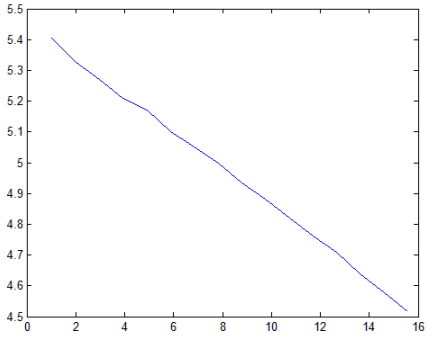
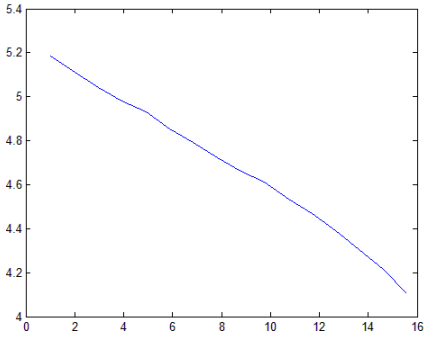

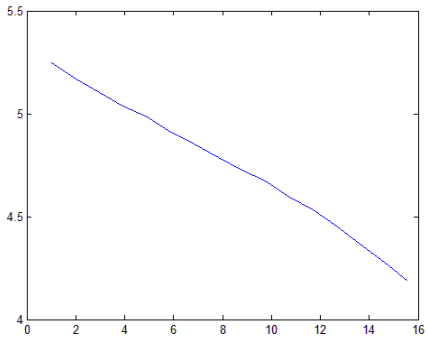

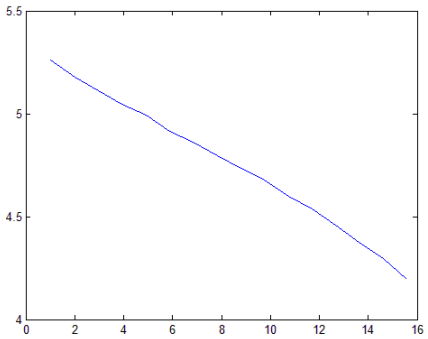

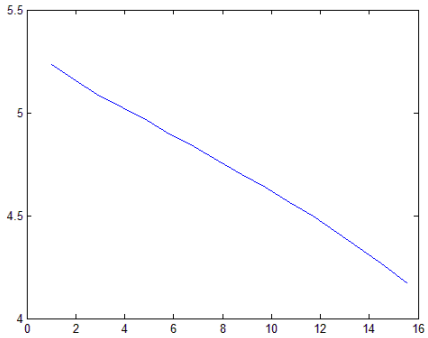

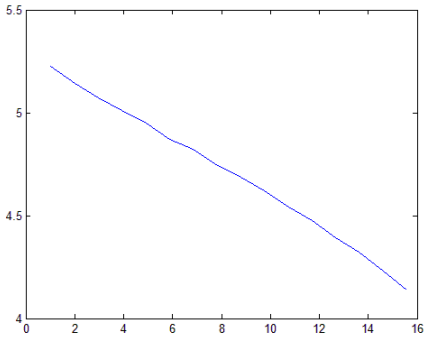

A.3 Signals of 0.03% volume concentration at different temperature

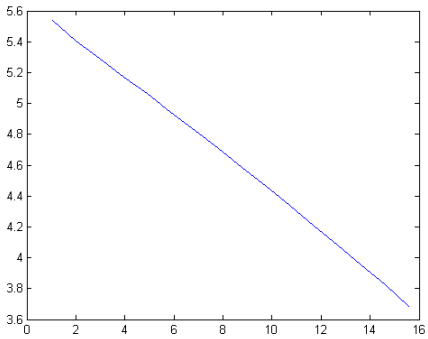

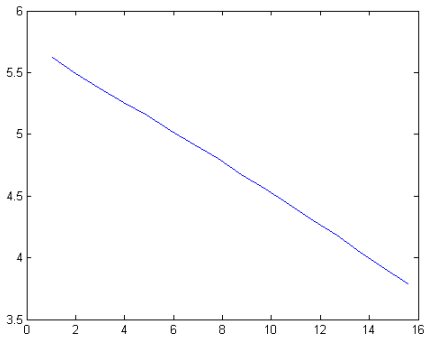

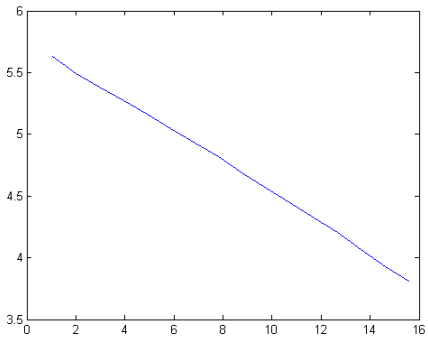
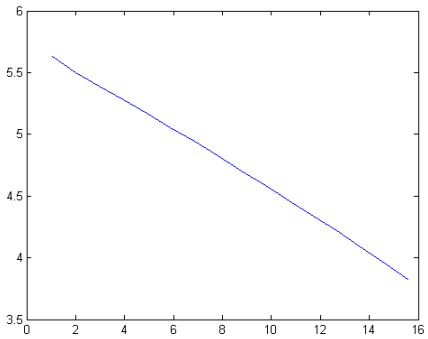
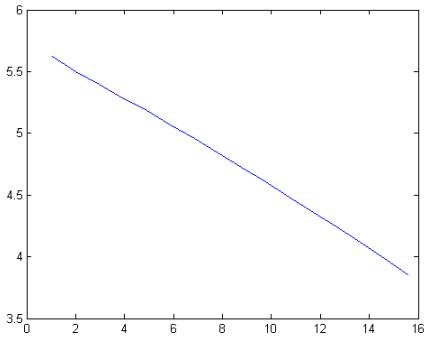
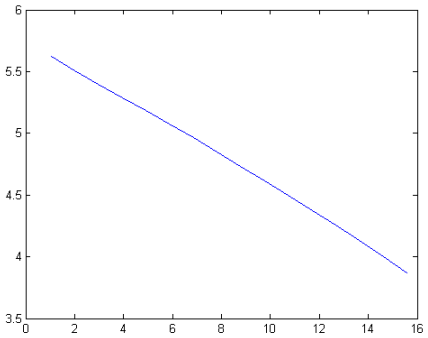
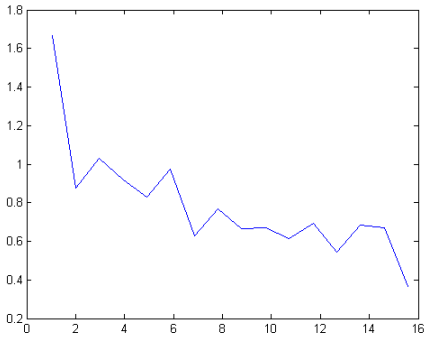
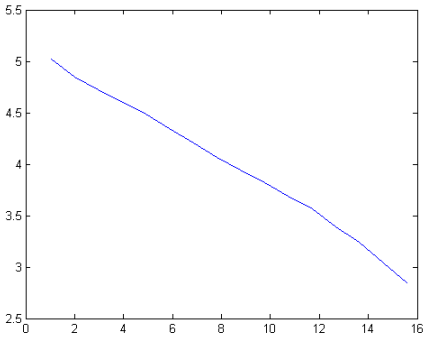
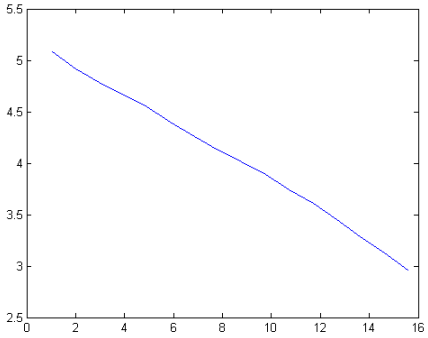
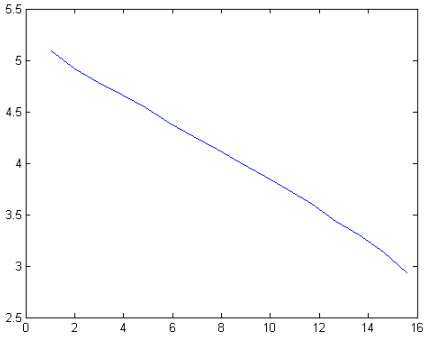

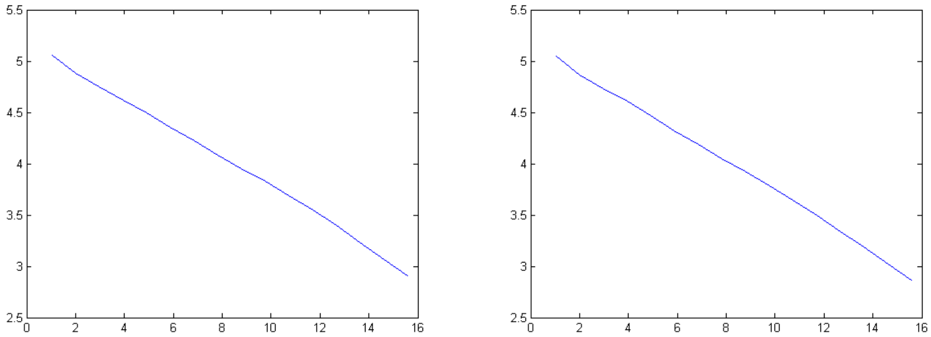

A.4 Signals of 0.05% volume concentration at different temperature

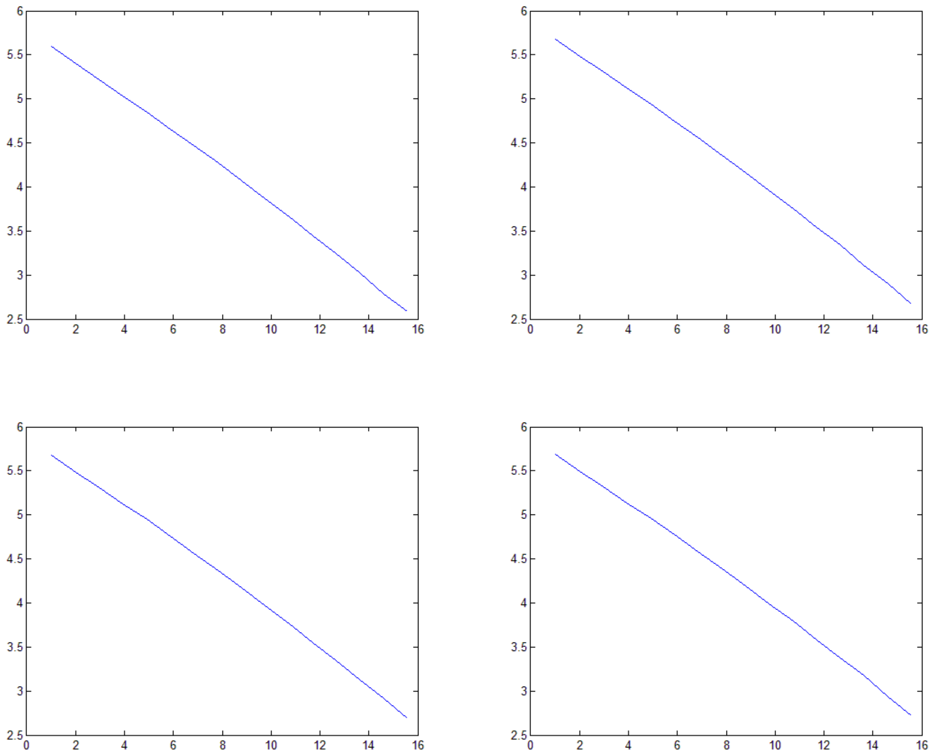

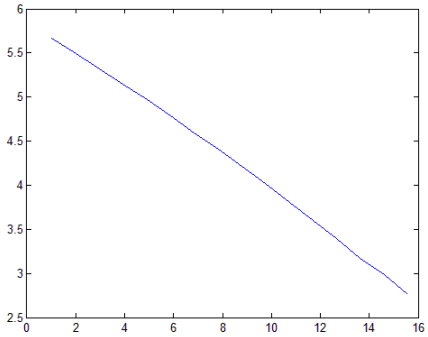
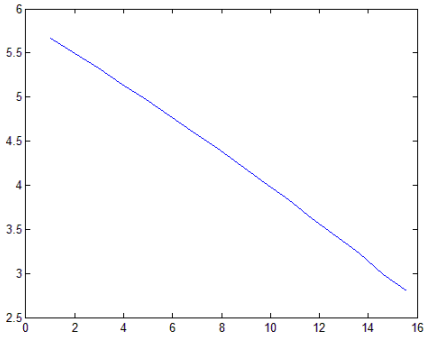
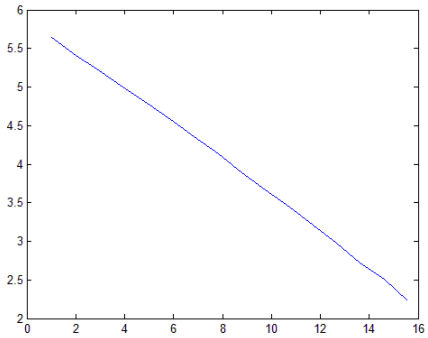
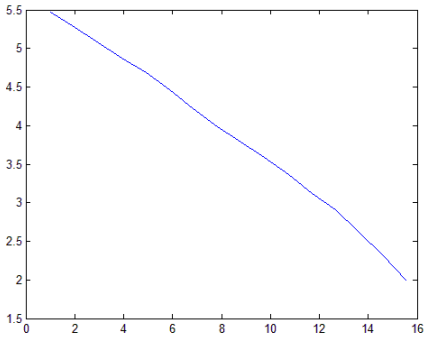
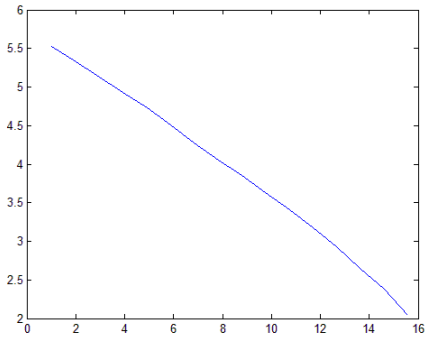
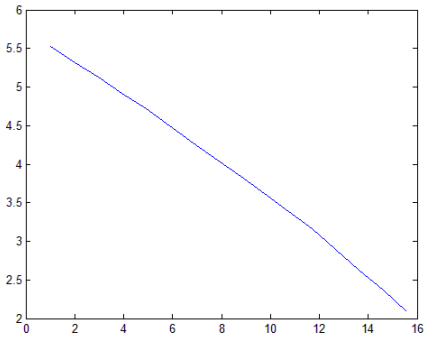
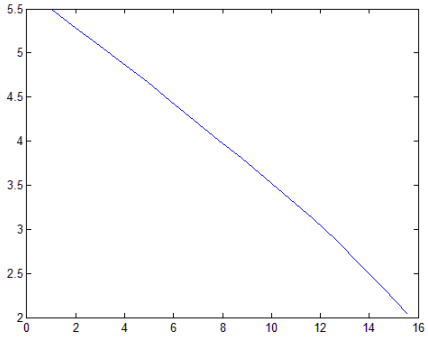
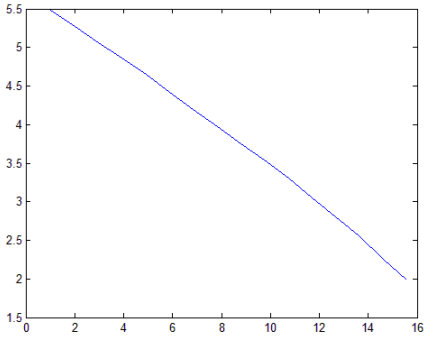

A.5 Signals of 0.07% volume concentration at different temperature

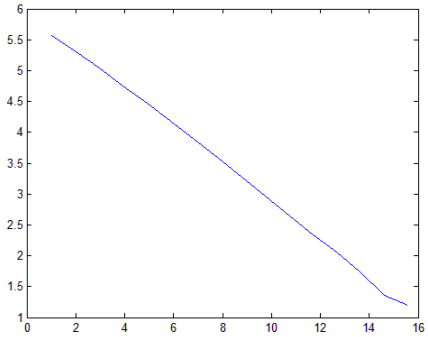
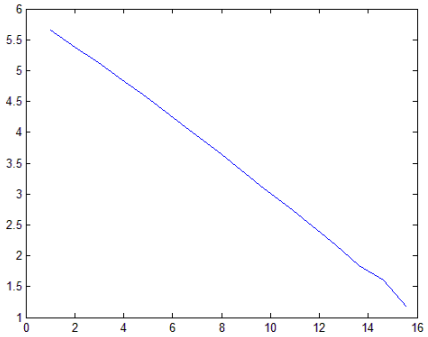
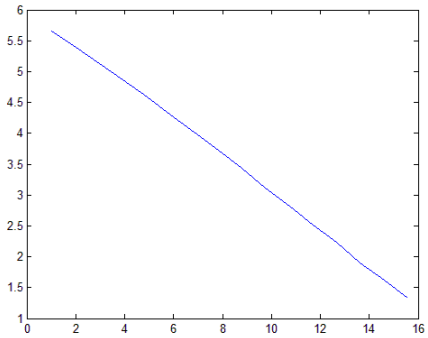
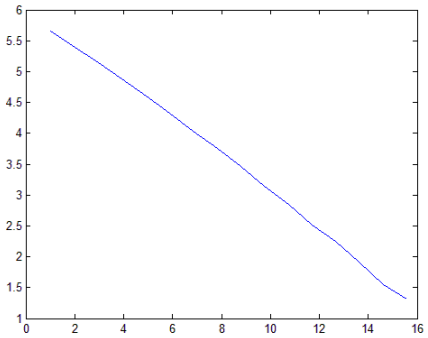
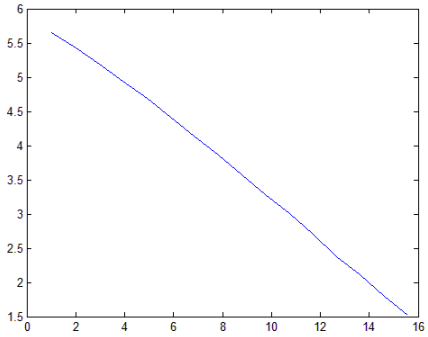
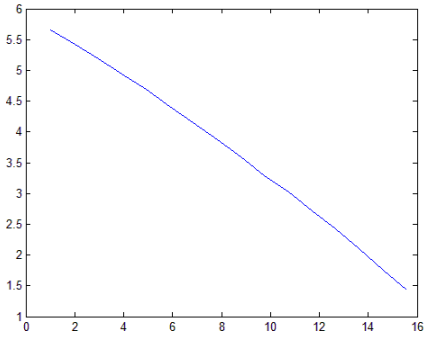
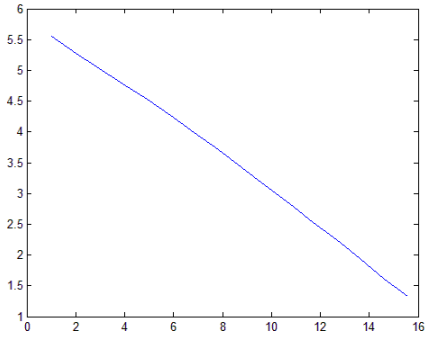
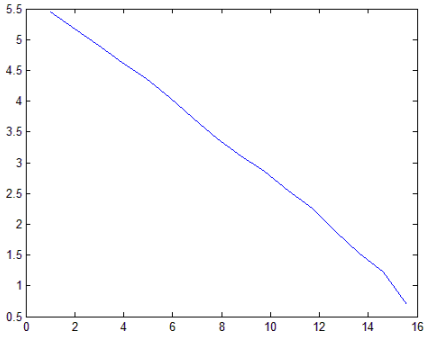

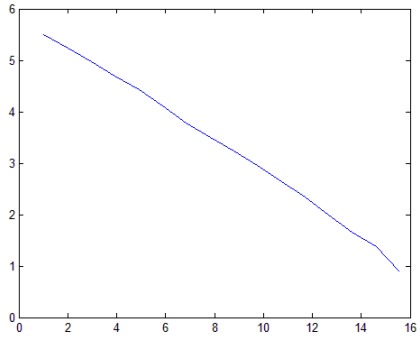
0
1
2
3
4
5
6
0
2
4
6
8
10
12
14
16

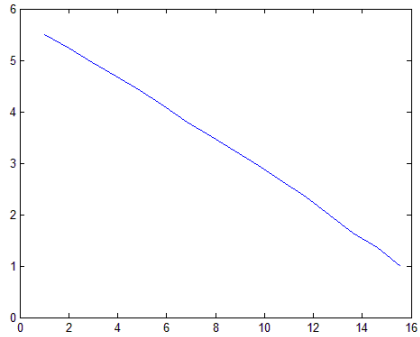
0
1
2
3
4
5
6
0
2
4
6
8
10
12
14
16

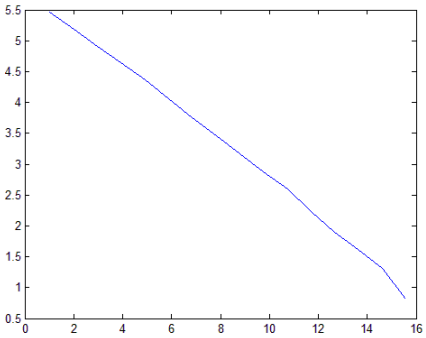
0.5
1
1.5
2
2.5
3
3.5
4
4.5
5
5.5
0
2
4
6
8
10
12
14
16

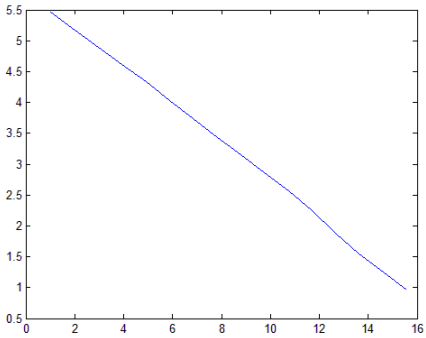
0.5
1
1.5
2
2.5
3
3.5
4
4.5
5
5.5
0
2
4
6
8
10
12
14
16

A.6 Signals of 0.1% volume concentration at different temperature

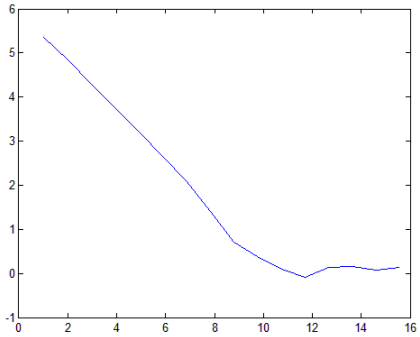
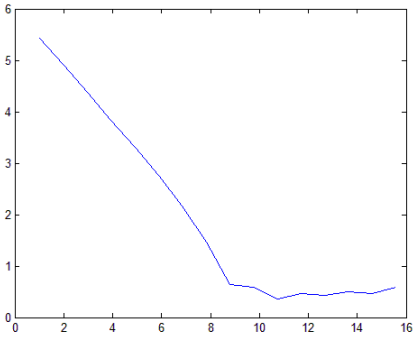
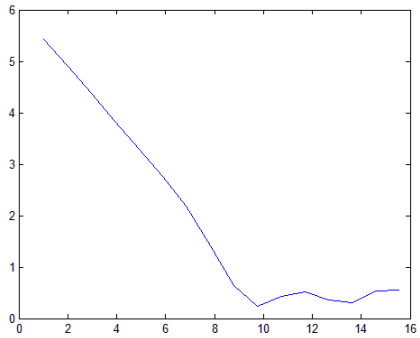
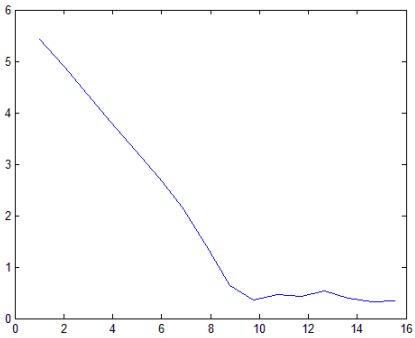
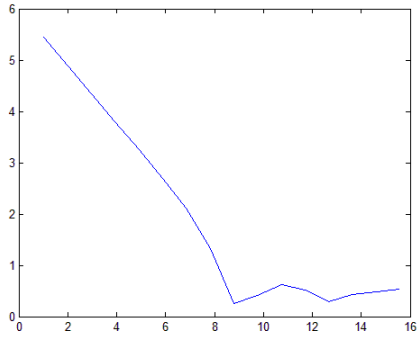
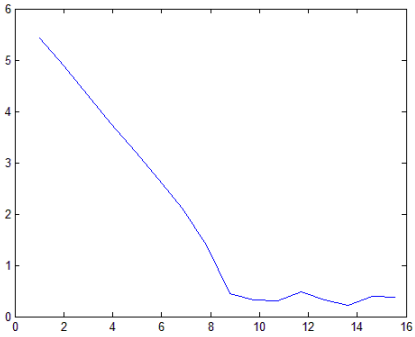
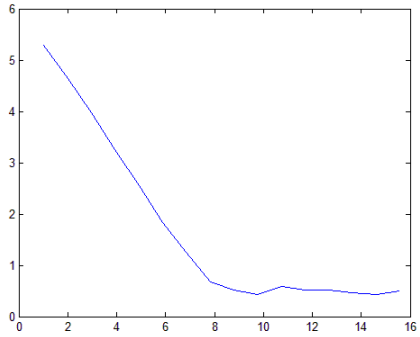
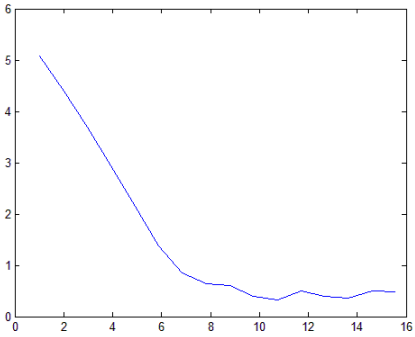

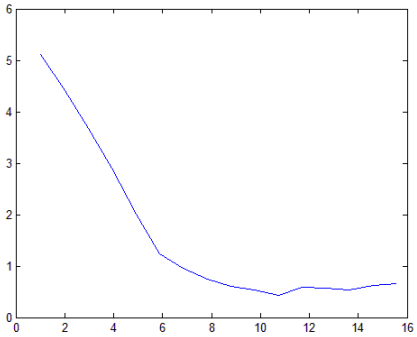
0 1 2 3 4 5 6
0 2 4 6 8 10 12 14 16

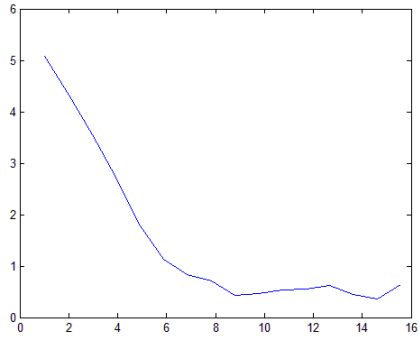
0 1 2 3 4 5 6
0 2 4 6 8 10 12 14 16

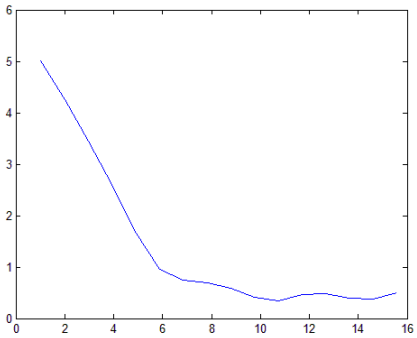
0 1 2 3 4 5 6
0 2 4 6 8 10 12 14 16

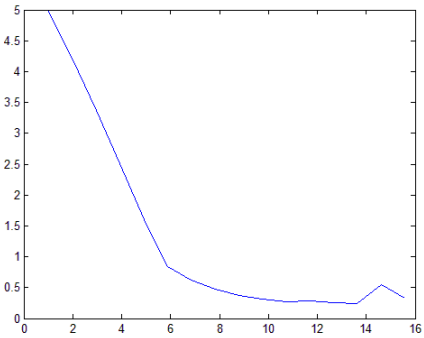
0 0.5 1 1.5 2 2.5 3 3.5 4 4.5 5
0 2 4 6 8 10 12 14 16

A.7 Log signals of different concentration

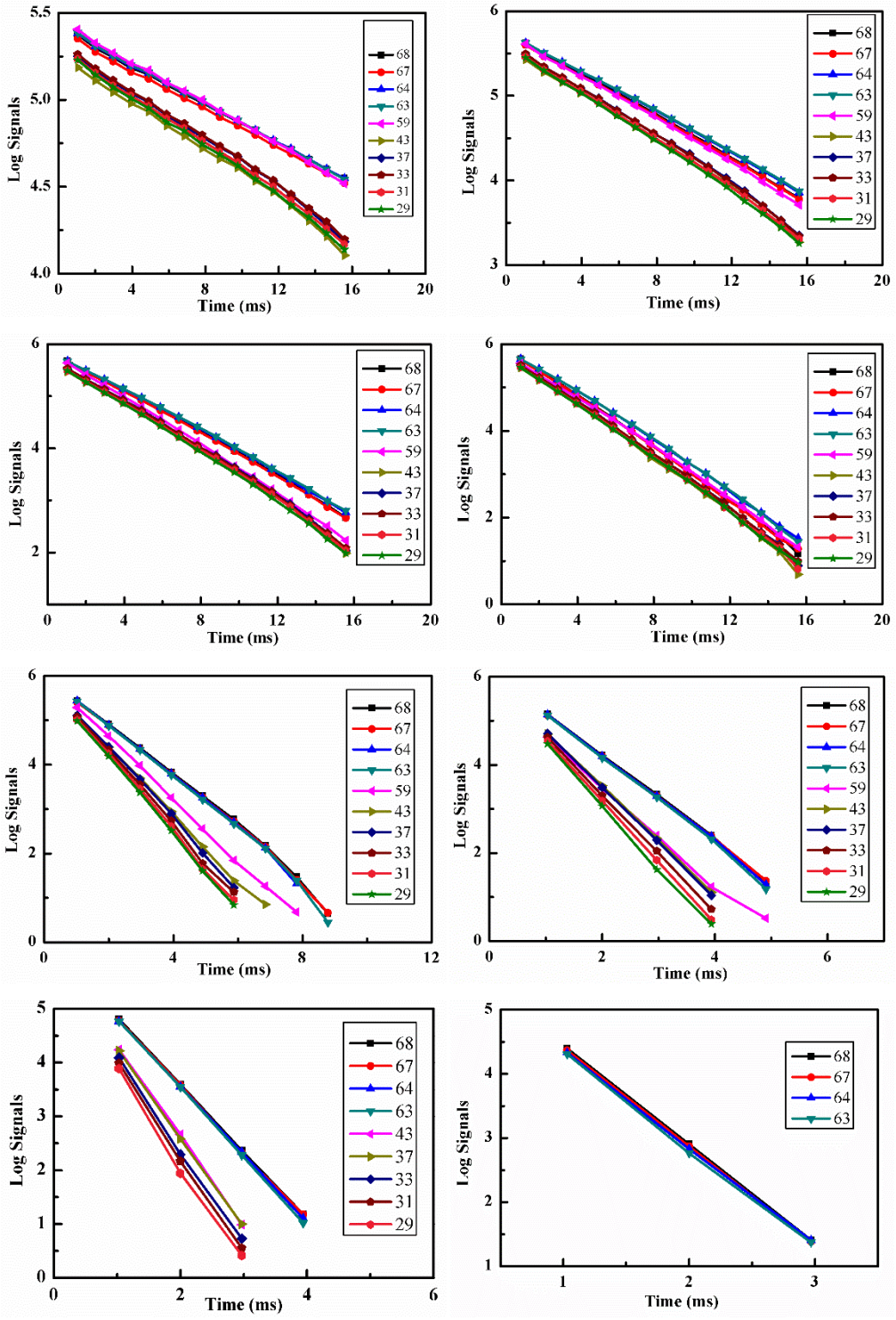

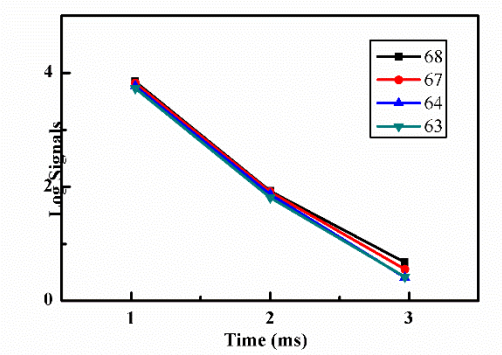

A.8 Log signals of different temperature

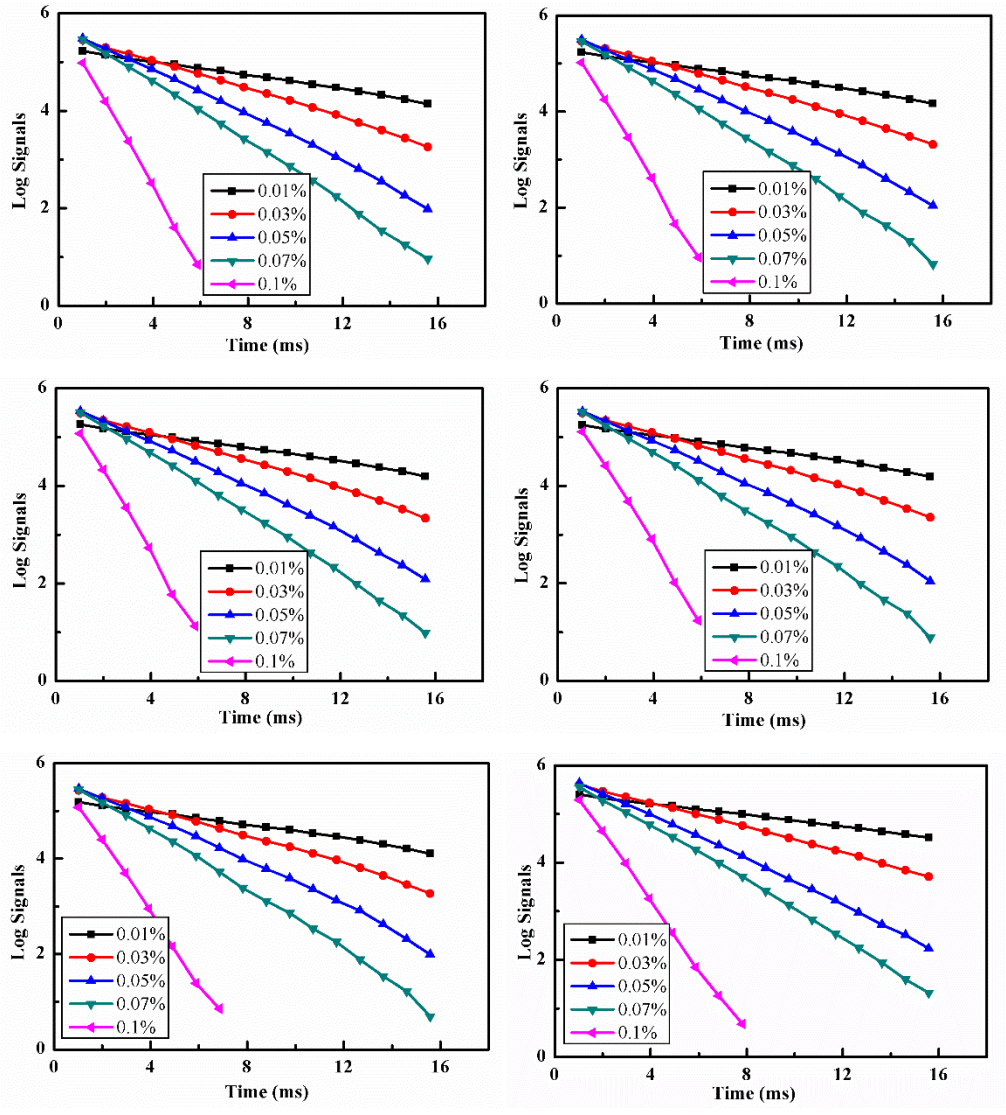

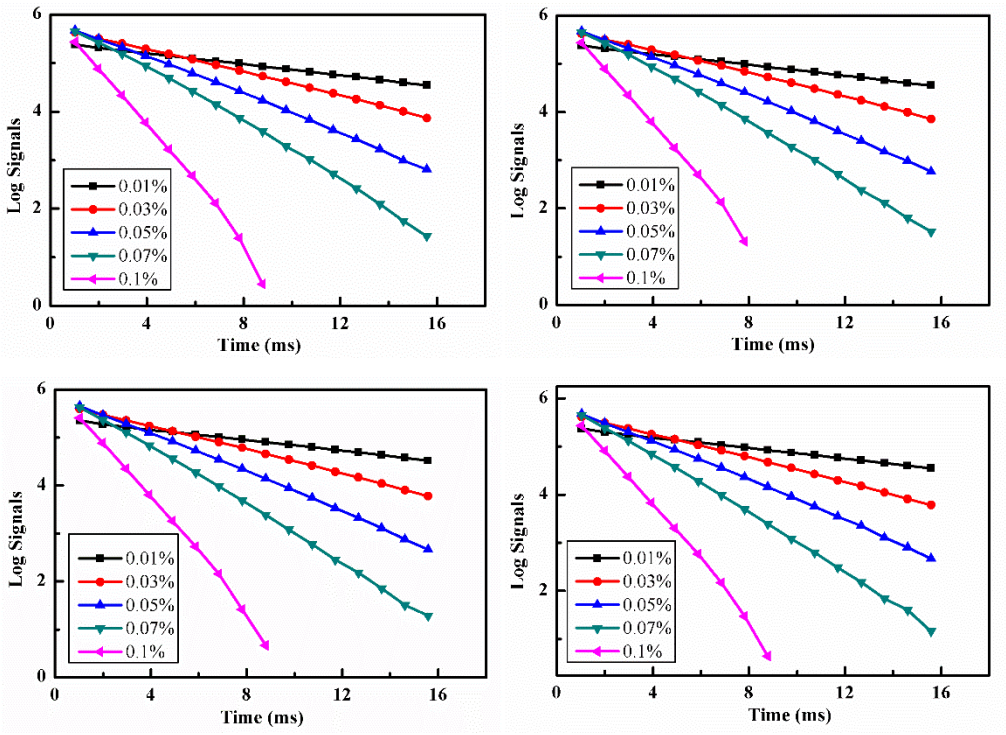
Log Signals
Time (ms)
0.01%
0.03%
0.05%
0.07%
0.1%

Appendix B: NMR performance of plant water migration

B.1 Profile for Cactus

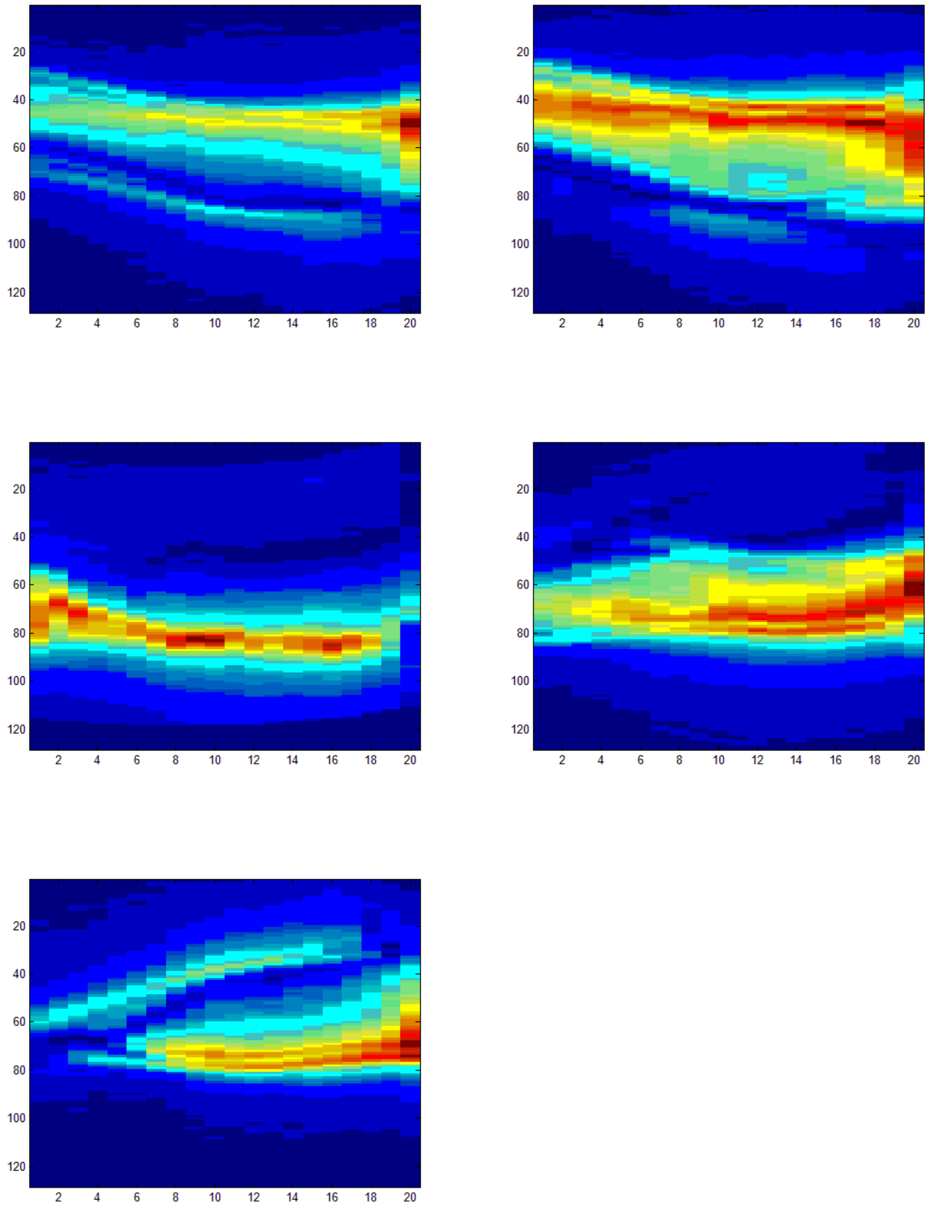

B.2 Profile for Musa × Paradisiaca

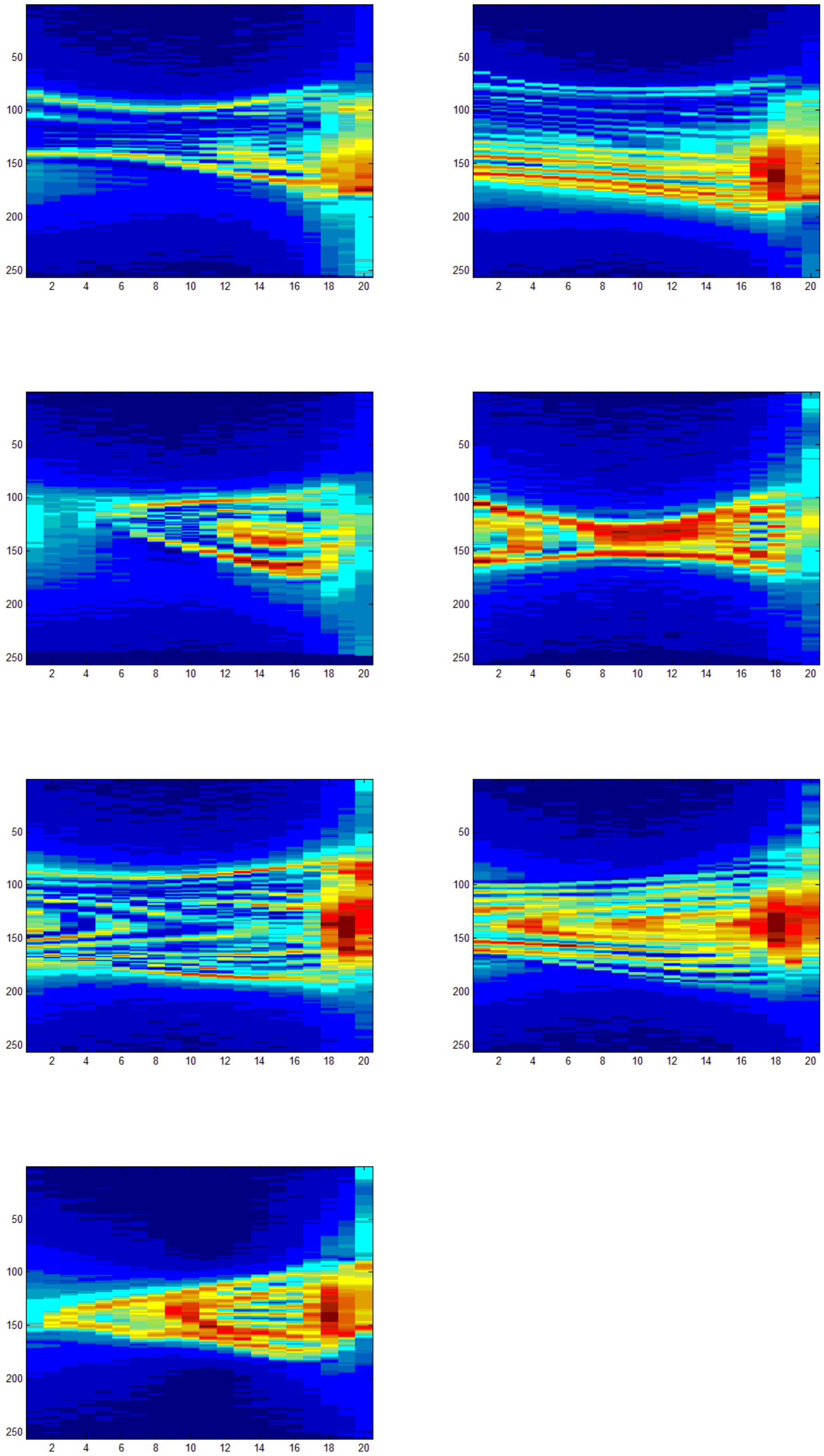

B.3 Profile for Salix Integra Flamingo

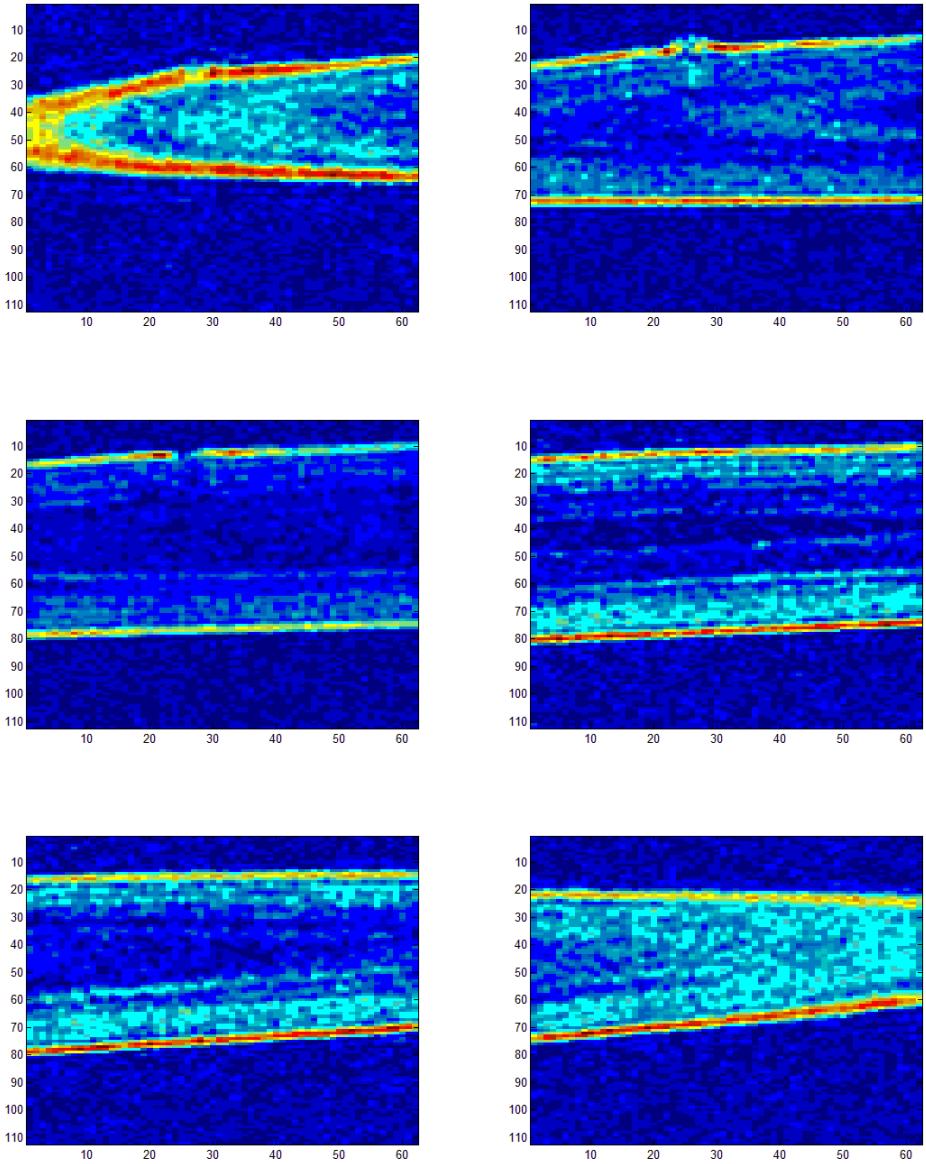

B.4 Water flow in xylem with noise

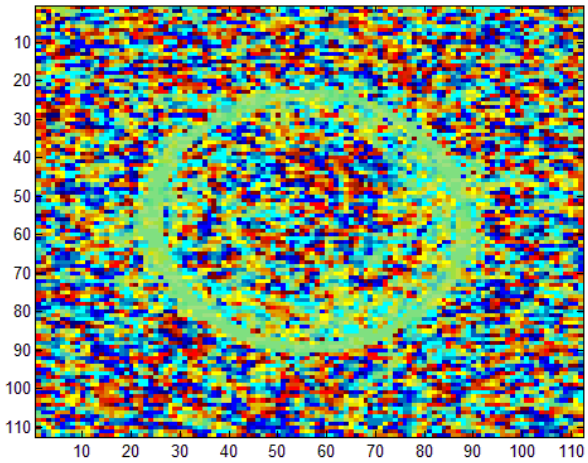

Appendix C: Matlab sample coding for NMR data

C.1 Coding for T_2 decay line from Figure 4.1

```
%    Obtain data from .mat file

%    Print and image

%    Pick out a box and plot a graph of amplitude (T2 decay)

close all

clear all


[file,pathname] = uigetfile('T2*.mat');

load([pathname,file])


% Images should be in matrix I

% plot an image


imagesc(I(:,:,1)');

% could be any image number 1 - 16

% note that imaged is transposed, use ' operator to get same image as scanner

% matrix images are printed by column, row

% example of plot of T2 decay

% the numbers for the region of interest come from the image
```

```
for i=1:16
    S(i) = sum(sum(I(82:89,143:148,i)));
    % change these for different tubes
end
figure
plot(S);
```

C.2 Coding for static concentration T_2 at different tubes in Figure 3.6

```
% get file data

images = 16;
columns = 144;
rows = 144;
[file,pathname] = uigetfile('*.REC');
%read data from file
%load([pathname,file]);

data_file1 = [pathname,file];
```

```
file_id = fopen(data_file1,'r','ieee-le');

data=fread(file_id,[2*columns*rows*images,'int16');


I = reshape(data,rows,columns,images);


A1(:,:) = I(:,:,1);

imagesc(A1);


% choose an image to plot.    The transpose is to show it on the screen

correctly

% Extract a region of interest and plot across TE values

% get the numbers from the image and remember to transpose.


for i=1:images

S(i) = sum(sum(I(20:40,40:100,i)));

% change these numbers for different tubes

% 20:40,40:100 is for the water outside

% 33:43,80:88 is for the 0.5%

% 59:69,80:88 is for the 0.4%

% 78:88,80:88 is for the 0.3%

% 103:113,80:88 is for the 0.2%
```

```
% 33:43,59:67 is for the 0.1%

% 59:69,59:67 is for the 0.05%

% 78:88,59:67 is for the 0.01%

% 103:113,59:67 is for SDS solution

% solution, image set 3


S(i)=S(i)/1281;

% change to average

TE(i) = 1.04 * 0.95 * (i-1);

% generate TE values in milli-sec

end


figure

Sln = log(S);

plot(TE,Sln);

% -1/T2* is the slope of this graph taking care to exclude any points which hit

the noise baseline

% save data as matrix file


[file,pathname] = uiputfile('*.mat');

save([pathname,file],'TE','S');
```

C.3 Coding for dynamic concentration distribution at each point

```
%% get file data


images = 16;

columns = 80;

rows = 80;


[file,pathname] = uigetfile('*.REC');

% read data from file

% load([pathname,file]);


data_file1 = [pathname,file];


file_id = fopen(data_file1,'r','ieee-le');

data=fread(file_id,[2*columns*rows*images],'int16');

I = reshape(data,rows,columns,images);

A1(:,:) = I(:,:,2);


% choose an image to plot.    The transpose is to show it on the screen

correctly
```

```
imagesc(A1);


% Extract a region of interest and plot across TE values

% get the numbers from the image and remember to transpose.


      for i=2:images

            for j=36:45

                  for k=37:47

                        S(j-35,k-36,i-1)=I(j,k,i);

                     % change these numbers for different tubes

                     % 38:43,40:43 is for overall

                     % solution, image set 3

                  end;

            end;

TE(i-1) = 0.53 * 0.974 * (i-1);

% generate TE values in milli-sec

end;


% use empirical equation to calculate concentration from T2


a=-7.38-0.028*45;

b=3.63+0.014*45;
```

```
c=-0.0043-0.000048*45;
NN=zeros(10,11);
concen=zeros(10,11);


for j=1:10
    for k=1:11
        for i=1:15
            ss(i)=log(S(j,k,i));
        end;
        p=polyfit(TE,ss,1);
        NN(j,k)=p(1);
        NN(j,k)=-1/NN(j,k);
        NN(j,k)=(a-NN(j,k))/b;
        concen(j,k)=exp(NN(j,k))-c;
        if concen(j,k)>0.1
            concen(j,k)=0.1;
        end;
    end;
end;
imagesc(concen);
```

C.4 Coding for dynamic concentration flow profile in Figure 5.2

```
% get file data


images = 2;

columns = 128;

rows = 128;

[file,pathname] = uigetfile('*.REC');

% read data from file

% load([pathname,file]);


data_file1 = [pathname,file];


file_id = fopen(data_file1,'r','ieee-le');

data=fread(file_id,[2*columns*rows*images],'int16');

I = reshape(data,rows,columns,images);


A1(:,:) = I(:,:,1)';

A2(:,:) = I(:,:,2)';

%A3(:,:) = I(:,:,3)';

% velocity phase

RI = -50.00000 ;

%-50.00000       0.02442 4.09500e+001
```

```
RS = 0.02442 ;

SS = 4.09500e+001 ;

DV = A2 * RS + RI;

FP = DV / (RS * SS);

%    fsvel = 70; %mm/s


Flow = FP; % already vencoded * fsvel/pi ;


imagesc(A1);

figure

imagesc(Flow);


% save data as matrix file


[file,pathname] = uiputfile('*.mat');

save([pathname,file],'A1','Flow')
```

C.5 Coding for noise elimination in nanofluid dynamic concentration measurement

```
A2(:,:)=A1(:,:);
for i=1:128
    for j=1:128
        if A1(i,j)<1000
            A2(i,j)=0;
        else
            A2(i,j)=1;
        end;
    end;
end;
A3=A2.*Flow;
imagesc(A3);
```

C.6 Coding for noise elimination in Salix Integra Flamingo water flow velocity measurement

```
load Image7.mat
thred=zeros(112,112);
s=0;
```

```
n=0;
se=0;
for i=1:112
    for j=1:112
        if A(i,j)>=100
            thred(i,j)=A(i,j);
            n=n+1;
        end;
    end;
end;
%imagesc(thred);
news=zeros(112,112);
for i=1:112
    for j=1:112
        if thred(i,j)~=0
            news(i,j)=Flow(i,j);
            s=s+news(i,j);
        else
            news(i,j)=0;
        end;
    end;
end;
```

```
imagesc(news);
s=s/n;
for i=1:112
    for j=1:112
        if thred(i,j)~=0
            se=se+(news(i,j)-s)*(news(i,j)-s);
        end;
    end;
end;
s
se=sqrt(se/n);
se
```

Reference

1. Gidaspow, D., *Multiphase flow and fluidization: continuum and kinetic theory descriptions*. 1994: Academic press.
2. Prosperetti, A. and G. Tryggvason, *Computational methods for multiphase flow*. 2007: Cambridge Univ Pr.
3. Bergman, T.L., et al., *Fundamentals of heat and mass transfer*. 2011: John Wiley & Sons.
4. Pletcher, R.H., J.C. Tannehill, and D. Anderson, *Computational fluid mechanics and heat transfer*. 2012: CRC Press.
5. Patankar, S., *Numerical heat transfer and fluid flow*. 1980: CRC press.
6. Wang, X.-Q. and A.S. Mujumdar, *Heat transfer characteristics of nanofluids: a review.* International journal of thermal sciences, 2007. **46**(1): p. 1-19.
7. Nkurikiyimfura, I., Y. Wang, and Z. Pan, *Heat transfer enhancement by magnetic nanofluids—A review.* Renewable and Sustainable Energy Reviews, 2013. **21**: p. 548-561.
8. Sivashanmugam, P., *Application of nanofluids in heat transfer*. 2012: INTECH Open Access Publisher.
9. Minkowycz, W., E.M. Sparrow, and J.P. Abraham, *Nanoparticle Heat Transfer and Fluid Flow*. Vol. 4. 2012: CRC press.
10. Das, S.K., et al., *Nanofluids: science and technology*. 2007: John Wiley & Sons.
11. Kakaç, S. and A. Pramuanjaroenkij, *Review of convective heat transfer enhancement with nanofluids.* International Journal of Heat and Mass Transfer, 2009. **52**(13–14): p.

3187-3196.

12. Kim, S.H., S.R. Choi, and D. Kim, *Thermal Conductivity of Metal-Oxide Nanofluids: Particle Size Dependence and Effect of Laser Irradiation.* Journal of Heat Transfer, 2006. **129**(3): p. 298-307.

13. Vincent, J.F., et al., *Biomimetics: its practice and theory.* Journal of the Royal Society Interface, 2006. **3**(9): p. 471-482.

14. ISBE, *Bionic engineering images.*

15. Serrano, E., G. Rus, and J. Garcia-Martinez, *Nanotechnology for sustainable energy.* Renewable and Sustainable Energy Reviews, 2009. **13**(9): p. 2373-2384.

16. Maxwell, J.C., *A treatise on electricity and magnetism*. Vol. 1. 1881: Clarendon press.

17. Wong, K.V. and O. De Leon, *Applications of nanofluids: current and future*. Advances in Mechanical Engineering, 2010. **2010**.

18. Kim, S., et al., *Surface wettability change during pool boiling of nanofluids and its effect on critical heat flux.* International Journal of Heat and Mass Transfer, 2007. **50**(19): p. 4105-4116.

19. Chopkar, M., P.K. Das, and I. Manna, *Synthesis and characterization of nanofluid for advanced heat transfer applications.* Scripta Materialia, 2006. **55**(6): p. 549-552.

20. Singh, D., J. Toutbort, and G. Chen, *Heavy vehicle systems optimization merit review and peer evaluation.* Annual Report, Argonne National Laboratory, 2006. **23**: p. 405-411.

21. Kao, M., et al., *Copper-oxide brake nanofluid manufactured using arc-submerged nanoparticle synthesis system.* Journal of Alloys and Compounds, 2007. **434**: p.

672-674.

22. Kleinstreuer, C., J. Li, and J. Koo, *Microfluidics of nano-drug delivery.* International Journal of Heat and Mass Transfer, 2008. **51**(23): p. 5590-5597.

23. Bica, D., et al., *Sterically stabilized water based magnetic fluids: Synthesis, structure and properties.* Journal of Magnetism and Magnetic Materials, 2007. **311**(1): p. 17-21.

24. Wasan, D.T. and A.D. Nikolov, *Spreading of nanofluids on solids.* Nature, 2003. **423**(6936): p. 156-159.

25. Borbath, T., et al., *Leakage-free rotating seal systems with magnetic nanofluids and magnetic composite fluids designed for various applications.* International Journal of Fluid Machinery and Systems, 2011. **4**(1): p. 67-75.

26. Saidur, R., K. Leong, and H. Mohammad, *A review on applications and challenges of nanofluids.* Renewable and sustainable energy reviews, 2011. **15**(3): p. 1646-1668.

27. Mukherjee, S. and S. Paria, *Preparation and stability of nanofluids-A Review.* IOSR Journal of Mechanical and Civil Engineering, 2013. **9**(2): p. 63-69.

28. Yu, W. and H. Xie, *A review on nanofluids: preparation, stability mechanisms, and applications.* Journal of Nanomaterials, 2012. **2012**: p. 1.

29. Wen, D., et al., *Review of nanofluids for heat transfer applications.* Particuology, 2009. **7**(2): p. 141-150.

30. Zhao, C.-X., *Multiphase flow microfluidics for the production of single or multiple emulsions for drug delivery.* Advanced drug delivery reviews, 2013. **65**(11): p. 1420-1446.

31. Zhou, J., et al., *Tribological behavior and lubricating mechanism of Cu nanoparticles in oil.* Tribology Letters, 2000. **8**(4): p. 213-218.

32. Vonarbourg, A., et al., *Parameters influencing the stealthiness of colloidal drug delivery systems.* Biomaterials, 2006. **27**(24): p. 4356-4373.

33. Singh, R. and J.W. Lillard, *Nanoparticle-based targeted drug delivery.* Experimental and molecular pathology, 2009. **86**(3): p. 215-223.

34. Bianco, A., K. Kostarelos, and M. Prato, *Applications of carbon nanotubes in drug delivery.* Current opinion in chemical biology, 2005. **9**(6): p. 674-679.

35. Sharma, T., et al., *Development of carbon nanotubes and nanofluids based microbial fuel cell.* International journal of hydrogen energy, 2008. **33**(22): p. 6749-6754.

36. Chol, S., *Enhancing thermal conductivity of fluids with nanoparticles.* ASME-Publications-Fed, 1995. **231**: p. 99-106.

37. Choi, S., *Nanofluids for improved efficiency in cooling systems, In; Heavy vehicle system review.* Argonne National Laboratroy: April, 2006: p. 18-21.

38. Liu, M.-S., et al., *Enhancement of thermal conductivity with Cu for nanofluids using chemical reduction method.* International Journal of Heat and Mass Transfer, 2006. **49**(17): p. 3028-3033.

39. Choi, S., et al., *Anomalous thermal conductivity enhancement in nanotube suspensions.* Applied physics letters, 2001. **79**(14): p. 2252-2254.

40. Hwang, Y., et al., *Investigation on characteristics of thermal conductivity enhancement of nanofluids.* Current Applied Physics, 2006. **6**(6): p. 1068-1071.

41. Eastman, J.A., et al., *Anomalously increased effective thermal conductivities of*

ethylene glycol-based nanofluids containing copper nanoparticles. Applied physics letters, 2001. **78**(6): p. 718-720.

42. Jana, S., A. Salehi-Khojin, and W.-H. Zhong, *Enhancement of fluid thermal conductivity by the addition of single and hybrid nano-additives.* Thermochimica Acta, 2007. **462**(1): p. 45-55.

43. Yoo, D.-H., K. Hong, and H.-S. Yang, *Study of thermal conductivity of nanofluids for the application of heat transfer fluids.* Thermochimica Acta, 2007. **455**(1): p. 66-69.

44. Lee, J.-H., et al., *Effective viscosities and thermal conductivities of aqueous nanofluids containing low volume concentrations of Al< sub> 2</sub> O< sub> 3</sub> nanoparticles.* International Journal of Heat and Mass Transfer, 2008. **51**(11): p. 2651-2656.

45. Mintsa, H.A., et al., *New temperature dependent thermal conductivity data for water-based nanofluids.* International Journal of Thermal Sciences, 2009. **48**(2): p. 363-371.

46. Vajjha, R.S. and D.K. Das, *Experimental determination of thermal conductivity of three nanofluids and development of new correlations.* International Journal of Heat and Mass Transfer, 2009. **52**(21): p. 4675-4682.

47. Shen, B., *Minimum quantity lubrication grinding using nanofluids*. 2008: ProQuest.

48. Eastman, J., et al. *Enhanced thermal conductivity through the development of nanofluids*. in *MRS proceedings*. 1996. Cambridge Univ Press.

49. Xuan, Y. and Q. Li, *Heat transfer enhancement of nanofluids.* International Journal of Heat and Fluid Flow, 2000. **21**(1): p. 58-64.

50. Hong, T.-K., H.-S. Yang, and C. Choi, *Study of the enhanced thermal conductivity of Fe nanofluids.* Journal of Applied Physics, 2005. **97**(6): p. 064311.

51. Patel, H.E., et al., *Thermal conductivities of naked and monolayer protected metal nanoparticle based nanofluids: Manifestation of anomalous enhancement and chemical effects.* Applied Physics Letters, 2003. **83**(14): p. 2931-2933.

52. Wang, X., X. Xu, and S.U. S. Choi, *Thermal conductivity of nanoparticle-fluid mixture.* Journal of thermophysics and heat transfer, 1999. **13**(4): p. 474-480.

53. Xie, H., et al., *Thermal conductivity enhancement of suspensions containing nanosized alumina particles.* Journal of Applied Physics, 2002. **91**(7): p. 4568-4572.

54. Xie, H., et al., *Study on the thermal conductivity of SiC nanofluids.* J. Chin. Ceram. Soc., 2001. **29**(4): p. 361-364.

55. Murshed, S., K. Leong, and C. Yang, *Enhanced thermal conductivity of TiO 2—water based nanofluids.* International Journal of thermal sciences, 2005. **44**(4): p. 367-373.

56. Biercuk, M., et al., *Carbon nanotube composites for thermal management.* Applied physics letters, 2002. **80**(15): p. 2767-2769.

57. Abareshi, M., et al., *Fabrication, characterization and measurement of thermal conductivity of Fe 3 O 4 nanofluids.* Journal of Magnetism and Magnetic Materials, 2010. **322**(24): p. 3895-3901.

58. Li, D., et al., *An easy fabrication of monodisperse oleic acid-coated Fe 3 O 4 nanoparticles.* Materials Letters, 2010. **64**(22): p. 2462-2464.

59. Maxwell, G.F., *Ferrofluid on glass, with a magnet underneath.*

60. Ghasemi, B. and S. Aminossadati, *Periodic natural convection in a nanofluid-filled*

enclosure with oscillating heat flux. International Journal of Thermal Sciences, 2010. **49**(1): p. 1-9.

61. Wright, B., et al., *Magnetic field enhanced thermal conductivity in heat transfer nanofluids containing Ni coated single wall carbon nanotubes.* Applied Physics Letters, 2007. **91**(17): p. 173116.

62. Thakur, H.V., et al., *Photonic crystal fiber injected with Fe3O4 nanofluid for magnetic field detection.* Applied Physics Letters, 2011. **99**(16): p. 161101.

63. Soelberg, S.D., et al., *Surface plasmon resonance detection using antibody-linked magnetic nanoparticles for analyte capture, purification, concentration, and signal amplification.* Analytical chemistry, 2009. **81**(6): p. 2357-2363.

64. Salloum, M., et al., *Controlling nanoparticle delivery in magnetic nanoparticle hyperthermia for cancer treatment: experimental study in agarose gel.* International Journal of Hyperthermia, 2008. **24**(4): p. 337-345.

65. Mahendran, V. and J. Philip, *An optical technique for fast and ultrasensitive detection of ammonia using magnetic nanofluids.* Applied Physics Letters, 2013. **102**(6): p. 063107.

66. Kodama, S., *Dynamic ferrofluid sculpture: organic shape-changing art forms.* Communications of the ACM, 2008. **51**(6): p. 79-81.

67. Kuzubov, A. and O. Ivanova, *Magnetic liquids for heat exchange.* Journal de Physique III, 1994. **4**(1): p. 1-6.

68. Philip, J., P. Shima, and B. Raj, *Evidence for enhanced thermal conduction through percolating structures in nanofluids.* Nanotechnology, 2008. **19**(30): p. 305706.

69. Vékás, L., D. Bica, and M.V. Avdeev, *Magnetic nanoparticles and concentrated magnetic nanofluids: synthesis, properties and some applications.* China Particuology, 2007. **5**(1): p. 43-49.

70. Yamaguchi, H., et al., *Experimental and numerical investigation of natural convection of magnetic fluids in a cubic cavity.* Journal of Magnetism and Magnetic Materials, 2009. **321**(22): p. 3665-3670.

71. Ghofrani, A., et al., *Experimental investigation on laminar forced convection heat transfer of ferrofluids under an alternating magnetic field.* Experimental Thermal and Fluid Science, 2013. **49**: p. 193-200.

72. Lajvardi, M., et al., *Experimental investigation for enhanced ferrofluid heat transfer under magnetic field effect.* Journal of Magnetism and Magnetic Materials, 2010. **322**(21): p. 3508-3513.

73. Li, Q. and Y. Xuan, *Experimental investigation on heat transfer characteristics of magnetic fluid flow around a fine wire under the influence of an external magnetic field.* Experimental Thermal and Fluid Science, 2009. **33**(4): p. 591-596.

74. Zhu, H., et al., *Effects of nanoparticle clustering and alignment on thermal conductivities of Fe3O4 aqueous nanofluids.* Applied Physics Letters, 2006. **89**(2): p. 23123-23123.

75. Junhong, L., et al., *Experiments and mechanism analysis of pool boiling heat transfer enhancement with water-based magnetic fluid.* Heat and mass transfer, 2004. **41**(2): p. 170-175.

76. Şeşen, M., et al., *Heat transfer enhancement with actuation of magnetic*

nanoparticles suspended in a base fluid. Journal of Applied Physics, 2012. **112**(6): p. 064320.

77. Kamiyama, S. and J. Ishimoto, *Boiling two-phase flows of magnetic fluid in a non-uniform magnetic field.* Journal of magnetism and magnetic materials, 1995. **149**(1): p. 125-131.

78. Shuchi, S., T. Mori, and H. Yamaguchi, *Flow boiling heat transfer of binary mixed magnetic fluid.* Magnetics, IEEE Transactions on, 2002. **38**(5): p. 3234-3236.

79. Taslimifar, M., et al., *Overall thermal performance of ferrofluidic open loop pulsating heat pipes: An experimental approach.* International Journal of Thermal Sciences, 2013. **65**: p. 234-241.

80. Bar-Cohen, Y., *Biomimetics? using nature to inspire human innovation.* Bioinspiration & biomimetics, 2006. **1**(1): p. P1.

81. Zang, H., S. Zhang, and K. Hapeshi, *A Review of Nature-Inspired Algorithms.* Journal of Bionic Engineering, 2010. **7**: p. S232-S237.

82. Cruiziat, P., H. Cochard, and T. Améglio, *Hydraulic architecture of trees: main concepts and results.* Annals of forest science, 2002. **59**(7): p. 723-752.

83. Zimmermann, M.H., *Hydraulic architecture of some diffuse-porous trees.* Canadian Journal of Botany, 1978. **56**(18): p. 2286-2295.

84. Tyree, M.T. and J.S. Sperry, *Vulnerability of xylem to cavitation and embolism.* Annual review of plant biology, 1989. **40**(1): p. 19-36.

85. Tyree, M.T. and F.W. Ewers, *The hydraulic architecture of trees and other woody plants.* New Phytologist, 1991. **119**(3): p. 345-360.

86. Pallardy, S.G., et al. *Hydraulic architecture and conductivity: an overview*. in *Structural and functional responses to environmental stresses: water shortage. XIV International Botanical Congress, Berlin, 24 July-1 August 1987.* 1989. SPB Academic Publishing bv.

87. Tyree, M.T., *Plant hydraulics: The ascent of water.* Nature, 2003. **423**(6943): p. 923-923.

88. Amritphale, D. and S.K. Sharma, *Xylem hydraulics: Rising up and higher!* Resonance, 2010. **15**(3): p. 223-231.

89. Pennisi, E., *The Sky Is Not the Limit.* Science, 2005. **310**(5756): p. 1896-1897.

90. Milburn, J.A., *Water flow in plants*. 1979: Longman Inc.

91. boundless.com, *Water movement in xylem.*

92. Dixon, H.H. and J. Joly, *On the ascent of sap.* Philosophical Transactions of the Royal Society of London. B, 1895: p. 563-576.

93. Hodson, M.J. and J.A. Bryant, *Functional biology of plants*. 2012: John Wiley & Sons.

94. Rabi, I.I., et al., *A New Method of Measuring Nuclear Magnetic Moment.* Physical Review, 1938. **53**(4): p. 318-318.

95. Filler, A.G., *The history, development and impact of computed imaging in neurological diagnosis and neurosurgery: CT, MRI, and DTI.* Nature Precedings, 2009. **7**(1): p. 1-69.

96. Abraham, R.J., J. Fisher, and P. Loftus, *Introduction to NMR spectroscopy*. 1988: Wiley.

97. Morris, P.G., *Nuclear magnetic resonance imaging in medicine and biology.* 1986.

98. Bottomley, P.A., *Human in vivo NMR spectroscopy in diagnostic medicine: clinical tool*

or research probe? Radiology, 1989. **170**(1): p. 1-15.

99. Günther, H., *NMR spectroscopy: basic principles, concepts and applications in chemistry*. 2013: John Wiley & Sons.

100. Maierhofer, C., H.-W. Reinhardt, and G. Dobmann, *Non-destructive Evaluation of Reinforced Concrete Structures: Non-destructive Testing Methods*. 2010: Elsevier.

101. Hirasaki, G.J., S.-W. Lo, and Y. Zhang, *NMR properties of petroleum reservoir fluids.* Magnetic resonance imaging, 2003. **21**(3): p. 269-277.

102. Robert Powell, H., et al., *The application of functional MRI of memory in temporal lobe epilepsy: a clinical review.* Epilepsia, 2004. **45**(7): p. 855-863.

103. Jack, C., et al., *Comparison of different MRI brain atrophy rate measures with clinical disease progression in AD.* Neurology, 2004. **62**(4): p. 591-600.

104. Osman, N.F., E.R. McVeigh, and J.L. Prince, *Imaging heart motion using harmonic phase MRI.* IEEE transactions on medical imaging, 2000. **19**(3): p. 186-202.

105. Hinshaw, W.S. and A.H. Lent, *An introduction to NMR imaging: From the Bloch equation to the imaging equation.* Proceedings of the IEEE, 1983. **71**(3): p. 338-350.

106. Brown, M.A. and R.C. Semelka, *MRI: basic principles and applications*. 2011: John Wiley & Sons.

107. Callaghan, P.T., *Principles of nuclear magnetic resonance microscopy*. Vol. 3. 1991: Clarendon Press Oxford.

108. Rinck, P., *Magnetic resonance in medicine. The basic text-41. book of the European Magnetic Resonance Forum*. 2003, Blackwell, London.

109. Runge, V.M., et al., *Work in progress: potential oral and intravenous paramagnetic*

NMR contrast agents. Radiology, 1983. **147**(3): p. 789-791.

110. Babes, L., et al., *Synthesis of iron oxide nanoparticles used as MRI contrast agents: a parametric study.* Journal of Colloid and Interface Science, 1999. **212**(2): p. 474-482.

111. Bulte, J.W. and D.L. Kraitchman, *Iron oxide MR contrast agents for molecular and cellular imaging.* NMR in Biomedicine, 2004. **17**(7): p. 484-499.

112. Runge, V.M., et al., *Paramagnetic agents for contrast-enhanced NMR imaging: a review.* American Journal of Roentgenology, 1983. **141**(6): p. 1209-1215.

113. Ward, J.L., J.M. Baker, and M.H. Beale, *Recent applications of NMR spectroscopy in plant metabolomics.* Febs Journal, 2007. **274**(5): p. 1126-1131.

114. Kim, H.K., Y.H. Choi, and R. Verpoorte, *NMR-based metabolomic analysis of plants.* Nat Protoc, 2010. **5**(3): p. 536-49.

115. Mesnard, F. and R.G. Ratcliffe, *NMR analysis of plant nitrogen metabolism.* Photosynth Res, 2005. **83**(2): p. 163-80.

116. Eisenreich, W. and A. Bacher, *Advances of high-resolution NMR techniques in the structural and metabolic analysis of plant biochemistry.* Phytochemistry, 2007. **68**(22-24): p. 2799-815.

117. Kim, H.K., Y.H. Choi, and R. Verpoorte, *NMR-based plant metabolomics: where do we stand, where do we go?* Trends Biotechnol, 2011. **29**(6): p. 267-75.

118. Ward, J.L. and M.H. Beale, *NMR Spectroscopy in Plant Metabolomics*, in *Plant Metabolomics*, K. Saito, R.A. Dixon, and L. Willmitzer, Editors. 2006, Springer Berlin Heidelberg: Berlin, Heidelberg. p. 81-91.

119. Mahrous, E.A. and M.A. Farag, *Two dimensional NMR spectroscopic approaches for*

exploring plant metabolome: A review. J Adv Res, 2015. **6**(1): p. 3-15.

120. Farag, M.A., *Comparative mass spectrometry & nuclear magnetic resonance metabolomic approaches for nutraceuticals quality control analysis: a brief review.* Recent Pat Biotechnol, 2014. **8**(1): p. 17-24.

121. Bottomley, P.A., H.H. Rogers, and T.H. Foster, *NMR imaging shows water distribution and transport in plant root systems in situ.* Proceedings of the National Academy of Sciences, 1986. **83**(1): p. 87-89.

122. Van As, H. *NMR IN HORTICULTURE: IN SITU PLANT WATER BALANCE STUDIES WITH NMR*. 1992. International Society for Horticultural Science (ISHS), Leuven, Belgium.

123. Scheenen, T.W.J., et al., *Quantification of water transport in plants with NMR imaging.* Journal of Experimental Botany, 2000. **51**(351): p. 1751-1759.

124. Eccles, C.D. and P.T. Callaghan, *High-resolution imaging. The NMR microscope.* Journal of Magnetic Resonance (1969), 1986. **68**(2): p. 393-398.

125. Kuchenbrod, E., et al., *Measurement of water flow in the xylem vessels of intact maize plants using flow‐sensitive NMR imaging.* Botanica Acta, 1996. **109**(3): p. 184-186.

126. Ishida, N., M. Koizumi, and H. Kano, *The NMR microscope: a unique and promising tool for plant science.* Annals of Botany, 2000. **86**(2): p. 259-278.

127. Clark, C., et al., *Application of magnetic resonance imaging to pre-and post-harvest studies of fruits and vegetables.* Postharvest Biology and Technology, 1997. **11**(1): p. 1-21.

128. McCarthy, M. and R. Kauten, *NMR for internal quality evaluation of fruits and*

vegetables. Transactions of the ASAE, 1989. **32**(5): p. 1747-1753.

129. Garnczarska, M., T. Zalewski, and M. Kempka, *Changes in water status and water distribution in maturing lupin seeds studied by MR imaging and NMR spectroscopy.* Journal of experimental botany, 2007. **58**(14): p. 3961-3969.

130. Petty, J., *Fluid flow through the vessels of birch wood.* Journal of Experimental Botany, 1978. **29**(6): p. 1463-1469.

131. Van As, H. and T. Schaafsma, *Noninvasive measurement of plant water flow by nuclear magnetic resonance.* Biophysical journal, 1984. **45**(2): p. 469.

132. Melkus, G., et al., *Dynamic 13C/1H NMR imaging uncovers sugar allocation in the living seed.* Plant biotechnology journal, 2011. **9**(9): p. 1022-1037.

133. Wang, S.Y., P.C. Wang, and M. Faust, *Non-destructive detection of watercore in apple with nuclear magnetic resonance imaging.* Scientia horticulturae, 1988. **35**(3-4): p. 227-234.

134. Koizumi, M., et al., *Observation of water and Na+ in tissues of theBruguiera gymnorrhiza by1H-and23Na-NMR imaging.* The botanical magazine= Shokubutsu-gaku-zasshi, 1992. **105**(1): p. 1-11.

135. Jagannathan, N., V. Govindaraju, and P. Raghunathan, *In vivo magnetic resonance study of the histochemistry of coconut (Cocos nucifera).* Magnetic resonance imaging, 1995. **13**(6): p. 885-892.

136. Gribble, K., et al., *Position of water in vitrified plants visualised by NMR imaging.* Protoplasma, 1998. **201**(1-2): p. 110-114.

137. Tamiya, T., et al., *Movement of water in conjunction with plant movement visualized*

by NMR imaging. Journal of biochemistry, 1988. **104**(1): p. 5-8.

138. Millard, M., et al., *Thermodynamic analysis of the physical state of water during freezing in plant tissue, based on the temperature dependence of proton spin‐spin relaxation.* Plant, Cell & Environment, 1996. **19**(1): p. 33-42.

139. Iwahashi, Y., et al., *The study of heat stress in tomato fruits by NMR microimaging.* Magnetic resonance imaging, 1999. **17**(5): p. 767-772.

140. Chudek, J., et al., *An application of NMR microimaging to investigate nitrogen fixing root nodules.* Magnetic resonance imaging, 1997. **15**(3): p. 361-368.

141. Wang, C. and P. Wang, *Differences in nuclear magnetic resonance images between chilled and non-chilled zucchini squash.* Environmental and experimental botany, 1992. **32**(3): p. 213-219.

142. Köckenberger, W., et al., *A non-invasive measurement of phloem and xylem water flow in castor bean seedlings by nuclear magnetic resonance microimaging.* Planta, 1997. **201**(1): p. 53-63.

143. Brown, J.M., et al., *Magnetic resonance microscopy of stem tissues of Pelargonium hortorum.* Botanical Gazette, 1988: p. 253-259.

144. Donker, H., et al., *Quantitative 1 H-NMR imaging of water in white button mushrooms (Agaricus bisporus).* Magnetic resonance imaging, 1997. **15**(1): p. 113-121.

145. Carr, H.Y. and E.M. Purcell, *Effects of diffusion on free precession in nuclear magnetic resonance experiments.* Physical review, 1954. **94**(3): p. 630.

146. Singer, J., *NMR diffusion and flow measurements and an introduction to spin phase*

graphing. Journal of Physics E: Scientific Instruments, 1978. **11**(4): p. 281.

147. Packer, K., *The study of slow coherent molecular motion by pulsed nuclear magnetic resonance.* Molecular Physics, 1969. **17**(4): p. 355-368.

148. Quemada, D. and C. Berli, *Energy of interaction in colloids and its implications in rheological modeling.* Advances in colloid and interface science, 2002. **98**(1): p. 51-85.

149. Evans, W., J. Fish, and P. Keblinski, *Role of Brownian motion hydrodynamics on nanofluid thermal conductivity.* Applied Physics Letters, 2006. **88**(9): p. 093116.

150. Alsaady, M., et al., *Thermo-physical properties and thermo-magnetic convection of ferrofluid.* Applied Thermal Engineering, (0).

151. Zeinali Heris, S., S.G. Etemad, and M. Nasr Esfahany, *Experimental investigation of oxide nanofluids laminar flow convective heat transfer.* International Communications in Heat and Mass Transfer, 2006. **33**(4): p. 529-535.

152. Zhou, D., *Heat transfer enhancement of copper nanofluid with acoustic cavitation.* International Journal of Heat and Mass Transfer, 2004. **47**(14): p. 3109-3117.

153. Mondragón, R., et al., *Experimental characterization and modeling of thermophysical properties of nanofluids at high temperature conditions for heat transfer applications.* Powder Technology, 2013. **249**: p. 516-529.

154. Molz, F.J., *Models of water transport in the soil‐plant system: A review.* Water Resources Research, 1981. **17**(5): p. 1245-1260.

155. Fiscus, E.L., A. Klute, and M.R. Kaufmann, *An interpretation of some whole plant water transport phenomena.* Plant Physiology, 1983. **71**(4): p. 810-817.

156. Sperry, J., et al., *Limitation of plant water use by rhizosphere and xylem conductance: results from a model.* Plant, Cell & Environment, 1998. **21**(4): p. 347-359.

157. Stratton, L., G. Goldstein, and F. Meinzer, *Stem water storage capacity and efficiency of water transport: their functional significance in a Hawaiian dry forest.* Plant, Cell & Environment, 2000. **23**(1): p. 99-106.

158. Takeda, M., et al., *Physical properties of iron-oxide scales on Si-containing steels at high temperature.* Materials transactions, 2009. **50**(9): p. 2242-2246.

159. Buongiorno, J., *Convective transport in nanofluids.* Journal of Heat Transfer, 2006. **128**(3): p. 240-250.

160. Maïga, S.E.B., et al., *Heat transfer behaviours of nanofluids in a uniformly heated tube.* Superlattices and Microstructures, 2004. **35**(3): p. 543-557.

161. Xuan, Y. and W. Roetzel, *Conceptions for heat transfer correlation of nanofluids.* International Journal of heat and Mass transfer, 2000. **43**(19): p. 3701-3707.

162. Feynman, R.P., R.B. Leighton, and M. Sands, *The Feynman Lectures on Physics, Desktop Edition Volume I*. Vol. 1. 2013: Basic books.

163. McNab, G. and A. Meisen, *Thermophoresis in liquids.* Journal of Colloid and Interface Science, 1973. **44**(2): p. 339-346.

164. Lister, D., *Corrosion products in power generating systems*. 1980: Chalk River Nuclear Laboratories.

165. Müller-Steinhagen, H., *Cooling-water fouling in heat exchangers.* Advances in Heat Transfer, 1999. **33**: p. 415-496.

166. Boker, A., et al., *Self-assembly of nanoparticles at interfaces.* Soft Matter, 2007. **3**(10):

p. 1231-1248.

167. Malvandi, A. and D. Ganji, *Brownian motion and thermophoresis effects on slip flow of alumina/water nanofluid inside a circular microchannel in the presence of a magnetic field.* International Journal of Thermal Sciences, 2014. **84**: p. 196-206.

168. Denny, M., *Tree hydraulics: how sap rises.* European Journal of Physics, 2012. **33**(1): p. 43.

169. Sperry, J.S., et al., *Spring filling of xylem vessels in wild grapevine.* Plant Physiology, 1987. **83**(2): p. 414-417.

170. Tibbetts, T.J. and F.W. Ewers, *Root pressure and specific conductivity in temperate lianas: exotic Celastrus orbiculatus (Celastraceae) vs. native Vitis riparia (Vitaceae).* American Journal of Botany, 2000. **87**(9): p. 1272-1278.

171. Van den Honert, T., *Water transport in plants as a catenary process.* Discussions of the Faraday Society, 1948. **3**: p. 146-153.

172. Zimmerman, M.H. and C.L. Brown, *Trees: structure and function*. 1971: New York, USA, Springer-Verlag.

173. JEJE, A.Y.A. and M.H. ZIMMERMANN, *Resistance to Water Flow in Xylem Vessels.* Journal of Experimental Botany, 1979. **30**(4): p. 817-827.

174. Dimond, A., *Pressure and flow relations in vascular bundles of the tomato plant.* Plant Physiology, 1966. **41**(1): p. 119-131.

175. Fiscus, E.L., L.R. Parsons, and R.S. Alberte, *Phyllotaxy and water relations in tobacco.* Planta, 1973. **112**(4): p. 285-292.

176. Wistuba, N., et al., *Xylem Flow and its Driving Forces in a Tropical Liana: Concomitant*

Flow‐Sensitive NMR Imaging and Pressure Probe Measurements. Plant Biology, 2000. **2**(6): p. 579-582.

177. Tyree, M.T., *The cohesion-tension theory of sap ascent: current controversies.* Journal of Experimental Botany, 1997. **48**(10): p. 1753-1765.

178. Kohonen, M.M. and Å. Helland, *On the function of wall sculpturing in xylem conduits.* Journal of Bionic Engineering, 2009. **6**(4): p. 324-329.

179. Holbrook, N.M. and M.A. Zwieniecki, *Transporting water to the tops of trees.* Physics Today, 2008. **61**(1): p. 76-77.

180. Giordano, R., et al., *Flow in xylem vessels and Poiseuille's law.* Canadian Journal of Botany, 1978. **56**(3): p. 333-338.

181. Siau, J.F., *Permeability*. 1984: Springer.

182. Calkin, H., A. Gibson, and P. Nobel, *Biophysical model of xylem conductance in tracheids of the fern Pteris vittata.* Journal of Experimental Botany, 1986. **37**(7): p. 1054-1064.

183. *Darcy Friction factor for Re between 10 and 10E8 for values of relative roughness*, in *ArthurOgawa*. https://commons.wikimedia.org/wiki/File:Darcy_Friction_factor_for_Re_between_10_and_10E8_for_values_of_relative_roughness.svg.

184. Hinckley, T.M., et al., *Water flux in a hybrid poplar stand.* Tree Physiology, 1994. **14**(7-8-9): p. 1005-1018.